SMART NANOCOMPOSITES

Volume 6, Number 2, 2015

TABLE OF CONTENTS

nova publishers
New York

Smart Nanocomposites

This Journal presents new studies in the fast growing area of smart materials, in particular, composite nanostructured materials. It focuses on the physics and physical chemistry of surfaces, interfaces, thin films and coatings, nanoparticles and other nanostructures, as well as on their new and smart applications. Original approaches in fabrication and applications of nanostructured materials will get special attention. Nanostructured ceramics, alloys, various nanocarbon forms (nanotubes, fullerenes, graphene) and their composites used in sensors (including single molecule sensing) and actuators, artificial metabolism, drug delivery, selective membranes, fuel cells, energy storage, and photovoltaics are just a few examples of new classes of materials and applications that are within the scope of the Journal. It features the results of interdisciplinary research from universities, national labs, and privately owned companies.

The Journal is peer-reviewed with the highest standards and quality of publications. The purpose of this Journal is to bring the most up-to-date advances in nanotechnology together, and to give research groups the opportunity to compare their results with other groups' data. To achieve this, the Journal focuses mostly on practical applications of nanodevices, and on proof of the concept publications. Areas of interest include (but not are limited to): sensors, smart membranes, smart coatings for corrosion protection, aspects of significance to nanorobots: power supplies, nanorobot manipulating devices, and microchips for artificial intelligence. The Journal also deals with safety issues: safety of nanotechnology to the environment, controlling the nanodevices, and other aspects.

Smart Nanocomposites
is published in two issues per year by

Nova Science Publishers, Inc.
400 Oser Avenue, Suite 1600
Hauppauge, New York 11788-3619, U.S.A.
E-mail: nova.main@novapublishers.com
Web: www.novapublishers.com

ISSN: 1949-4823

Subscription Rate per Volume
Print: $245 Electronic: $245 Combined Print + Electronic: $367

Additional color graphics might be available in the e-version of this journal.

Smart Nanocomposites
Volume 6, Number 2
ISSN: 1949-4823

CHARACTERISTICS OF THE INTERFACES AND THE PROPERTIES OF CHROMIUM OXIDE NANOLAYERS ON GALLIUM ARSENIDE

Yu. K. Ezhovskii*
St. Petersburg Technological Institute (Technical University)
St. Petersburg, Russia

ABSTRACT

This paper reports on the experimental results of investigations into the electrical properties of chromium oxide ultrathin layers (nanostructures) synthesized on the GaAs(100) and GaAs(110) surfaces through the molecular layer-by-layer growth (atomic layer deposition). It is established that the synthesis conditions and the layer composition affect the characteristics of the semiconductor–dielectric interface.

INTRODUCTION

The design of microelectronic and nanoelectronic devices has been determined in many respects by the considerable advances made in research into the mechanism of formation and the properties of low-dimensional systems, which, in turn, has given impetus to the development of nanotechnology for these systems. Among the large variety of methods used in the chemical nanotechnology of low-dimensional systems, the atomic layer deposition, or the so-called ALD technology, has enjoyed the widest application [1, 2]. This technology is based on the physicochemical principles developed even in the 1970s by the school of Russian scientists under the supervision of Aleskovskii [3]. The technology involves chemical surface reactions between low-temperatures reagents and functional groups of surfaces. This makes it possible to prepare dielectric and semiconductor nanolayers whose composition and thickness can be controlled within a monolayer.

Ultrathin dielectric layers of chromium oxides are very promising for use as components of metal–insulator–semiconductor structures, as well as adhesive and diffusion barrier layers, in silicon and gallium arsenide integrated devices [4]. In this case, the layer thickness should not exceed a few nanometers. The possibility of easily changing the valence state of

* E-mail: ezhovski@pochta.ru

chromium from Cr(III) to Cr(VI) allows one to affect not only the dielectric characteristics of layers but also the quality of the semiconductor–dielectric interface.

This paper reports on the experimental results of investigations into the properties of chromium oxide nanostructures on gallium arsenide and evaluation of the electrical properties and the quality of the semiconductor–dielectric interface.

SAMPLE PREPARATION AND EXPERIMENTAL TECHNIQUE

Chromium oxide nanolayers were synthesized in a vacuum–flow type reactor (the residual pressure was no higher than 10^{-2} Pa) at temperatures in the range T_s=373-473K by using alternate treatment of the surfaces of gallium arsenide with the (110) and (110) orientation in vapors of chromium oxychloride CrO_2Cl_2 with different hydroxylating reagents according to the following technological schemes.

1. Alternate treatment of the surface in CrO_2Cl_2 and H_2O (the neutral hydroxylating reagent) vapors.
2. Alternate treatment of the surface in CrO_2Cl_2 and CH_3OH (or $CH_3OH + H_2O$) (the reducing hydroxylating reagent) vapors.
3. Alternate treatment of the surface in CrO_2Cl_2 and H_2O_2 (or $H_2O_2 + H_2O$) (the oxidizing hydroxylating reagent) vapors.

In all cases, the reagent vapor pressure was approximately equal to 1.3 Pa.

The use of hydroxylating reagents with reducing or oxidizing properties permits one to vary the oxide composition and, hence, its properties.

Immediately before synthesis, the substrates were etched in a methanol–bromine etchant. The thickness of the residual oxide layer on the GaAs surface according to ellipsometric estimates did not exceed 1 nm [6].

The thickness of the synthesized layers was determined by measuring the elliptic polarization angles Δ and Ψ and was then calculated in the framework of the Drude–Tronston single-layer model [7]. The angles Δ and Ψ were measured on an ellipsometer assembled according to the PQSA scheme [8] with a static compensator. An LG-75 laser with an emission wavelength of 632.8 nm served as a source of linearly polarized light. In order to increase the accuracy of measurement, the light beam was subjected to magnetic modulation. The error in determining the angles Δ and Ψ did not exceed $\pm$ 0.10′ (plane angle)]. The layer thickness was calculated using the refractive indices, which were determined by the Holmes method [8, 9].

The composition of nanostructures was controlled using x-ray photoelectron spectroscopy. The x-ray photoelectron spectra were recorded on NR-5950A (Al K_α radiation, E = 1486 eV) and SER-1 (Mg $K\alpha$ radiation, E = 1253 eV) spectrometers. The energy was measured with respect to the $C1s_{1/2}$ line (E_{st} = 285,0 eV). The maximum depth of penetration of the probe into the surface layer at the above energies did not exceed 8 nm [10]. The assignment of the lines observed at energies E_s for the elements under investigation in the x-ray photoelectron spectra was performed according to the data taken from [11, 12]. For quantitative analysis of the composition of the surface layers, we used the relationship [10]

$$I_1 / I_2 = n_1 \sigma_1 \sqrt{E_{K2}} \Big/ n_2 \sigma_2 \sqrt{E_{K1}} \quad , \tag{1}$$

where I_1 and I_2 are the intensities of the lines of given atoms, respectively; σ_1 and σ_2 are the relative ionization cross sections of the corresponding energy levels; n_1 and n_2 are the concentrations of atoms, respectively; and E_{K1} and E_{K2} are the kinetic energies of electrons. Here, $E_K = E_{K\alpha} - F_s$, where F_s is the work function of the spectrometer material. The spectra were processed with a special computer program using the Gaussian approximation of the curves.

The current–voltage characteristics were measured on EM-1 and IT-2 electrometers. A vacuum-evaporated tin layer (the work function of tin is close to that of gallium arsenide) served as a counter electrode.

The capacitance–voltage characteristics were measured for two systems, namely, the metal–dielectric–semiconductor system for dielectric layer thicknesses ranging from 50 to 150 nm and the electrolyte–dielectric–semiconductor system in the case of thicknesses smaller that 50 nm.

The capacitance–voltage characteristics of metal–dielectric–semiconductor structures were determined in the frequency range 6–170 kHz and at a fixed frequency of 1 MHz. The measurements were performed with the use of a differential compensation circuit at frequencies up to 170 kHz and from the reactive component of the current passing through the sample at a frequency of 1 MHz.

The properties of the GaAs–chromium oxide structures with ultrathin layers (8–50 nm thick) were investigated in the electrolyte–dielectric–semiconductor system with a 1% Na_2SO_4 solution as an electrolyte, because the evaporation of a metal electrode can lead to heating of the surface layer and metal diffusion over the entire depth of the ultrathin dielectric [13, 14]. The measurements were carried out using a bridge circuit in the frequency range 0.6–170 kHz. A conventional silver chloride electrode served as a reference electrode.

The capacitance–voltage characteristics were used to calculate the density of surface states at the interface by the Terman method [15]. When measuring in the electrolyte–dielectric–semiconductor system, the structures can be considered Schottky diodes with a Bardeen barrier [16]. In this case, the capacitance of the space-charge region of the semiconductor surface and the surface potential are related by the Schottky–Mott equation

$$\frac{1}{C^2} = \frac{2}{\varepsilon \cdot \varepsilon_0 e N_d} \left(\varphi_0 + \varphi_b - \frac{kT}{e} \right), \tag{2}$$

where C is the specific capacitance, ε is the permittivity of the semiconductor, φ_0 is the potential of the semiconductor, φ_b is the height of the barrier on the emiconductor surface, and N_d is the concentration of ionized donors in the semiconductor. The extrapolation of the dependence $C^{-2} = f(\varphi)$ to the intersection with the abscissa axis enables one to determine the barrier height (the potential of flat bands)

$$\varphi_b = -\varphi_0 + \frac{kT}{e}, \tag{3}$$

furthermore, the dopant concentration in the surface region of the semiconductor can be estimated from the slope of the dependence $C^{-2} = f(\varphi)$. An analysis of a deviation of the experimental Dependence $C^{-2} = f(\varphi)$ from the theoretical dependence provides a means for obtaining information on the charge state of the semiconductor–dielectric interface and calculating the density of surface states [15, 17].

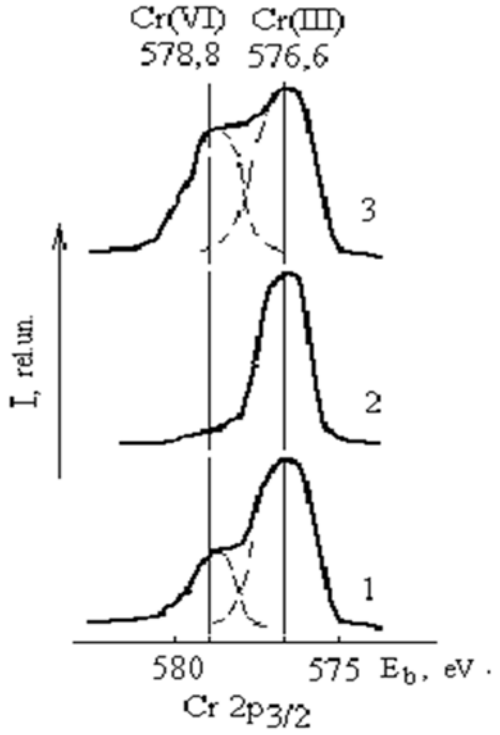

Figure 1. X-ray photoelectron spectra of the chromium oxide layers (d = 15 nm) synthesized according to different technological schemes with (*1*) CrO_2Cl_2 and H2O, (*2*) CrO_2Cl_2 and CH_3OH, and (*3*) CrO_2Cl_2 and H_2O_2. Synthesis conditions for all cases were as follows: contact time of the reagents τ = 60 s, pressure $P \approx 1.3$ Pa, and temperature Ts = 423 K.

The examination of the composition of the synthesized products with the use of the X-ray photoelectron spectra (Figure 1) showed that all layers prepared at temperatures $T_s > 400$K contained Cr(III) and Cr(VI) ions. The presence of Cr(III) ions in the products prepared upon hydrolysis in the oxidizing medium indicates that pyrolytic processes play an important role in the formation of the oxide layers.

The composition of the synthesized products was also studied from the infrared diffuse reflection spectra of the samples prepared on gallium arsenide powders of the aforementioned

grades. The analysis of these data demonstrated that only the Cr_2O_3 and CrO_3 oxides are observed in the chromium oxide nanostructures synthesized [5].

Electron diffraction investigation of the nanostructures revealed that the chromium oxide layers in all cases have an amorphous structure. This circumstance did not allow us to identify their composition from structural characteristics.

RESULTS AND DISCUSSION

The use of the chromium (VI) oxyhalide possessing oxidizing properties in the synthesis of the chromium oxide layers could substantially affect the chemical composition of the GaAs surface, because the oxidation of the matrix surface can occur in the given system in addition to the reactions with hydroxyl groups on the surface and pyrolytic decomposition. In this respect, the GaAs–chromium oxide interface was analyzed from the x-ray photoelectron spectroscopic dataobtained for the thin (≈5 nm) layers. The x-ray photoelectron spectra of these samples (Figure 2) contain information on the chemical composition of both the formed dielectric layer and the surface layer of the substrate.

The processing and analysis of these spectra showed that the interface involves the Ga_2O_3 oxide. Most likely, the interface also contains the As_2O_3 oxide; however, the characteristic As3*d* maximum at E_b = 44.5eV could not be separated, because it coincided with the Cr3*p* maximum at E_b = 44.4eV. It should be noted that the Ga and As spectra virtually did not depend on the technological scheme for synthesizing the chromium oxide layer. This suggests that the medium of deposition has a weak effect on the composition of the matrix surface. The ratio of the elements in the surface layer of the GaAs substrate was calculated from the x-ray photoelectron spectroscopic data with allowance made for the photoionization cross sections for the Ga 3*d* and As 3*d* levels (σ_{Ga}/σ_{As} =1.67) [10]. It was found that [Ga]/[As]≈1. The same ratio is characteristic of the GaAs surface subjected to chemical etching. Consequently, the inference can be made that the deposition of the chromium oxide layers is not accompanied by significant oxidation of the matrix surface.

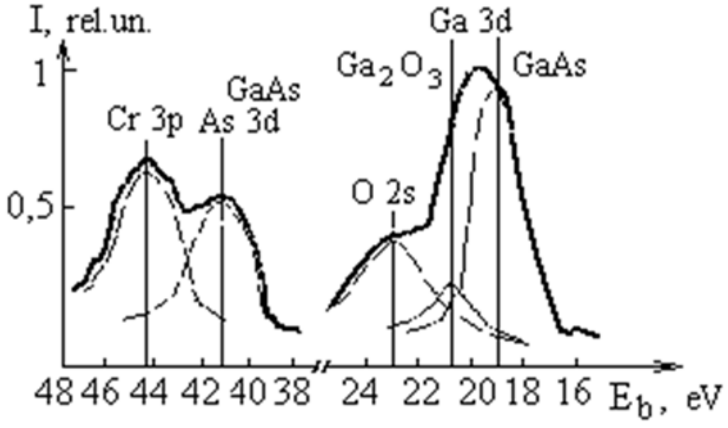

Figure 2. X-ray photoelectron spectra of the GaAs–chromium oxide system synthesized according to the second technological scheme. The thickness of the chromium oxide layer is d ≈5 nm.

The conductivity of the chromium oxide layers depends on the synthesis temperature and is governed by the layer composition [the Cr(III)/Cr(VI) ratio]. The lowest conductivity ($\sigma < 10^{-11}$ Ω cm^{-1}) is observed for the layers prepared at temperatures of 373–423 K with ratios [Cr(III)]/[Cr(VI)] ≈ 2. The low conductivity of these chromium oxide nanolayers is associated with their structure, i.e., the layered distribution of supramolecular clusters formed by the Cr_2O_3 and CrO_3 oxides over the layer thickness [5]. In the case of molecular layer-by-layer deposition and the layer mechanism of growth, a zonal distribution of Cr(III) and Cr(VI) ions is most probable. However, the size of these clusters can be very small and correspond to one monolayer. As a consequence, these clusters depending on the predominant component should manifest themselves as donor or acceptor centers in the layer structure and the conductivity of the layer should be determined by the Coulomb barrier associated with the charge state of chromium. The barrier model is confirmed by the analysis of the current–voltage characteristics of the layers (Figure 3). The conductivity of the nanolayers in weak electric fields is close to ohmic, whereas the current–voltage characteristics at $E > 10^4$ V cm^{-2} are well linearized in the Poole–Frenkel coordinates, when the conductivity is governed by the electron emission through the barrier φ_0; that is

$$I = n_0 \mu E \exp\left[-\frac{e(\varphi_0 - \beta E^{1/2})}{rkT}\right], \tag{4}$$

where n_0 is the equilibrium concentration of electrons in the conduction band, μ is the electron drift mobility, and r is coefficient taking into account the energy distribution of donor and acceptor states. For noncrystalline materials, this coefficient varies from 1 to 3 [18] and is determined by fitting.

With the use of the function

$$\beta e E^{1/2} = e\Delta\varphi = (e^3 E/\pi\varepsilon\varepsilon_0)^{1/2}, \tag{5}$$

one can determine the decrease $\Delta\varphi$ in the Coulomb barrier of the donor and to calculate the permittivity ε.

The current–voltage characteristics of the layers synthesized at temperatures $T_s > 373$K exhibit two linear portions (Figure 3). The conductivity in the initial portion is governed by the decrease (associated with the field) in the effective barrier height, which at the point of inflection is estimated to be approximately equal to 0.18 eV. The barrier height determined from the temperature dependence of the conductivity (with due regard for the field strength) is 0.23 eV. Therefore, the decrease in the barrier height amounts to 0.23–0.18 eV = 0.05 eV ≈ 2 kT and is also retained for the current–voltage characteristics measured at temperatures of 293 and 138K. This suggests that the barrier plays a decisive role. An increase in the field strength results in an increase in the electron emission through the barrier. The decrease in the barrier height in the electric field is governed by the permittivity of the components. Since the permittivities of the Cr_2O_3 and CrO_3 oxides are different, the slope of the current–voltage characteristic is determined by the limiting component.

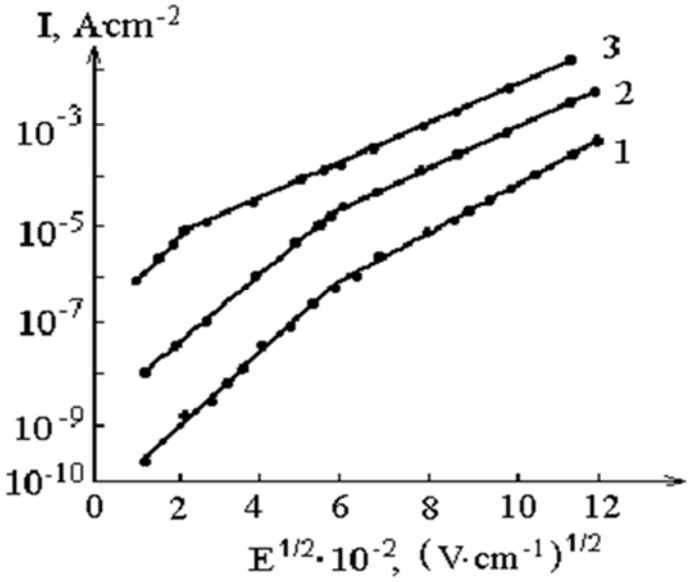

Figure 3. Current–voltage characteristics of the chromium oxide films prepared at temperatures T = (*1*) 423, (*2*) 453, and (*3*) 373 K. The thickness of the chromium oxide layer is $d \approx 100$ nm.

Examination of the characteristics of the semiconductor–dielectric interface with the chromium oxide layers prepared under different conditions revealed that the minimum density of surface states N_{ss} is observed in the structures synthesized through alternate treatment of the etched GaAs surface in CrO_2Cl_2 and CH_3OH vapors. The x-ray photoelectron spectrum of the interface of this structure is depicted in Figure 2. Similar results were obtained in the synthesis of the dielectric layer without using the hydroxylating agents upon direct pyrolysis of the CrO_2Cl_2 compound.

The capacitance-voltage characteristics for the GaAs-chromium oxide structures exhibit a normal frequency dispersion. Figure 4 shows the typical capacitance-voltage characteristics measured in the electrolyte-dielectric-semiconductor (Figure 4a) and metal–dielectric–semiconductor (Figure 4b) systems. Since the dispersion of the capacitance measured in the electrolyte–dielectric–semiconductor system for the dielectric layer with a small thickness (d < 50 nm) is insignificantly changed with an increase in the frequency from 53 to 170 kHz, it is believed that the capacitance–voltage characteristic at f =170kHz can be treated as a high-frequency characteristic.

A comparison of the experimental and theoretical dependences $C^{-2} = f(\varphi)$ for the systems under investigation (Figure 4) allowed us to calculate the density of surface states at the GaAs–chromium oxide interface. The results obtained (Figure 5) indicate that the maximum density of states occurs in the range $E–Ev$ = 0.47eV and is most likely governed by the acceptor states of the dielectric. However, according to the capacitance–voltage characteristics measured for the nanostructures with thin dielectric layers in the electrolyte–dielectric–semiconductor system, the density of these states appears to be one order of magnitude lower. Moreover, these states were not revealed at all for the nanostructures synthesized at the temperature T_s = 373K. In our opinion, these discrepancies can be explained by both the structural transformations proceeding during the layer growth and the

increase in the synthesis temperature. Most probably, the origin of these states is associated with the formation of misfit dislocations at the interface in the course of crystallization processes that occur with an increase in the dielectric layer thickness or the increase in the synthesis temperature.

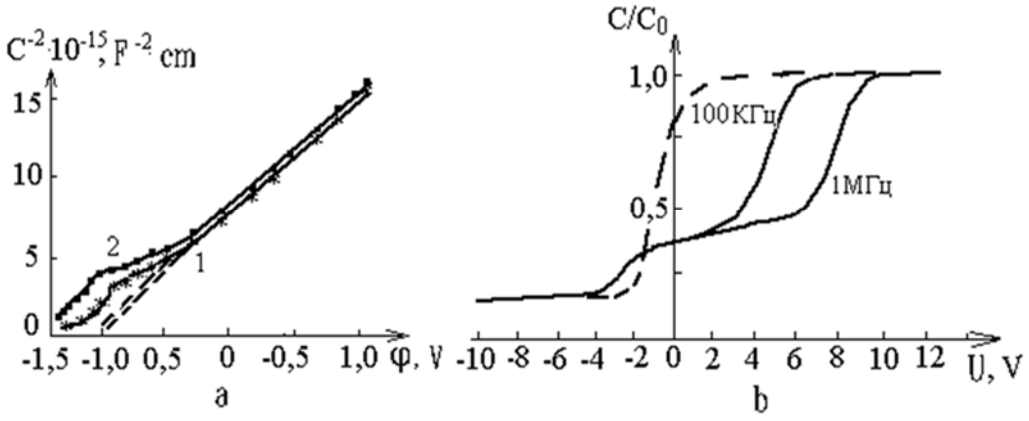

Figure 4. Capacitance–voltage characteristics of (a) the GaAs–chromium oxide–electrolyte system (d=11 nm) at frequencies f = 53 (*1*) and 170 (*2*) kHz and (b) the GaAs–chromium oxide–Sn system (d =130 nm) in different coordinates. Dashed lines indicate theoretical capacitance–voltage characteristics.

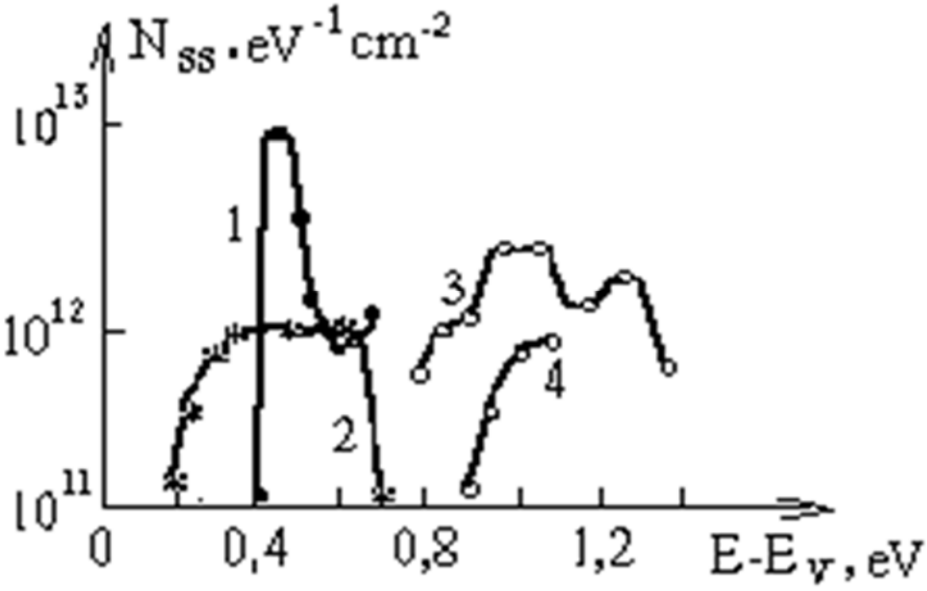

Figure 5. Densities of surface states at the GaAs–chromium oxide interface according to the calculations from the results of measurements in the (*1*, *3*) metal–dielectric–semiconductor and (*2*, *4*) electrolyte–dielectric–semiconductor systems for (*1*, *2*) acceptor states and (*3*, *4*) donor states in the chromium oxide layers synthesized at the temperature T_s = 423K. The thicknesses of the chromium oxide layers are d = 130 (*1*, *3*) and 11 nm (*2*, *4*).

As follows from our results, the lowest density of states at the interface is observed for the chromium oxide dielectric layers prepared at low temperatures. It seems likely that this circumstance is primarily explained by the formation of ordered chemical bonds with the matrix surface and the more favorable layer mechanism of nanostructure growth at low synthesis temperatures [5]. It is not improbable that free arsenic can undergo mild oxidation at the GaAs surface under the action of the chromium oxychloride. The preparation of the nanostructures with the use of different technological schemes enables us to vary the density of surface states N_{ss} by three orders of magnitude. The performed experiments demonstrate that, in the case of dielectrics based on the chromium oxide, it is possible to control the density of surface states and to prepare nanostructures with $N_{ss} < 10^{12}$ eV^{-1} cm^{-2} on the GaAs surface. Note that the weak dependence of the parameters of the semiconductor-dielectric interface on the GaAs surface on the technique and conditions for the preparation of the dielectric layers confirms the assumption made by Alekhin et al. [19] that a natural oxide layer on the surface of $A^{III}B^{V}$ semiconductors plays a crucial role in the formation of nanostructures.

REFERENCES

[1] *Nanotechnology Research Directions: Vision for Nanotechnology in the Next Decade* Ed. by M. C. Roco, S. Williams, and P. Alivisatos (Kluwer, Boston, 2000; Mir, Moscow, (2002).

[2] T. Seidel, A. Londergan, and L. Winkler, Solid State Technol. **5**, 67 (2003).

[3] V. B. Aleskovskioe, Vestn. Akad. Nauk SSSR **6**, 52 (1975).

[4] J. Gelatos, L. Chen, H. Chung, and R. Thakur, Solid State Technol. **2**, 44 (2003).

[5] Yu. K. Ezhovskii, A. L. Egorov. Neorg. Mater. **42** (4), 421 (2006) [Inorg. Mater **42** (4), 368 (2006)].

[6] L. Egorov, Yu. K. Ezhovskioe, and P. V. Rogovskioe, Zh. Prikl. Khim. (St. Petersburg) **57**, 2126 (1984).

[7] R. Azzam and N. Bashara, *Ellipsometry Polarized Light* (North-Holland, Amsterdam, 1977; Mir, Moscow, 1981).

[8] V. K. Gromov, *Introduction to the Ellipsometry* (Leningrad State University, Leningrad, 1986) [in Russian].

[9] D. A. Holms, Appl. Opt. **6**, 168 (1967).

[10] V. I. Nefedov and V. T. Cherepin, *Physical Methods for Investigating Surfaces of Solids* (Nauka, Moscow, 1983) [in Russian].

[11] V. I. Nefedov, *X-Ray Photoelectron Spectroscopy of Chemical Compounds* (Khimiya, Moscow, 1984) [in Russian].

[12] *Handbook of X-Ray Photoelectron Spectroscopy* (Perkin-Elmer, Edom Prairie, Minnesota, 1978).

[13] J. Lindau, P. Chye, and P. Pianettu, J. Vac. Sci. Technol. **5**, 1332 (1978).

[14] E. H. Nicollian and A. K. Sinha, in *Thin Films: Interdiffusion and Reactions*, Ed. by J. Poate, K. Tu, and J. Mayer (Wiley, New York, 1978; Mir, Moscow, 1982).

[15] S. M. Sze, *Physics of Semiconductor Devices* (Mir, Moscow, 1972; Wiley, New York, 1981).

[16] E. H. Roderick, *Metal–Semiconductor Contacts* (Clarendon, Oxford, 1978; Radio i Svyaz', Moscow, 1982).
[17] V. Lyashenko, Yu. A. Tarantov, and A. P. Baraban, Poverkhnost, No. 7, 74 (1982).
[18] R. Hill, Philos. Mag. **23**, 59 (1971).
[19] P. Alekhin, S. V. Belotelov, and A. V. Emel'yanov, *Elektron. Tekh*., Ser. 3: Mikroélektron., No. 1 (52), 32 (1988).

Smart Nanocomposites
Volume 6, Number 2
ISSN: 1949-4823

STUDY OF THE DEPOSITION PROCESS OF VINPOCETINE ON THE SURFACE OF POROUS SILICON

Yu. A. Polkovnikova*, P. V. Seredin, A. S. Lenshin, and A. V. Prochorova
Voronezh State University, Russia

ABSTRACT

Currently the most prospective way in pharmacotherapy is the obtaining of nanoparticles involving pharmaceutical substances. Application of porous inorganic materials on the basis of silicon is among the main tendencies in solving of this problem. The present work is concerned with the problem of the deposition of pharmaceutical drug with nootropic activity – vinpocetine – into porous silicon. Silicon nanoparticles were obtained by electrochemical anodic etching of Si plates. The process of vinpocetine deposition was studied in a dependence of the deposition time. As a result of the investigations it was found that infrared transmission spectra of porous silicon with the deposited vinpocetine revealed the absorption bands characteristic of vinpocetine substance.

Keywords: nanoparticles, porous silicon, vinpocetine

1. INTRODUCTION

At present the idea concerned with the use of nanostructured containers for the targeted delivery of pharmaceutical drugs is of a great interest among the experts in the field of medicine and pharmacy. The reason of this is due not only to the successes in development of the new nanomaterials but rather low efficiency of the routine ways of the drug's introduction [1]. It is well-known that only a small part of the introduced pharmaceutical drug gets directly into a nidus [2]. Moreover, pharmaceutical drugs, as a rule, cause drug side effects. Therefore, their dosage is strictly limited. A prospective tendency in solving of these problems is the use of porous inorganic materials on the basis of silicon.

Quite simple technology of production, large surface area and adjustable pores diameter in mesoporous Si make its use rather appealing for the targeted drug delivery. Si-encapsulated

* E-mail: juli-polk@mail.ru

pharmaceutical preparation avoids physico-chemical impacts and it can be released in a controllable manner. Porous containers can be used for the payload of both hydrophilic and hydrophobic molecules [1, 3].

Recently Si nanoparticles have been more and more applied in therapy of the nervous system diseases [4].

An important role in complex therapy of the chronic cerebral circulatory disorder is concerned with the drugs improving cerebral circulation. One of the most widely applied medications is vinpocetine [5, 6].

Vinpocetine has been shown to improve cerebral circulation and metabolism in the treatment of various types of cerebrovascular circulatory disorder, e.g., cerebral infarction, cerebral hemorrhage residual and cerebral arteries cirrhosis, etc. Due to its poor aqueous solubility and extensively metabolized during the first pass, its clinical use is greatly restricted by the low bioavailability after oral administration and so there is a need to improve its poor aqueous solubility to increase the oral bioavailability. An oral formulation with a high degree of oral absorption would, therefore, be highly desirable [7].

The purpose of this work was the study of sorption process of vinpocetine onto porous silicon in a dependence on the deposition time.

2. EXPERIMENTAL SETUP AND SAMPLES

In the experiments vinpocetine (Figure 1) was used as an active pharmaceutical substance and additives registered for medical use and corresponding to the requirements of normative documents.

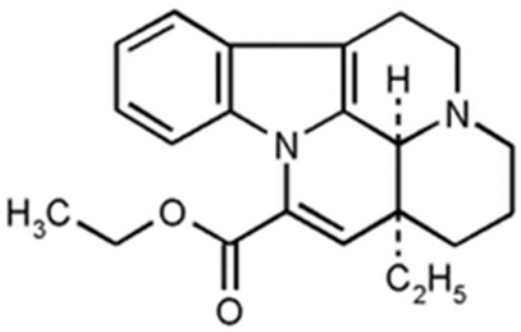

Figure 1. Structural formula of vinpocetine.

Mesoporous silicon with a transverse pores size of 5 to 25 nm and high enough porosity (>50%) proves to be most suitable for the use as biocompatible container materials for the pharmaceutical drugs delivery. Such size of the pores makes it possible to hold large organic molecules while the large specific surface area and the possibility to provide this material as hydrophobic as hydrophilic properties support its high adsorption capacity and the ability of selective adsorption.

Porous silicon samples were obtained by electrochemical anodic etching of silicon plates with n-type conductivity KEF (100) with the use of hydrofluoric acid, isopropyl alcohol and

hydrogen peroxide according to the technique described in [9]. Scanning electron images of the samples cleavages were obtained with the scanning electron microscope produced by JEOL Company – JSM 6380LV.

Infrared Fourier spectroscopy was applied for the study of chemical bonds in PSi nanoparticles at the different stages of the process of their fabrication within the wavelength range of 500- 4000 cm^{-1}.

Deposition of vinpocetine on the surface of porous silicon was performed from a solution prepared by solving of 0,005 g of vinpocetine in 1 ml of distilled water for 20 and 60 minutes.

3. EXPERIMENTAL RESULTS

The observed SEM images of the cleavage and surface of porous silicon are presented in Figure 2.

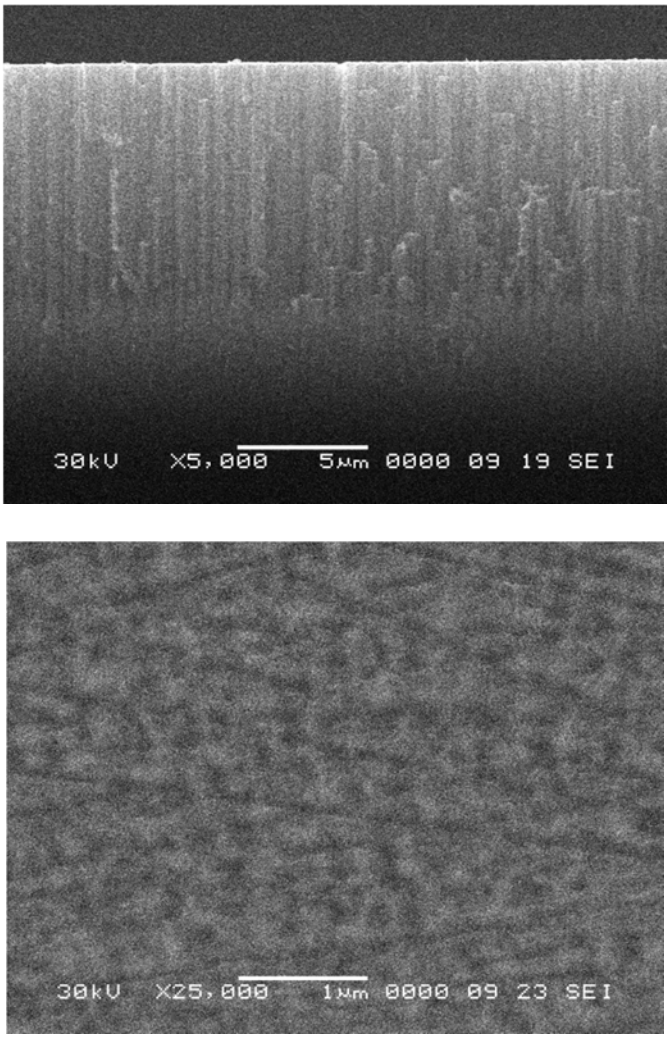

Figure 2. SEM image of the cleavage and surface of porous silicon.

Maximum size of pores in porous silicon did not exceed 100-150 nm, specific surface area of the samples was of 250 m^2/g (Figure 2).

The presence of vinpocetine was identified by the degree of coincidence and characteristic frequencies of the functional groups in the investigated substances according to the reference data [8], that are partially given in Table 1.

Table 1. Assignment of characteristic frequencies of absorption in IR spectra to the functional groups

Functional group (structural fragment)	Wavenumbers, cm^{-1}	Notes
Carbonyl group -C = O	1700–1680 1800–1680	Strong, as a part of carboxylic group
Amides	3500–3200; 830–850 3450–3310 и 1650–1550 1780; 1380; 830	Primary amide, double band Secondary amide Characteristic shape of the peaks
Carboxylic acids	1650–1550; 1440–1335; 770–400; 1690	

IR transmission spectra of porous silicon with the deposited vinpocetine in a dependence on the deposition time are presented in **Figure** 3.

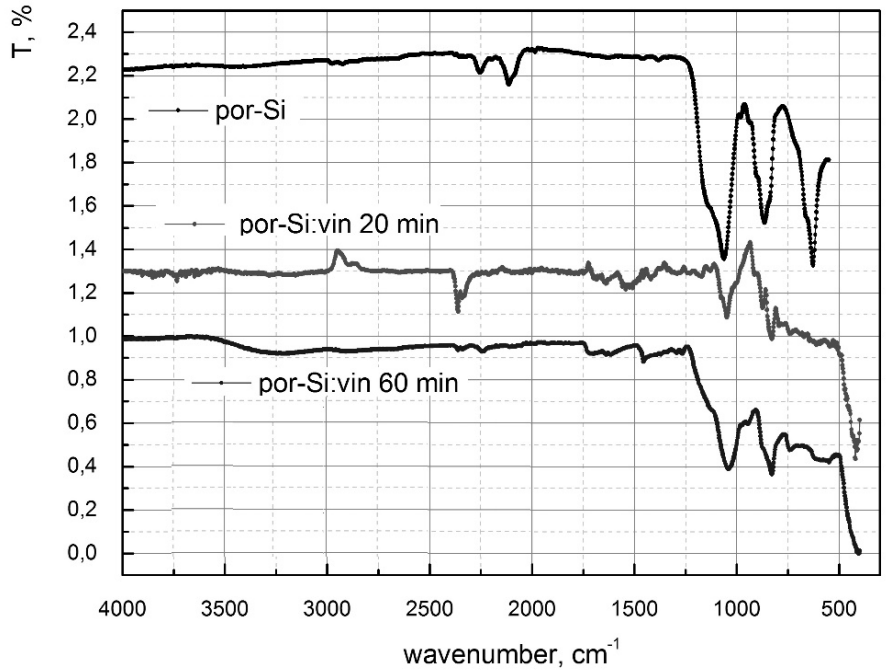

Figure 3. IR transmission spectra of porous silicon with deposited vinpocetine in a dependence of the deposition time.

Analysis of the obtained data indicated at the increase of vinpocetine concentration on the deposition time that was observed as an increase of intensity of the absorption peaks related to vinpocetine. No chemical bonds between silicon and vinpocetine molecules were detected. Porous silicon composition did not considerably change as compared with the original samples. It means that physical adsorption of the drug preparation on porous silicon is a prevailing process in the investigated system.

CONCLUSION

The feasibility of pSi as vinpocetine delivery device was investigated in this study. The device was fabricated by electrochemical etching of silicon wafer, resulting in porous microparticles, which were further stabilized by thermal oxidation.Overall, pSi nanoparticles present optimal vinpocetine delivery capabilities and together with its intrinsic optical properties and biocompatibility have the potential to be used as wearable devices for point of care.

REFERENCES

[1] Ksenofontova O. I., Vasin A. V., Egorov V. V. et al. Porous silicon and its applications in biology and medicine//*Technical Physics*. 2014. Vol. 84, №. 1. P. 67–78.

[2] Tao S. L., Desai T. A. Micromachined devices: The impact of controlled geometry from cell-targeting to bioavailability//*J. Control Release*. 2006. № 109. P. 127-138.

[3] Lenshin A. S., Kashkarov V. M, Seredin P. V. et al./The optical characteristics of the various structures of porous silicon//*Technical Physics*. 2014. Vol.84, № 2. P. 70-75.

[4] Shin J. A., Jeong S. I., Kim M. S. et al. Visceral adipose tissue inflammation is associated with age-related brain changes and ischemic brain damage in aged mice//*Brain Behav Immun*. 2015.№ 8. 456-465.

[5] Torres K. J., Göttle P., Kremer D. et al. Vinpocetine Inhibits Oligodendroglial Precursor Cell Differentiation//*Cell Physiol Biochem* 2012. Vol. 30. P. 711-22.

[6] Ogunrin A. Effect of vinpocetine (cognitol™) on cognitive performances of a nigerian population. *Ann Med Health Sci Res*. 2014. № 4. P. 654-61.

[7] Szakács T., Veres Z., Vereczkey L. In vitro –in vivo correlation of the pharmacokinetics of vinpocetine//*Pol. J. Pharmacol*. 2001. № 53. P. 623–628.

[8] "Spectral Database for Organic Compounds, SDBS." URL: http://sdbs.db.aist.go.jp/ sdbs/cgi-bin/direct_frame_top.cgi.

Smart Nanocomposites
Volume 6, Number 2
ISSN: 1949-4823

RELAXATION PHENOMENA IN $Bi_{12}SiO_{20}$ SINGLE CRYSTAL

M. P. Sevryugina[1], N. S. Pshchelko[1,*], and V. A. Moshnikov[2]
[1]National University of Mineral Resources "The University of Mines,"
St. Petersburg, Russia
[2]Saint-Petersburg State Electrotechnical University, St. Petersburg, Russia

ABSTRACT

Charge transfer in $Bi_{12}SiO_{20}$ structures is investigated. Electric current dependences on time at temperature of 300 K in the dc electric field strength of the $2 \cdot 10^5 - 10^6$ V/m range are measured. Flowing of relaxation polarizing current is shown to result in charge accumulation in the sample surface area. Experimental regularities coordinate with provisions of the relay mechanism of transfer of a charge with the participation of deep local levels.

Keywords: electric field, charge transfer, charge accumulation, conductivity, polarization, local states

INTRODUCTION

Sillenite possess electrooptical and magnetooptical properties that in combination with photoconductivity puts them forward in number of perspective materials for creation electro - and the magnetooptical modulators of laser radiation, memory units and other devices. Keen interest to these chemical compounds is caused by their use in instrument making, first of all, in devices of spatial temporary modulation of light as an active element, and also in the electrician and the electronic engineering. Thanks to similarity of electronic structure of all undoped sillenite, it is possible to state that they are materials with the wide energy gap, high specific resistance and low mobility of charge carriers.

Further improvement of devices operating quality based of materials with a sillenite structure is connected with need of obtaining information about the probable defective structure defining distribution of energy levels in the semiconductor energy gap. The specified data can be received, in particular, by studying of the mechanism of conductivity and currents of polarization kinetics in crystals of BSO doped by various impurities. Charge

* nikolsp@mail.ru

relaxation in semiconductor bulk can be assumed as one of the factors that determine the stability of characteristics of electronic elements The investigation of temporal dependence of the currents of isothermal relaxation makes it possible to acquire information on the population kinetics of capture centers arranged nonuniformly over the semiconductor thickness as well as on the capture processes in near-electrode regions [1, 2]. In the following, the results of the study of the polarization relaxation in photoconductive $Bi_{12}SiO_{20}$ single crystals are presented.

EXPERIMENTAL

Kinetic dependences of polarization currents were measured for the $Bi_{12}SiO_{20}$ single crystals. Currents of isothermal polarization were detected using a Keithley 6517A electrometric amplifier. The electric field strength was varied in the range $E = 2 \times 10^5$–10^6 V/m. The furnace was dc-supplied by a stabilized current source. Conductivity measurements in the frequencies range of $f = 10^3 \ldots 10^5$ Hz of the measuring field were performed when using the precision immitance measuring instrument E7-20 at the room temperature.

RESULTS AND DISCUSSION

Figure 1 shows the results of the study of the kinetics of isothermal polarization currents in $Bi_{12}SiO_{20}$ single crystal measured for different electric fields.

The shape of the polarization relaxation curves for $Bi_{12}SiO_{20}$ indicates that there are two phases of the process (fast and slow) corresponding to time intervals Δt_1 =1–20 s and Δt_2 = 20–200 s.

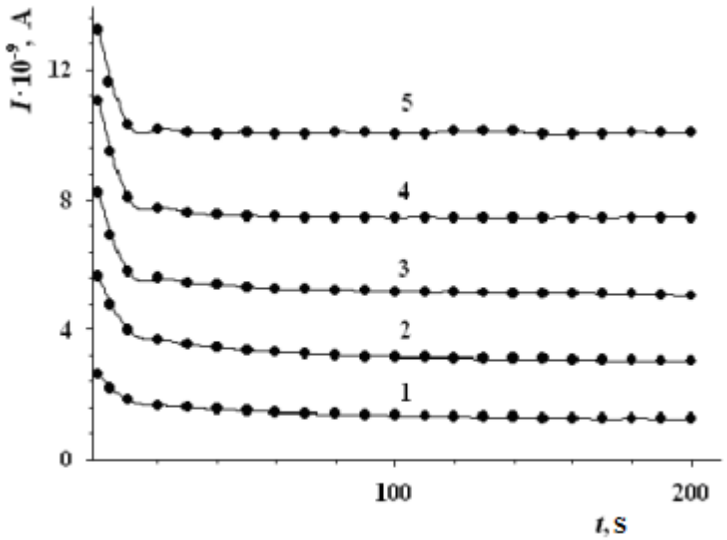

Figure 1. Kinetics of the polarization current measured for $Bi_{12}SiO_{20}$ single crystals at electric fields 1 - $2 \cdot 10^5$, 2 - $4 \cdot 10^5$, 3 - $6 \cdot 10^5$, 4 - $8 \cdot 10^5$, 5 - 10^6 V/m. T = 300 K.

At the initial stage after switching the voltage on, rapid current decay is observed in $Bi_{12}SiO_{20}$ single crystals, obeying the empirical Curie–von Schweidler relation $I \sim t^{-n}$ ($n = 0.8$). A slow polarization kinetics component corresponds to the exponential dependence. As the voltage increases, the temporal range of the initial portion of the kinetics of the polarization current decreases, while the decay rate of function $I(t)$ increases.

The data on the kinetics of the isothermal relaxation currents was interpreted within a model according to which the transfer of an electric charge injected into a crystal occurs through the relay-race mechanism [2, 3, 4, 5]. The charge transfer from the contact into the sample occurs through the mechanism of hopping conduction over the trap centers, which are located in the band gap and have deep trapping levels of free charge carriers. This process is also accompanied by the formation of an energy barrier at the boundary with the anode, which hinders the transfer of electrons (injected from the cathode) to the anode. The energy barrier at the boundary with the anode arises from the energy difference between the electron affinity for the local center and the work function of the anode metal. Thus, the electric current is limited by both the space charge in the bulk of the semiconductor and the energy barrier at the boundary with the anode, which leads to a redistribution of the voltage across the crystal and decrease of electric current passing through the crystal.

The current relaxation decay observed for the structure is accompanied by the accumulation of charge whose value can be determined from the area lying under the curve of the time dependence of the current. In Figure 2, the values of this charge are plotted as functions of the applied electric field. We can notice that in low electric fields, the accumulated charge increases to a first approximation by the quadratic law, while with the further increase, the polarization varies according to linear dependence.

As follows from the theory developed in [4], the electric current passing through the system and the accumulated charge are related by the expression

$$Q = C_c U - \sqrt{\frac{C_c L^3 I}{\mu_{eff} d_c}} \tag{1}$$

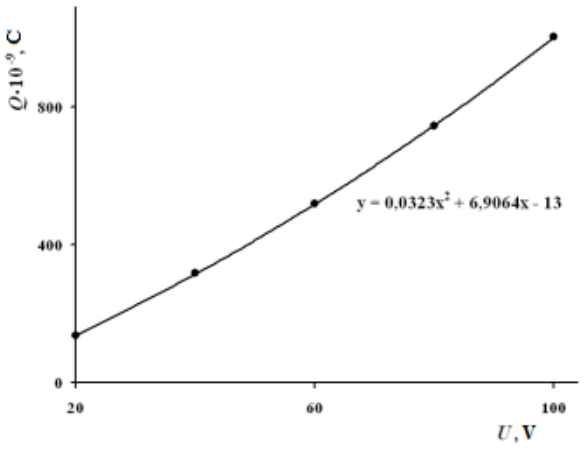

Figure 2. Charge accumulated in $Bi_{12}SiO_{20}$ single crystals and measured as a function of the electric field U. $T = 300$ K.

It can be seen from expression (1) that, at each instant of time, the accumulated charge is proportional to the square root of the current flowing through the system. Relationship (1) holds for the voltages and times corresponding to the descending branches of the relaxation characteristics. It is worth noting that the lower the voltage and the shorter the time, the better the fit of relationship (1) to the experimental data.

In Figure 3. frequency dependence of conductivity σ is given at low frequencies (f) for a sample of a BSO:Ge single crystal which corresponds to a function of $\sigma(f) \sim f^s$. The obtained curve is character zed by two consecutive parts corresponding to frequencies range of 10^3 – $2 \cdot 10^4$ Hz, where s = 0.98 and to an interval of f = $2 \cdot 10^4$ … 10^5 Hz, where s = 1.4. The frequency dependence of conductivity σ at high frequencies given in Figure 3, is characteristic for hopping.

According to conclusions made in [6] the obtained dependences (with the value of s close to 1 ($1 < s < 2$) correspond to jumps on local states with casual dispersion both on crystal volume and on local states energy, in this way the value of s - indicator can change from 0 to 2 depending on spatial and energy distribution of local levels radius of localization, wave function of the carrier localized on defective and impurity states. It is also various at different multiplicity, that is number of links in a chain of jumps [7].

At the impurity doping of the studied single crystals, distortion of oxygen tetrahedrons of structure of BSO with formation of the oxygen vacancies capable to take an electron according to compensation condition is probable. Other option of a structure change in the considered chemical compound is bismuth replacement with the introduced germanium in the distorted octahedrons. Thus it is necessary to expect larger value of s for undoped crystals of BSO and, respectively, decrease in this case in multiplicity of jumps. Defects of crystals of BSO prove also in relaxation processes which existence can be connected with quasidipolar polarization. The crystal lattice of BSO is high-polarizable and the deep centers of strong localization can interact with it.

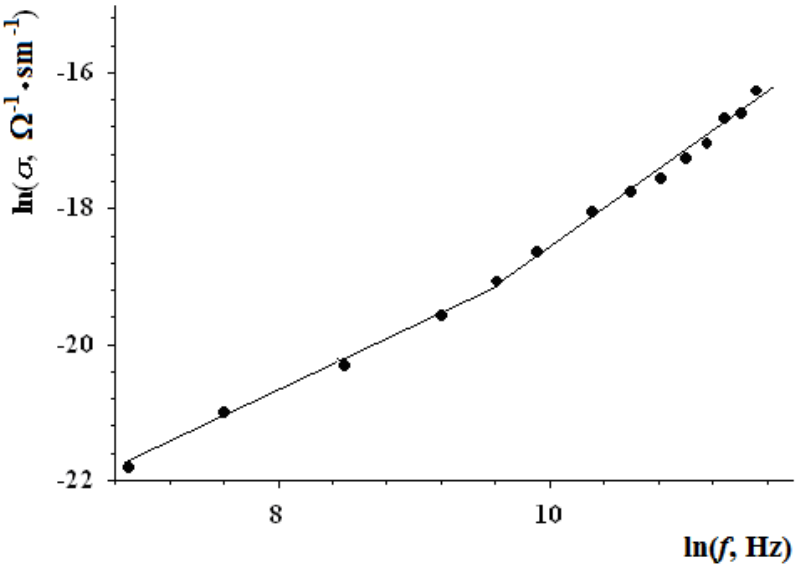

Figure 3. Frequency dependence of ac-conductivity for $Bi_{12}SiO_{20}$ single crystals. T = 300 K.

The real component of the hopping nature electrical migration conductivity corresponds to the expression [7]:

$$\sigma_{ac}(f) = (\pi^3 / 96) \cdot e^2 kTN_F^2 a^5 f[\ln(\nu_{ph} / f)]^4, \tag{2}$$

where e - electron charge, k - Boltzmann constant, T - absolute temperature, N_F - density of localized states near the Fermi level, α - decay constant of the wave function, the inverse radius of the largest localization, ν_{ph} - phonon frequency, assumed equal to 1012 Hz.

According to the theory of hopping the average length of carriers jumps is defined as

$$R = \frac{1}{2\alpha} \ln\left(\frac{\nu_{ph}}{f}\right). \tag{3}$$

Localized states, used for charge carriers jumps, are randomly distributed in the bulk and separated by an energy barrier. The observed experimental dependence $\sigma \sim f^{0.98}$ may be associated with transitions of charge carriers tunnel and classic jumping over barriers. Parameter s allows to estimate also a difference in energy values between the main minimum energy state and a free state when the carrier can move over a crystal

$$W_m = \frac{6\ kT}{1 - s}. \tag{4}$$

The calculations executed by a formula (3) result to W_m = 7,6 eV in BSO:Ge single crystal. The obtained W_m value and the value of dielectric permeability of the studied doped single crystal of a sillenit structure in the range of frequencies where the law of $\sim f^{0.98}$ takes place, allow to determine the Bohr radius of the localized charge carrier:

$$r = \frac{e^2}{2\ \varepsilon\varepsilon_0 W_m}. \tag{5}$$

The value of the localization radius, defined by the formula (4), is r = 0,6 Å.

Calculation using formulas (1) and (2) leads to values of the density of localized states near the Fermi level $N_F = 3{,}9 \cdot 10^{20}$ $eV^{-1} \cdot cm^{-3}$ and the average distance of jumps R = 5,5 Å.

At known average distance of jumps of charge carriers it is possible to determine the average time of jumps:

$$\tau^{-1} = \nu_{ph} \cdot \exp(-2\alpha R) \tag{6}$$

In Figure 4 a direct current temperature dependence of conductivity of a single crystal BSO:Ge sample is presented. The obtained experimental results demonstrate that the considered characteristic corresponds to exponential function of temperature which is well approximated by a formula:

$$\sigma = \sigma_o \exp\left(-\frac{E_a}{kT}\right), \tag{7}$$

where E_a represents the energy of activation.

According to expression (5) it is possible to allocate two consecutive temperature sites with various values of energy of activation of E_a = 0,07 eV (T < 340 K) and E_a = 0,12 eV (T > 340 K) which correspond to various length of clusters of local states near a valence zone. Changing of the conductivity mechanism is the reason of the specified behavior of experimental curves.

At low temperatures probably leaping of charge carriers from one defective knot on another is realized. Above T = 340 K increase in current of conductivity can be caused by change of mobility and concentration of carriers. Generally transfer on local states near Fermi's level can be expressed by dependence [8]

$$\sigma(T) \sim T^{l}, \tag{8}$$

where l is the constant depending on character of jumps.

For single jumps between the neighbouring states (pair model) l ~ 0, while for jumps on chains of states (multiplet jumps) – l ~ (i – 1), where characteristic i is the average number of jumps in a chain.

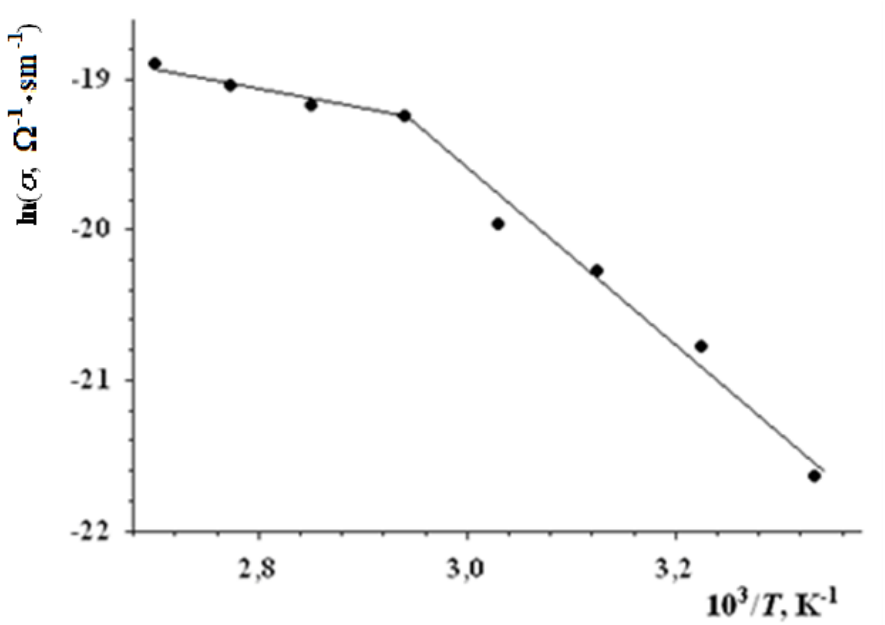

Figure 4. Temperature dependence of ac-conductivity for $Bi_{12}SiO_{20}$ single crystals. U = 50 V.

CONCLUSION

Thus, for the studied BSO single crystals with Germany impurity it was revealed that in all studied interval of temperatures multiplet jumps of charge carriers with i =7 takes place (T < 340 K) and i = 2 (T > 340 K). The behavior of main characteristics of the charge transfer processes occurring in $Bi_{12}SiO_{20}$ single crystals are in agreement with the theory of the relay mechanism of charge transport under the conditions of nonuniform distribution of local centers in metal–(high-resistivity semiconductor)–metal structures. The results of $Bi_{12}SiO_{20}$:Ge single crystals conductivity research found out in this work are well coordinated with the data obtained earlier for the crystals of similar structure doped by various impurities (Rh, Re, Ru, Os, etc. [9]). That allows to make a conclusion about nature of charge carriers transfer in the studied structure connected with multiplet jumps between the localized states in the conditions of casual distribution of energy barriers.

REFERENCES

[1] Mustafayeva S. N., Hasanov A. I. 2004 *Physics of the Solid State* 46 (11) 1937.
[2] Sevrugina M. P., Pshchelko N. S. Kadi Ya. S. 2015. *Journal of Physics: Conference Series* 586 1.
[3] Timan B. L. 1973 *Semiconductors* 7 (2) 225.
[4] Timan B. L. 1973 *Semiconductors* 7 (2) 230.
[5] Avanesyan V. T., Bordovskii V. A., Potachev S. A. 2002 *J. Non-Cryst. Solids* 305 136 [6] Pollak M. 1971 *Phylos. Magazinen* 23 519.
[6] Panchenko T. V., Karpova L. M., Duda V. M., 2000 Physics of the Solid State 42 (4) 671
[7] Kudzin A. Yu., Plyaka S. N., Sokolyansky G. H. 2000 *Physics of the Solid State* 42 (5) 839.
[8] Milenov T. I., Veleva M. N., Petrova D. P., Gospodinov M. M. 2005 *Inorganic Materials* 41 (2) 152.

Smart Nanocomposites
Volume 6, Number 2
ISSN: 1949-4823

ATOMIC-FORCE MONITORING OF POTENTIAL RELIEF ON THE VO_2 NANOCRYSTAL THIN FILM

A. V. Il'inskiy[1], V. A. Moshnikov[2,3], M. E. Pashkevich[3], N. V. Permyakov[2], and E. B. Shadrin[1,*]

[1]Ioffe Physical Technical Institute, Russian Academy of Sciences, St. Petersburg, Russia
[2]St. Petersburg Electrotechnical University LETI, St. Petersburg, Russia
[3]St. Petersburg State Polytechnical University, St. Petersburg, Russia

ABSTRACT

The structure that is formed on the surface of VO_2- nanocrystal thin film using electron-beam irradiation at energies (5–8 keV) is formed with the purpose of its optical microscopic, optical diffraction, and atomic force investigations. The electron beam was used to change the of the metal-semiconductor phase transition temperature, and creation of a jump of reflectance of the thin film by phase transition. The physical principle of such a change is based on the donor properties of the broken off σ-bonds that result from variations in the structure of the oxygen octahedron under electron-beam irradiation.

Keywords: phase transition, vanadium dioxide, strong correlation

INTRODUCTION

Recent interest in the methods for control of parameters of vanadium-oxide nanocrystal thin film has been driven by the application of such materials in ultrafast devices (e.g., microwave visalisators and limiters of high-power femtosecond optical radiation) with almost instantaneous electronic semiconductor-metall phase transition (SMPT). The control procedure can be implemented with the purposes of doping of nanocrystal thin film with transition elements [1, 2], hydrogenisation [3], introduction of controlled nonstoichiometry by synthesis [1, 4], influence of ultrahigh (gigapascal) pressure [5], laser annealing [6], etc. Ions-beam irradiation is among the most efficient methods for control of SMPT-parameters [7]. The purpose of this work is a detailed study of the macro- and microtransformation of the physical parameters of SMPT in nanocrystal vanadium-oxide thin film under electron-beam irradiation at energies of 5–8 keV and a current density of 200 μ C/cm2 s.

* E-mail: shadr@mail.ioffe.ru.

SAMPLES AND EXPERIMENTAL PROCEDURE

The samples for study represent vanadium-oxide nanocrystal thin film that are synthesized as thin film Fabry–Perot interferometers with sizes of 2 × 2 c and a VO_2-working element (polycrystalline VO_2 film with a thickness of 80 nm) that is placed between mirrors. An aluminum sublayer with a thickness of 50 nm and the outer surface of the film play a role of the mirrors of interferometer. Such structure enables to employ the interference method for contrast enhancement of the image that is formed by electron beam on the front surface of the interferometer.

In general, the recording of electron beam images on the surface of film samples that is implemented in this work can be performed by an electron beam influence that is raster scanned and modulated by a video signal. For the readout of image, we can use the reflected optical beams with different spectral compositions. In this work, the target represents a thin film vanadium oxide interferometer evacuated to a pressure of 10^{-5} Torr at room temperature, which is lower than the temperature of structural PT (67° C). In the course of recording of a test image, the electron beam irradiation is performed using a broad electron beam with a beam energy of 7 keV through a metal grid with square cells of 65 × 65 μm and a wire width of 35 μm that is pressed to the sample. Such a relatively simple procedure allows to make a high contrast and high resolution recording and with various of the diffraction efficiency of the recorded diffraction grating. It is convenient that the recorded image remains unchanged over a relatively long time interval (several months) at room temperature and atmospheric pressure, so that conventional experimental methods can be used. The reflection spectra of electron beam irradiated regions and original regions of thin film interferometer in the spectral interval 400–1000 nm give systems of interference peaks whose spectral positions depend on the irradiation dose and sample temperature. In additives to this the radiation of He–Ne and Ar lasers is used for the Raman spectroscopy of irradiated and unirradiated thin film samples. The spectroscopic study is aimed at identification of structural changes in the nanocrystallites of the VO2 film related to the SMPT.

EXPERIMENTAL RESULTS

Figure 1 shows the profile of the metal grid that is obtained on the irradiated sample. Variations in the spectral positions of the reflection maxima of the Fabry–Perot interferometer upon electron beam irradiation in comparison to the peak positions of unirradiated regions that are hidden under wires of the grid lead to the changes of interference color of the surface of irradiated regions and the formation of the color contrast image of the grid.. The maximum irradiation dose (200 μC/cm^2) leads to the shift of the loop by 25°C toward lower temperatures and a simultaneous decrease (virtually to zero) of the jump of reflectance at the SMPT point. The resulting reflection coefficient of the film becomes close to the reflection coefficient of by heating metallized samples.

An increase in the irradiation dose leads to the blue shift by 62–70 nm toward the position that is typical of the thermally metallized sample. The Raman spectra of the vanadium oxide nanocrystal thin film are substantially modified due to electron irradiation. In particular, the Raman spectrum that is typical of monoclinic VO_2 is observed at low and phonon bands are overlapped by the broad Raman band typical of the tetragonal phase. At the

maximum irradiation, the Raman spectrum remains qualitatively unchanged but the shape of the broad band is slightly modified and the band is blue shifted by 20–30 cm^{-1} in accordance with the thermal transformation of the Raman spectra in [7] except for the fact that the shift is greater than the shift induced by the heating of the sample to 100°C. The optical color contrast image of the metal grid that serves as a transparency upon electron beam irradiation exhibits relatively high (submicron) resolution medium doses. However, we also observe an increasing broad band that is centered at 450 cm^{-1} and serves as a pedestal for narrow phonon bands of monoclinic phase. This result corresponds to the thermal transformation of the Raman spectra [8] and the evolution of spectra with an increase in the irradiation dose: narrow phonon bands are overlapped by the broad Raman band typical of the tetragonal phase. At the maximum irradiation, the Raman spectrum remains qualitatively unchanged but the shape of the broad band is slightly modified and the band is blue shifted by 20–30 cm^{-1} in accordance with the thermal transformation of the Raman spectra in [7] except for the fact that the shift is greater than the shift induced by the heating of the sample to 100°C. The optical color contrast image of the metal grid that serves as a transparency upon electron beam irradiation exhibits relatively high (submicron) resolution (Figure 1).

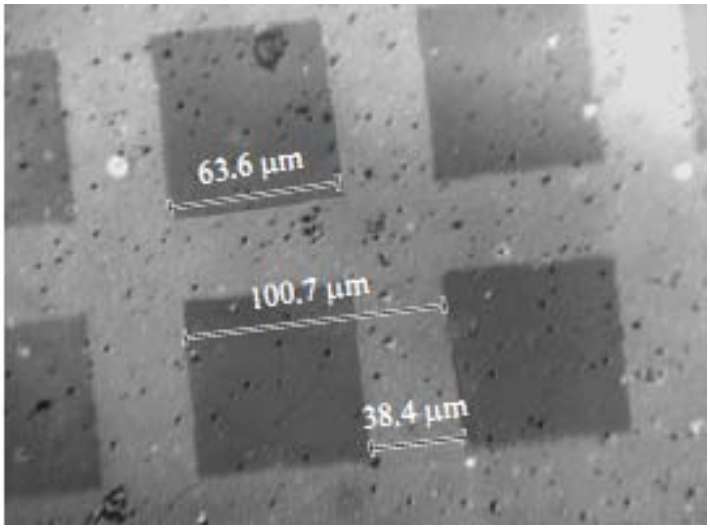

Figure 1. Image of the VO_2 film surface in reflected light after electron beam irradiation through the metal grid with a period of 100 μm. The image is obtained due to the difference of refractive indices in irradiated (squares of 65 ×65 μm) and unirradiated regions.

To additionally prove relatively high resolution of the vanadium oxide composites that serve as electron beam targets, we experimentally study the diffraction of the laser radiation with a wavelength of 532 nm by the 2D periodic structure that is recorded by electron beam. High intensity diffraction peaks of higher orders (up to sixths) indicate the presence of higher Fourier components in the spatial spectrum of the recorded image. The diffraction angles correspond to a spatial period of 200 nm that can be considered as the resolution of the synthesized electronic resist. The experimental results also show that an increase in the irradiation dose or temperature leads to the intensity redistribution over diffraction orders. Such a transformation related to irradiation or heating results from variations in the refractive

index and, hence, phase shifts of the optical radiation reflected from the irradiated and unirradiated regions. The intensity distribution over the diffraction orders can be estimated using the relationship that is obtained in the framework of the scalar diffraction theory. Here, η_n is the diffraction efficiency of the grating in the nth diffraction order; β is the filling coefficient of the diffraction element that is equal to the ratio of the wire width to the grating period; R1 and R2 are the reflection coefficients of the nanocrystal thin film under wire and in the grid cell, respectively; and $\Delta\varphi$ is the phase difference for the optical oscillations reflected from these regions. The facilities of the Ntergra Therma nanolaboratory are used in the comparative study of the conductivities of the neighboring irradiated and unirradiated fragments. The results make it possible to characterize the profile and the distribution of electric properties over the surface of nanocrystal thin film on which the periodic structure is recorded by electron beam. We study the samples using the spreading resistance method, Kelvin probe microscopy, and capacitance microscopy [9].

Figure 2 presents the image of a fragment with a size of 100 × 100 μm in the regime of the Kelvin probe microscopy in which the two pass mode makes it possible to form a signal that corresponds to the surface potential distribution (the right hand panel in Figure 2). The left hand panel demonstrates the profilometry data. The analysis of the images yields the absence of difference between the heights in the irradiated and unirradiated regions, whereas a significant potential difference between the irradiated and unirradiated regions corresponds to the difference of conductivities in the presence of voltage across the sample. We conclude that the electron beam irradiated square fragments exhibit higher conductivity and the potential profile is formed in spite of the topographical homogeneity of the film.

Figure 3 presents the axonometric images of the potential relief of the same fragment of the VO_2 film at a temperature of 20°C that is lower than the temperature of the structural PT in the film grains and a relatively high temperature of 100°C that is significantly higher than the temperature of the structural PT to the monoclinic phase. It is seen that an increase in the temperature to 100°C leads to a significant decrease in the contrast of the spatial distribution of the surface potential. At the high temperature irradiated and unirradiated fragments consist of metal phase grains with different degrees of metallicity.

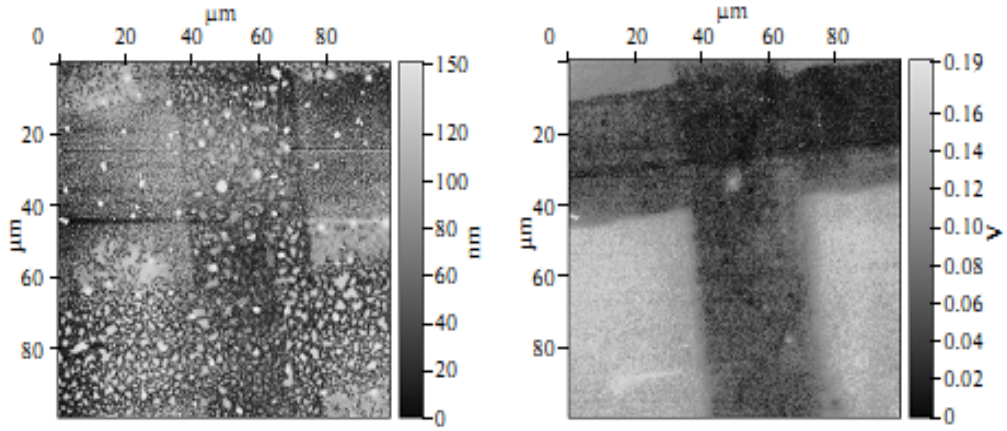

Figure 2. AFM images of a fragment of the VO_2 film that is irradiated by electron beam at a medium energy: (left hand panel) topography and (right hand panel) surface potential distribution.

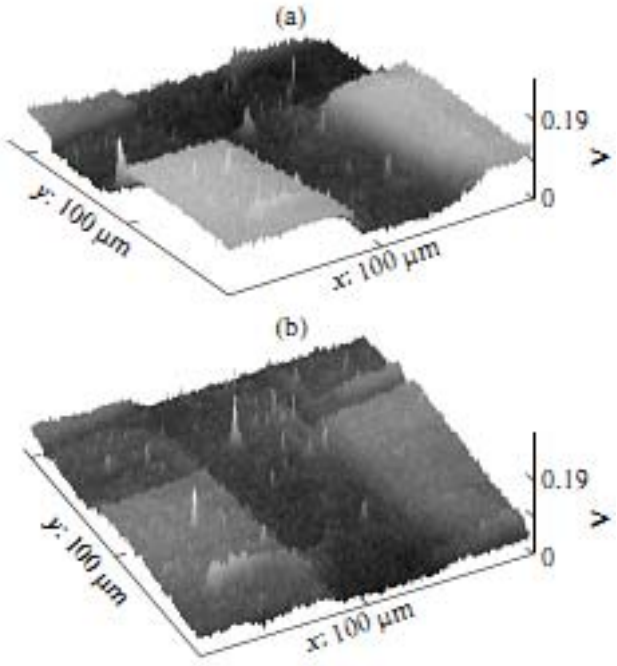

Figure 3. 3D surface potential distribution at temperatures of (a) 20 and (b) 100°C.

DISCUSSION

Variations in the PT parameters due to an increase in the electron beam irradiation dose are similar to variations related to the hydrogenation of the VO_2 film [10, 11] and incomplete oxidation of the metal vanadium grains in the synthesis [4]. Variations in the PT parameters indicate a decrease in the band gap between 3d|| and π^* bands that is normally related to the formation of the donor type defects in VO_2 [1]. The reasons for such an effect and its characteristics can be analyzed using the following facts.

The X-ray data of [1] show that the crystalline lattice of the vanadium dioxide at $T > Tc$ exhibits tetragonal symmetry and contains vanadium ions V4+ located along the CR rutile axis. Each vanadium ion is located at the center of the oxygen octahedron. When the temperature decreases to a point that is lower than the PT temperature ($T < Tc$), the lattice symmetry decreases to the monoclinic symmetry owing to the formation of stable ion pairs V4+– V4+ in the above chains. Such dimmers lead to the period doubling of the crystalline lattice along the chain. The structural transition (Peierls transition) leads to the electronic spectrum with a gap between fully occupied and free Hubbard subbands [3]. Thus, vanadium dioxide becomes a Peierls semiconductor with the monoclinic lattice.

The exact solution that is possible for the 1D quantum mechanical problem of the calculation of electronic spectrum for the system under study yields a gap of 0.2–0.5 eV. However, the experiments of [12] show that the splitting of the d subbands is 2.5 eV. Thus, a π^* band must be placed between these subbands at a distance of 0.7 eV from the lower occupied Hubbard subband. In addition, such a significant difference between the experimental and calculated results must be interpreted.

The above facts make it possible to describe the thermally induced transition of the material from the tetragonal semiconductor phase to the monoclinic metal phase as the thermal destruction of dimers owing to the electron transition through a gap of 0.7 eV. However, simple estimations yield relatively low efficiency of the transition through a wide gap of 0.7 eV at a temperature of Tc = 340 K (67°C). Thus, such a process cannot lead to significant destruction of dimmers needed for the transition of the material to the metal phase.

To solve the problem, we must take into account the correlation interaction of electrons. In this case, (i) the Fermi distribution of electrons with extremely low tails of about 0.03 eV at a temperature of 340 K is transformed into the Migdal distribution [13] with tails of about 0.4 eV, (ii) the positions of energy bands depend on electron populations [14], and (iii) a correlation correction of about 2.0 eV is provided for the gap between the 3d Hubbard subbands. Indeed, even a simple model in which the V4+–V4+ dimmer is represented as a hydrogen molecule yields a gap of about 2.5 eV when the correlation interaction of electrons is taken into account. Thus, we interpret an additional increase in the gap between the subbands to 2.5 eV using the correlation interaction (i.e., the formation of a large band gap semiconductor in which the band gap consists of the Mott gap (2.0 eV) and the Peierls gap (0.5 eV)).

In the course of PT, the correlation effects in the heated sample lead to a decrease in a gap of 0.7 eV between the lower 3d subband and π* band owing to the correlation motion of bands determined by the thermal transition of electrons from the lower 3d subband to the π* band (Figure 4). This circumstance leads to a positive feedback between the band gap and populations: a decrease in the band gap provides an increase in the rate of the thermal generation of electrons to the π* band, which causes a decrease in the band gap.

Thus, the population of the π* band by electrons provided by the donor type defects leads to a decrease (due to correlation effects) in the band gap from 0.7 eV to a level that is determined by the donor concentration. Therefore, we obtain a decrease in the temperature of the thermal structural PT of the material from semiconductor phase to metal phase.

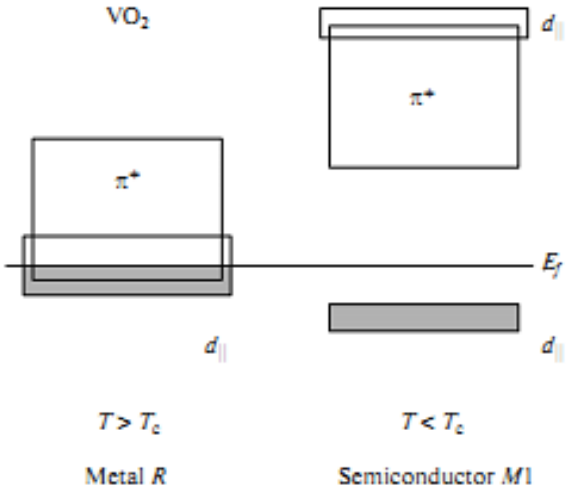

Figure 4. Bands of (a) high temperature metal and (b) low temperature semiconductor phases of vanadium dioxide.

We assume that the oxygen vacancies that are generated by electronbeam irradiation serve as donor defects. Indeed, the electron beam with a medium energy of 7 keV passes through the film with a thickness of 80 nm to the glassceramic substrate and generates secondary electrons with a solid energy spectrum in the interval 0–50 eV. The escape energy of the oxygen atom for the VO_2 lattice (several electronvolts) is close to the energy of the formation of oxygen vacancy in rutile (7.74 eV) [15]. Such an energy is available in the solid spectrum of secondary electrons. Thus, the beam of secondary electrons generates vacancies with donor properties. Donor electrons provide a decrease in the energy of the π^* band and, hence, a decrease in the temperature of the semiconductor–metal PT. A large decrease in the energy of the π^* band (by 0.7 eV) leads to the overlapping with the lower d|| Hubbard subband, so that the dielectric phase is transformed into the metal phase at room temperature.

The microscopic effect of the π^*-band saturationn with electrons is reduced to the transition of two electrons from the σ bonds of the oxygen octahedron that are broken when the oxygen atom is removed from the lattice. Indeed, each oxygen atom in the defect free lattice is bound with three oxygen–vanadium octahedra prior to the formation of vacancies. The oxygen atom in the 2S2(1)2P2(2) hybridization state donates 4/3 of the total electron density to each octahedron. The removal of a single oxygen atom and the formation of vacancy leads to the liberation of 2/3 of electron density from the σ bonds of each octahedron, which generally corresponds to two liberated electrons. In the absence of the oxygen atoms, the vanadium atoms of the neighboring octahedrons form a back donation donor-acceptor bond the strength of which is significantly less than the strength of a conventional σ bond [16]. The electrons of the back donation bond that is easily thermally broken at room temperature get into the conduction band (π^* band) and provide a decrease in its energy owing to the correlation interaction of electrons.

CONCLUSION

The electron beam irradiated VO_2 film exhibits the semiconductor–metal PT. Such a process leads to significant variations in the optical and electrophysical properties of the film, so that extremely high gradients of the refractive index (up to 0.5×10^6 m^{-1}) and conductivity (up to 10^9 S m^{-1}) can be formed on the film surface. This result is of practical importance for high capacity data recording and storage devices.

REFERENCES

[1] W. Bruckner, H. Opperman, W. Reichelt, E. I. Terukov, and F. A. Tschudnovskii, Vanadiumdioxide (Akamemie Verlag, Berlin, 1983).

[2] S. E. Nikitin, I. A. Khakhaev, F. A. Chudnovskii, and E. B. Shadrin, *Phys. Solid State* 35, 1393 (1993).

[3] V. Il'insky, O. E. Kvashenkina, and E. B. Shadrin, Semiconductors 45, 1153 (2011).

[4] R. A. Aliev and V. A. Klimov, *Phys. Solid State* 46, 532 (2004).

[5] T. Kikuzuki and M. Lippmaaa, *Appl. Phys. Lett*. 96, 132107 (2010); E. Arcangeletti, L. Baldassarre, D. Di Castro, S. Lupi, L. Malavasi, C. Marini, A. Perucchi, and P. Postorino, cond.mat.mtrl.sci/0611281v1 (2006).

[6] E. B. Shadrin, F. A. Chudnovskii, K. Sh. Tsibadze, and I. A. Khakhaev, *Tech. Phys*. 42, 403 (1997).
[7] V. Il'inskii, V. Yu. Davydov, R. A. Kastro, O. E. Kvashenkina, M. E. Pashkevich, and E. B. Shadrin, *Tech. Phys. Lett*. 39, 705 (2013).
[8] N. Goncharuk, A. V. Il'inskii, O. E. Kvashenkina, and E. B. Shadrin, Phys. Solid State 55, 164 (2013).
[9] O. A. Aleksandrova, P. A. Alekseev, I. E. Kononova, A. I. Maksimov, E. V. Maraeva, V. A. Moshnikov, E. N. Muratova, S. S. Nalimova, N. V. Permyakov, Yu. M. Spivak, and A. N. Titkov, Diagnostic of Materials by Methods of Scanning Probe Microscopy: Tutorial, Ed. by V. A. Moshnikov (SPbGETU LETI, St. Petersburg, 2012).
[10] E. B. Shadrin, D. A. Kurdyukov, A. V. Il'inskii, and V. G. Golubev, Semiconductors 43, 102 (2009).
[11] V. Il'inskii, O. E. Kvashenkina, and E. B. Shadrin, Semiconductors 45, 1163 (2011).
[12] S. Shin, S. Suga, M. Taniguchi, M. Fujisawa, H. Kanzaki, A. Fujimori, H. Daimon, Y. Ueda, K. Kosuge, and S. Kachi, *Phys. Rev*. B 41, 4993 (1990).
[13] V. V. Val'kov and D. M. Dzebisashvili, *Phys. Solid State* 51, 877 (2009).
[14] M. Gatti, F. Bruneval, V. Olevano, and L. Reining, *Phys. Rev*. 99, 26402 (2007).
[15] V. G. Zavodinskii and A. N. Chibisov, *Phys. Solid State* 51, 507 (2009).
[16] L. Knunyants and N. S. Zefirov, Chemical Encyclopedia (Sovetskaya Entsiklopediya, Moscow, 1999), Vol. 4.

Smart Nanocomposites
Volume 6, Number 2
ISSN: 1949-4823

THE FUEL QUALITY SENSOR BASED ON INFRARED OPTICAL CELL

T. V. Stoyanova[1,*], V. D. Smolyaninov[1], and A. V. Chernyaev[2]
[1]Mining University, St. Petersburg, Russia
[2]LED Microsensor NT, St. Petersburg, Russia

ABSTRACT

Absorption of an infrared radiation in petrol and diesel fuel samples in the spectral range from 1 μm to 4 μm was examined. Certain infrared spectrum areas, where the differences in the absorption of radiation by samples are the most significant were determined. Development project for the infrared LED petrol and diesel fuel quality control module was carried out.

Keywords: light-emitting diodes, infrared radiation, absorption, wavelength, petrol, diesel fuel, quality control, sensor

INTRODUCTION

The life time of an internal combustion engine highly depends on the quality of the fuel. A low-quality fuel significantly increases corrosion and deterioration of an engine, leading to frequent breakdowns and deviations of the operating mode. Despite rigor quality control procedures of the production process, occasionally the quality of petrol deviates from the standard requirements. This issue mostly affects car owners. Therefore, the urgent task is to create a low-cost sensor to control the quality of the fuel in the tank of a vehicle.

Modern automotive fuels are mixtures of components obtained by different technological processes. Petrol can contain more than 200 individual hydrocarbons of various structures. The content of individual hydrocarbons, as well as their interaction with each other determines properties of petrol [1].

The petrol and diesel fuel quality analyzer, based on an infrared optical cell is one of the possible solutions to the problem. Among the non-destructive methods of control, optical methods have the highest speed [2]. Developments in modern of light-emitting diodes (LED) industry raised optical analysis to a new level. Light-emitting diodes should be used in optical

* Corresponding author: Ph.D. Stoyanova Tatiana, associated professor, National Mineral Resources University, (Mining University), Saint Petersburg, Russian Federation, Tel.: 8 911760-87-58, E-mail: Stoyanova_tv@list.ru.

cells, because they have number of advantages over other types of radiation sources. Main advantages of light-emitting diodes: long live time (100000 hours of continuous operation), reliability, energy efficiency, small size (~0.1 mm^2), minimal heating (especially in pulse mode). The width of the light-emitting diode spectrum is comparable with the width of absorption bands of chemicals. Small size of the light-emitting diodes chips allows to create multi-wavelength light-emitting diodes matrices for controlling of different substances in the liquid [3]. Light-emitting diodes matrix can be integrated with photodetectors and electronics in one unit. It becomes possible to create compact LED-based optical cells and embed them in portable devices.

DESCRIPTION OF THE METHOD

Samples of petrol AI -92, AI- 95, AI- 98 and diesel fuel were examined in our research.

At the first stage of the research, measurements were carried out on equipment that consists of source of infrared radiation, mechanical modulator and monochromator MDR-41 [4].

Figure 1. The spectral analysis installation.

The photodiode based on InSb structure (the sensitive area with a diameter of 2 mm) was used as an optical receiver.

Measurements were carried out in the range of 1 μm to 4 μm (Figure 2). The transmission spectrum is a number of rather wide absorption and transmission bands. It has areas with almost complete absorption of infrared radiation. The most significant difference in the absorption of electromagnetic radiation was detected at wavelengths of 2.8 – 2.9 μm. The spectrum of diesel fuel is shifted to longer waves area. Diesel fuel absorbs more infrared radiation near the bandwidth of 1.8 – 2.2 μm.

The objective of the following measurement session was to examine the absorption of infrared LED radiation by different types of motor fuel and to determine certain wavelengths, where the differences in the absorption of radiation are the most significant. The portable

device (2) connected to the computer (3) was used for measurement (Figure 3). The device includes optical cell with six light-emitting diodes that emits at wavelengths 1.3 μm, 1.4 μm, 1.6 μm, 1.9 μm, 2.1 μm, 2.3 μm and one photodiode (1) (Figure 3). Light-emitting diodes operate in a pulse mode with pulse duration of 20 μs.

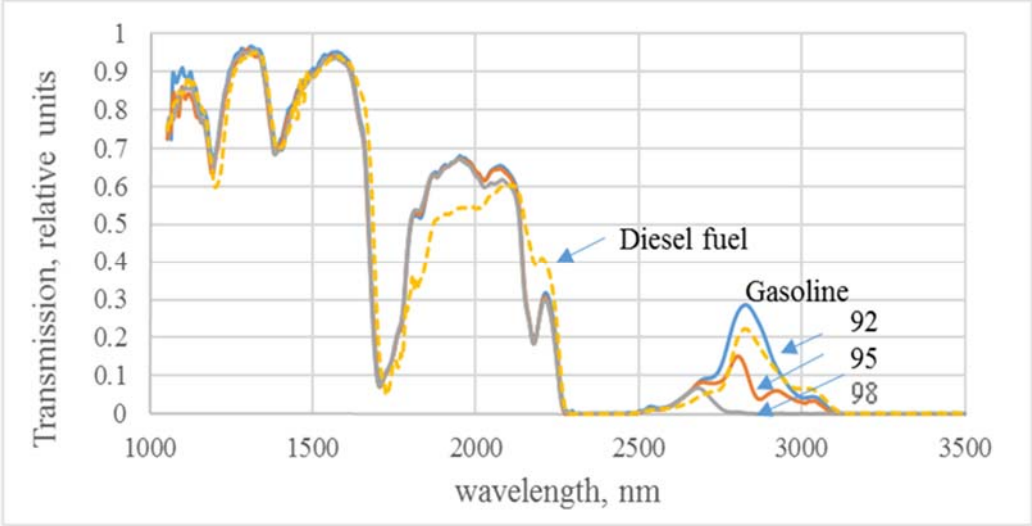

Figure 2. The transmission spectrum of petrol (solid lines) and diesel fuel (dashed line). Petrol brands shown in the figure.

The significant differences in absorption spectra of motor fuel samples were determined at the wavelengths 1.3 μm, 1.4 μm, 1.9 μm and 2.1 μm (Figure 4). The maximum difference was obtained upon irradiation of the light-emitting diode with a wavelength of 1.9 microns.

The absorption of different samples remains the same when radiation of light-emitting diodes with wavelengths of 1.6 μm and 2.3 μm was applied.

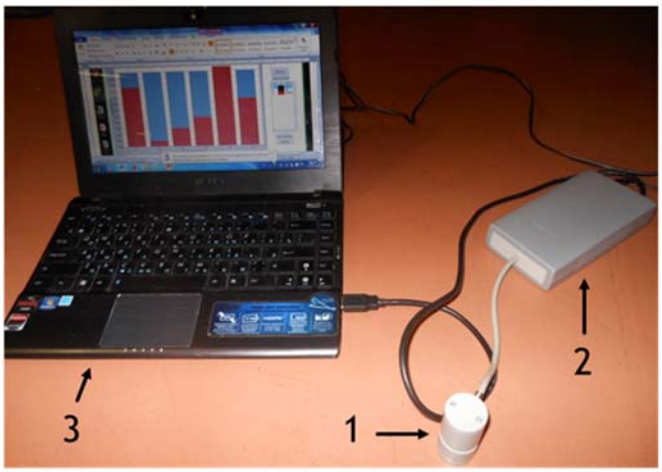

Figure 3. Equipment for analyzing of the absorption in infrared spectral range. Optical cell (1), electronic unit (2), computer (3).

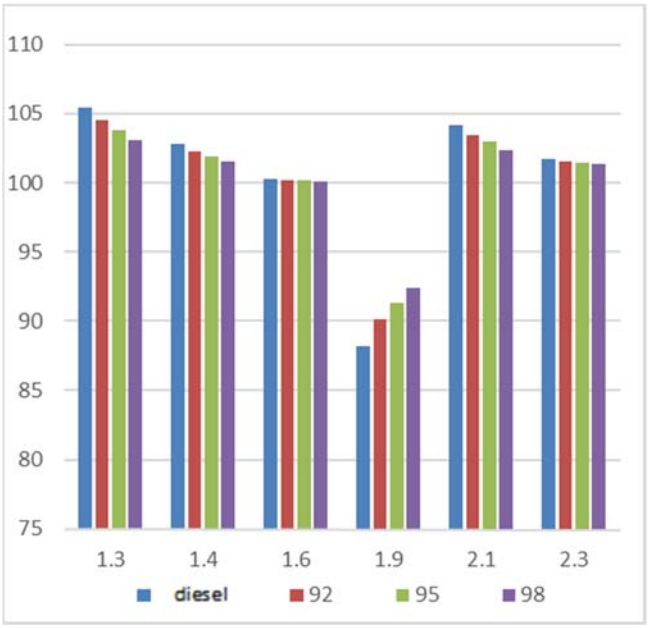

Figure 4. Absorption of infrared radiation for diesel fuel and different brands of petrol.

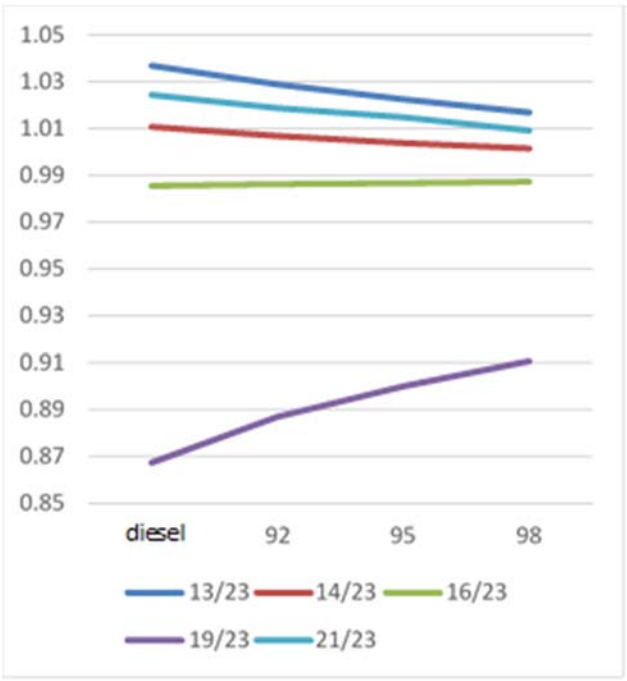

Figure 5. Relative absorption of infrared radiation at different wavelengths to 2.3 μm.

The relative change of the absorption of infrared radiation, shown in Figure 5, was obtained by dividing the absorption spectrum by the reference signal (2.3 μm).

From the obtained dependence in Figure 5 it can be concluded that the examined LED analyzer can be used for determination of the type of the motor-car fuel.

CONCLUSION

In this research two experiments were carried out. For this purpose, two types of equipment were used. In the first experiment absorption/transmission spectra of different types of petrol and diesel fuel were determined. We determined spectrum areas where the differences in absorption of radiation were the most significant. The aim of the second experiment was to examine the possibility to analise absorption of fuel samples using portable infrared LED sensor. Based on obtained results in these two experiments, it can be concluded that the examined LED analyzer can be used for determination of the type of the motor-car fuel.

ACKNOWLEDGMENT

Thanks are due to LED Microsensor NT for supporting this work.

REFERENCES

[1] www.rossibneft.ru.

[2] N. Stoyanov, Kh. Salikhov, K. Kalinina, B. Zhurtanov, S. Kizhaev, Middle infrared LEDs: key element for new generation chemical sensors, *Proceedings of the SPIE,* 8257, 82571E-6, 2012.

[3] Kalinina K.V., Molchanov S.S., Stoyanov N.D., Shestakov A.P., Salikhov H.M., Yakovlev Y.P., "Portable optical analyzer water content in oil-based optopair" LED matrix broadband photodiode "mid-infrared (1.6-2.4 microns)" *Technical Physics,* 2010, Volume 80, Issue 2, pp. 99-104.

[4] S.A. Gasanli, M.A. Avila Rees, T.V. Stoyanova, Portable analyzer automotive fuel, *Proceedings of the XVI International Scientific Conference "Severgeoecotech*-2015, Ukhta, USTU, 2016, Volume 1, pp. 25-29.

Smart Nanocomposites
Volume 6, Number 2
ISSN: 1949-4823

PROPERTIES OF THE LUBRICANTS AND ITS COMPONENTS CONTAINING SURFACE-MODIFIED ALUMINUM POWDER

A. G. Syrkov[1,*], M. O. Silivanov[1], and I. V. Pleskunov[2]
[1]Mining University, St. Petersburg, Russia
[2]IMC Montan, London, Great Britain

ABSTRACT

The priority measurings of friction coefficient (f) and friction force (F_{fr}) were carried out for the heterogeneous systems as oil I-20 with Al – additives modified by triamon (T), alkamon and ethylhydridesiloxane according to various programs. It was found that as a number of T –underlayers, included in Al-additives with chemisorpted external layer of ethylhydridsiloxane reduces from 3 to 1 the force of friction and coefficient of friction reduce. It was discovered that the value of summand (from 10,8 to 13,2 N) which stands for the amount of intermolecular forces in the boundary friction equation can be regulated in Al – additives by adding low-molecular T – underlayer.

Keywords: nanotribology, nonlinear effects, monomolecular layers surfactant, modifying of the aluminum surface, anti-frictional effect, intermolecular forces, boundary friction

INTRODUCTION

Consistent (mixed) chemisorption of quaternary ammonium compounds (triamon and alkamon, which are surfactants, based on quaternary ammonium compounds, with molecules having different size) proved to be a potentially successful method of regulation of water repellency, reaction potential and anti-frictional properties of modified metals [1, 2]. The most interesting research objects are modified aluminum samples and Al – containing lubricants. This due to properties listed above and the synergetic effects observed [1-3]. Hydrophobization of metal additives favorably affect anti-frictional properties of lubricants [1, 4], however the influence of location and number of underlayers on metal, with external hydrophobic layer, on adsorption properties of that metal and on characteristics of lubricants is still unknown. Also, fundamental tribological characteristic (F_{fr} and f) of systems with lubricants, which contain disperse metals with multiple layers (n = 1- 4) of quaternary

* Corresponding author: syrkovandrey@spmi.ru

ammonium compounds and hydrophobic ethylhydridsiloxane, were not yet measured and described. This work's aim was to solve the problems listed above.

MATERIALS AND METHODS

Aluminum powder (PAP-2) with specific surface area of 2,6 ± 0,2 m^2/g (BET) was chosen as a primary initial disperse metal. According to transmission electron microscopy (TEM) the size of particles of aluminum powder varies mainly from a few to tens microns, though there are smaller particles, the size of which varies from 45 to 70 nm. Modes of modification, used in the research, do not change a form and a size of particles. Aluminum powder was modified using different modes at a room temperature in vapors of triamon (T), alkamon (A) and hydrophobic silicone-organic liquid (HSL), which is based on ethylhydridsiloxane. Modes of modification of powder were fully described in prior researches [2, 5].

Composition of the samples was determined by using EDX-spectroscopy (analytical attachment EDAX/TSL, shooting mode – 6kV) and X-ray fluorescence spectroscopy (XRF, Bruker S4 Explorer). The water-repellent properties of the sample were measured gravimetrically using desiccator method at a relative water vapor pressure $p / p_0 = 0.98 \pm 0.02$. Al powder, modified in vapors of quaternary ammonium compounds and/or HSL, was added to an industrial oil I-20 (lubricant). Force of friction (F_{fr}) and coefficient of friction of the system with oil I-20 with Al-additives was determined by using friction testing machine (DM-29M). The tribological pair was Steel 45 (GOST 1050-88) – Bronze Br Aj 9-4 (GOST 18175-78). Tribological measurements data was compared with data obtained from another friction testing machine (MTU-01). Anti-frictional properties in friction testing machine MTU-01 are measured by the reduction of torque of friction force. Moreover, freshly obtained tribological properties of heterogeneus systems were compared with early obtained integral index of friction (D), which is proportional to force of friction. Integral index of friction was measured on certified device ARP-11 (frequency range: 20 - 300 kHz) using a method of acoustic emission. A measurement of D was carried out in accordance with GOST 21655-88.

Samples, based on aluminum powder PAP-2, which were examined, are listed below (except initial Al powder). Al/T – sample with chemisorpted triamon, Al/A – sample with chemisorpted alkamon, Al/(A+T) – sample, treated in vapors of mixture of triamon and alkamon; Al/T/A – sample treated consistently with alkamon and triamon, Al/A/T (changed the consistency of treating) and Al/T/T (2 layers of triamon). In order to examine the influence of number of low molecular triamon underlayers on the properties of external layer of ethylhydridsiloxane (HSL), we synthesized completely new samples (Al/T/HSL, Al/T/T/HSL, Al/T/T/T/HSL). Triamon has a molecular formula of $\left[(HOC_2H_4)_3N^+CH_3\right]\left[CH_3SO_3^-\right]$. The main difference between alkamon and triamon is that alkamon has much bigger radicals (C_{16} - C_{18}) [4]. The number of underlayer adsorpted can be controlled during the modification by the presence of S and N atoms on the surface of powder. According to EDX – spectroscopy and XRF – spectroscopy, initial Al powder does not contain significant amount N and S. Al/T sample contains 0,21 mol % N and 0,22 mol % S after the first treatment with triamon. The consistent treatment of aluminum with A and T leads to an increase of the amount of N up to 0,55 mol % and S up to 0,43 mol %. Also, the

amount of silicone, carbon and oxygen can be determined at all stages of the synthesis [2]. Modification of Al powder in vapors of quaternary ammonium compounds does not significantly affect the quantity of specific surface area. The specific surface area of the disperse Al samples is 2,7 ± 0,1 m^2/g [2].

RESULTS AND DISCUSSION

According to Figure 1 system with Al/(A+T) sample has the largest decline of coefficient of friction. Al – additive, which modified in vapors of HSL and which has the highest hydrophobicity [5], does not significantly improve the anti-frictional properties of initial lubricant (see also the characteristics of Al/HSL in Table. 1). The anti-frictional properties significantly improved with inclusion of 1-2 T-underlayers under HSL – layer. Similar effect was discovered for Al/T/A sample, using the friction testing machine DM-29M (Figure 1, 2). It is important to note that Al/A/T additive, with alkamon underlayer does not cause F_{fr} to decrease, as much as Al/T/A does (Figure 1, Table. 1).

Modification of aluminum powder in vapors of a mixture (A+T) gives a greater improvement in anti-frictional properties than samples modified in vapors of alkamon or triamon separately (Figure 1, 2). This synergetic effect can be better noticed by the reduction of integral index of friction using acoustic emission method (Figure 3). According to graphic, plotted using a data from research [5], D (friction) in the system with Al/(A+T) is several times smaller than in the system with Al/A or Al/T. Setting for acoustic emission (47 MPa) can produce a pressure almost 3 times greater than a friction machine (17 MPa) can. That explains why in the Figure 3 the decrease of friction in the system with Al/(A+T) is sharper than in the Figure 2.

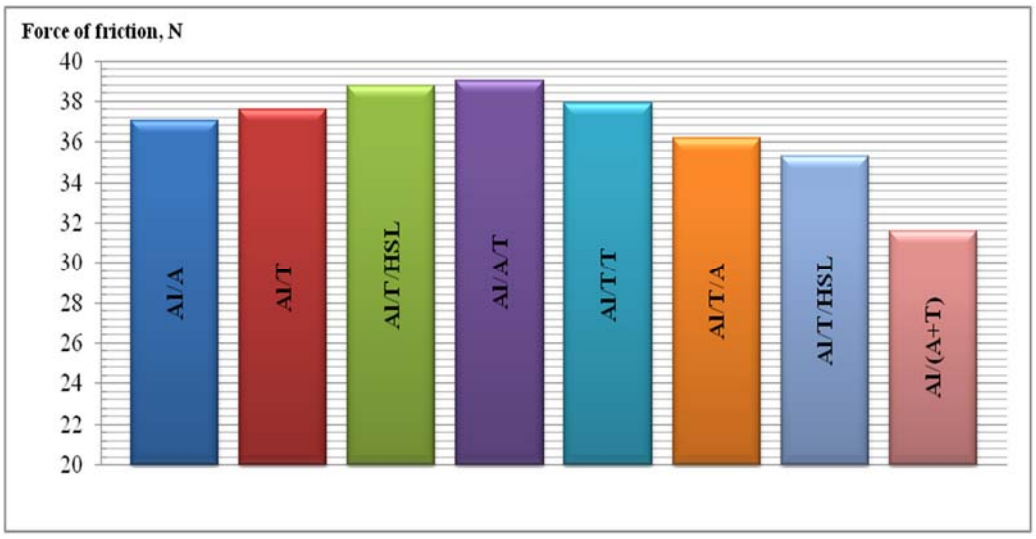

Figure 1. Force of friction in systems with lubricants, containing Al - additives, modified using different modes (the weight load was N = 5000 N; lubricants contained 0,5 % of additives by mass).

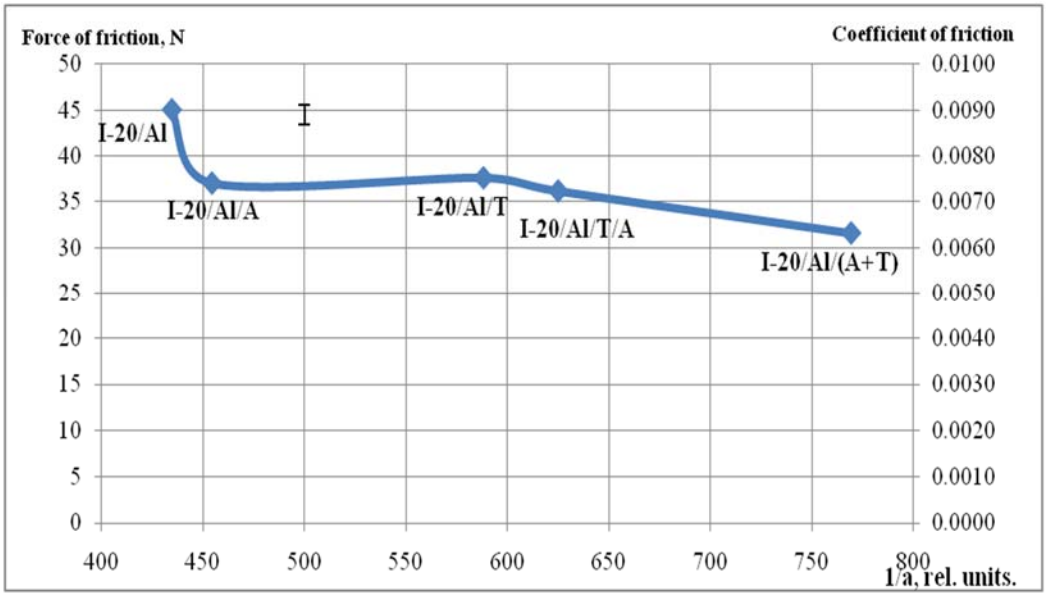

Figure 2. The dependence of F_{fr} and f on 1/a, where a – adsortion of water on Al – additive (N = 5 кN, P = 17 MPa).

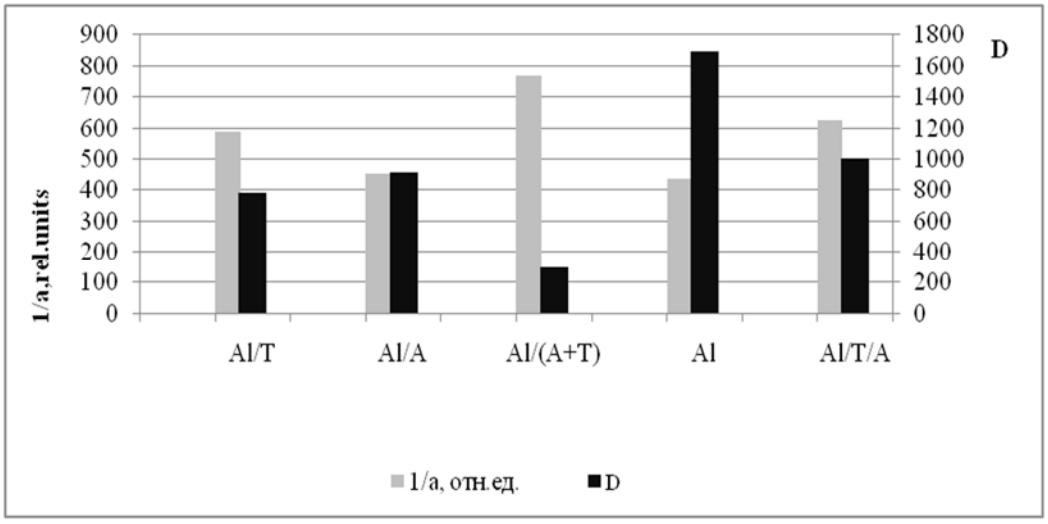

1/a, rel. units

Figure 3. The dependence of hydrophobiciy (~1/a) and integral index of friction D of lubricant, based on oil I-20, on the mode of modification (Pressure P = 47 MPa).

According to the ideas shown in the researches [1, 5, 7], at high load pressure as the liquid lubricant (I-20) is pressed out of the area of contact, system verges in the mode of "dry friction." Thus, anti-frictional properties of the system significantly depend on characteristics of the surface of solid additives. Therefore, it becomes evident that in the soft friction conditions (Figure 4) the effects caused by physical and chemical properties of Al – additives surface (Table. 1), become less obvious than in the data shown in Figure 3 and researches [1, 5].

The relationships between frictional force and the weight load of the lubricant with Al – additives and of the original oil I-20 (Table 1), can be approximated by the linear with the reliability degree R^2 measured between 0,986 – 0,999. Obtained y = kx + b form of equations are similar to the boundary friction equation in which intermolecular interaction of contacting surfaces is considered [8].

$$F_{fr} = k\left(N + Sp_0\right) = kN + kSp_0 ,$$

where k - friction coefficient in the measuring range N, N – the force of normal pressure, S – contact area between solids, p_0 – additional pressure, caused by intermolecular interaction forces. Equations with minimal proportionality factors k and the smallest value of R^2 (0,991 and 0,986) correspond to Al – additives (Al/(A+T), Al/T/HSL respectively) which reduce the force of friction the most. Free term of the equation, which is stands for intermolecular interaction, is the smallest for the additive Al/T/A and the biggest for the additive Al/HSL (Table 1). Lubricant with Al/T/A ranks among the top three lubricants with the best anti-frictional properties. Otherwise lubricant with Al/HSL has the largest friction coefficient f.

According to the data shown in the Table 1, Al – additives with external HSL – layer on the surface may be placed by the ability to reduce F_{fr} in the following way:

$$Al/T/HSL > Al/T/T/HSL > Al/T/T/T/HSL > Al/HSL$$

$$\longleftarrow$$

Reduction of F_{fr}

Thus, the additive with one T – underlayer improves the anti-frictional properties of lubricant the most. Such additives as Al/T/T/HSL and Al/T/T/T/HSL have a little positive impact on the F_{fr} in the weigth load range from 50 to 350 kgf. Moreover, they lower the anti-frictional properties of the oil I-20 (in the table 1 $\Delta F_{fr} > 0$) at the high weight load (more than 500 kgf).

In the research [9] it was established that the increase in the number of T – underlayers under the external A – layer on the aluminum powder reduces the water-repellent properties of the sample. So, it is possible that the best anti-frictional properties of the sample Al/T/HSL and the increase in hydrophobicity of the sample Al/T/A is just one more example of the monolayer effect, which was derived by Aleskovsky [10]. As a number of T-underlayers increases, the external hydrophobic layer becomes more distanced from the aluminum surface, which leads to the decline of some tribochemical properties of the samples. This fact indicates of influence of force of interaction between the metal surface and the external layer on tribochemical properties of the sample. According to Aleskovsky, after the layering of 3-4 layers the influence of aluminum surface nearly disappears. According to Abramzon [4], hydrophobization of the surface of metal and high level of adhesion between metal and a layer of surfactant are necessary to obtain good anti-frictional and protective properties of the sample. The results of this research confirm that the adhesion factor is a major factor among two factors listed above, which was earlier proved using the acoustic emission method for different metal-fillers [1, 11].

Table 1. The influence of type of Al - additive (0,5 % by mass) on $F_{fr} = \Phi(N)$ equation, the change of F_{fr} (ΔF_{fr}) and coefficient of friction (f) in comparison with the initial lubricant (I-20)

№	Al – additive (lubricant)	$F_{fr} = \Phi(N)$ equation	R^2	ΔF_{fr} (average), %	ΔF_{fr} (N = 5 кN), %	f (N = 3.5 кN)
1	Al/(A+T)	y = 0.037x + 12.47	0.991	-11.41	-15.92	0.0075
2	Al/T/HSL	y = 0.043x + 12.15	0.986	-7.42	-5.99	0.0075
3	Al/T/A	y = 0.048x + 10.81	0.992	-7.75	-3.69	0.0079
4	Al/A	y = 0.050x + 12.05	0.997	-1.05	-1.40	0.0089
5	I-20 (no additives)	y = 0.050x + 12.29	0.994	0	0	0.0089
6	Al/T	y = 0.050x + 11.86	0.999	-1.52	0.13	0.0087
7	Al/T/T/HSL	y = 0.049x + 12.49	0.993	-0.21	0.89	0.0085
8	Al/T/T/T/HSL	y = 0.048x + 12.50	0.995	-0.20	0.88	0.0086
9	Al/T/T	y = 0.051x + 11.59	0.994	-1.59	0.89	0.0086
10	Al/HSL	y = 0.048x + 13.22	0.994	2.32	3.80	0.0086
11	Al/A/T	y = 0.050x + 12.68	0.992	1.96	3.95	0.0085
12	Al (PAP-2)	y = 0.065x + 11.74	0.997	12.61	20	0.0101

Table 2. Dependence of f on weight load (50 – 500 kgf)

№	Al - additive (lubricant)	f, 50 kgf	f, 100 kgf	f, 150 kgf	f, 250 kgf	f, 500 kgf
1	Al/(A+T)	0.0299	0.0173	0.0125	0.0086	0.0064
2	Al/T/HSL	0.0293	0.0170	0.0129	0.0094	0.0072
3	Al/T/A	0.0275	0.0164	0.0127	0.0091	0.0074
4	Al/A	0.0299	0.0173	0.0133	0.0101	0.0076
5	I-20 (no additives)	0.0308	0.0185	0.0134	0.0098	0.0077
6	Al/T	0.0299	0.0173	0.0131	0.0101	0.0077
7	Al/T/T/HSL	0.0316	0.0182	0.0137	0.0097	0.0077
8	Al/T/T/T/HSL	0.0313	0.0183	0.0135	0.0099	0.0077
9	Al/T/T	0.0305	0.0176	0.0133	0.0096	0.0077
10	Al/HSL	0.0322	0.0185	0.0141	0.0105	0.0079
11	Al/A/T	0.0322	0.0185	0.0139	0.0102	0.0080
12	Al (PAP-2)	0.0316	0.0193	0.0146	0.0112	0.0092

The feature of Al-additives (based on PAP-2) is that the strengthening of adhesion of metal to a film (the heteroatomic interaction (M←N) [11] is made more difficult by the presence of stearin film (about 2 monolayers) on the aluminum particles [12]. The strengthening of adhesion of metal to a film occurs due to the heteroatomic interaction with the displacement of electron density (M←N). That is the main reason why according to the measurements obtained on friction testing machine (Table 1, 2) and on the certified device ARP-11 (Figure 3) Al/(A+T) samples has the greater positive impact than Al/T/A. According to the research [13], mixed treatment of PAP-2, when molecules of A and T reach the surface of metal together, is more favorable for stabilizing of T – A – layer, than the consistent treatment of A and T. For example, in case of addition of Cu-additives, which have purer metal surface, to the oil I-20 the greatest positive impact has Cu/T/A sample. The presence of heteroatomic interaction (M←N) in it was proved using X-ray photoelectron spectroscopy [11].

Using the friction testing machine MTU-01 (the center of collective use of the high-tech equipment of Mining university) it was determined that the addition of Al/(A+T) to the oil I-20 leads to the decrease in torque of friction by 2.6 times ($M_1 = 0.52$, $M_2 = 0.20$ rev. units.) at the weight load of N = 2 kN. Thus, the outstanding anti-frictional properties of Al/(A+T) additive were confirmed by 3 independent ways of analysis. The analysis of friction coefficient of 11 different lubricants (Table 2) shows that the Al/(A+T) additive has an advantage in the harsh weight load conditions. In milder weight load conditions (below 150 kgf, i.e., approximately 1500 N) such additives as Al/T/HSL и Al/T/A have a similar anti-frictional effect as Al/(A+T) does.

According to the Figure 2, the decrease of force of friction in the system is proportional to the decrease of the level of adsorption of the water vapor on the metal. In other words, the force of friction is indirectly proportional to the hydrophobicity of Al-additives.

The similar results were obtained earlier [7]. The integral index of friction D in similar tribosysems decreases symbatically with the increase of hydrophobicity of the Al – additive; the linear correlation coefficient for the D = Φ(a) is 0,82. However, the addition of the water-repellent (A or HSL) on the aluminum does not decrease F_{fr} of the lubricants by much (the samples 4 and 10 in the table 1) and does not increase the water-repellent properties (~1/a) of the metal (pic. 3). The most efficient out of all Al-additives are the additives which have external layer of triamon with the small ($C_1 – C_2$) organic substituents on the nitrogen atom. This fact leads to the penetration of the T-molecules to the gaps in the industrially applied stearic nanofilm on the aluminum. We have concluded that the steric availability of the nitrogen atoms in the triamon eases the forming of heteroatomic interaction between nitrogen and metal and between triamon and external layer A or HSL. Factors that are listed above contribute to the stabilization of the external layer of Al – additive and amplification of the anti-frictional effect of the lubricant with this additive.

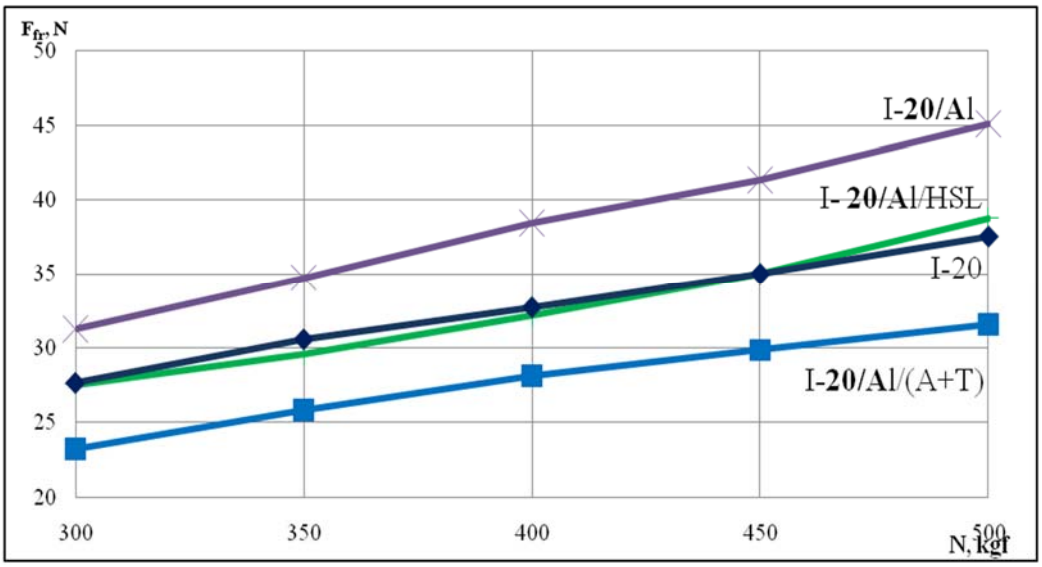

Figure 4. The dependence of force of friction on weight load for lubricants with Al-additives (lubricants contained 0.5 % of additives by mass).

Comparing the results to the data obtained for oil I-20 with nanopowder of soft metals (Cu, Zn, Pb, Brass) and received using electroexplosive method [14], shows the following. The synthesized Al – additives allow us to form the lubricants with anti-frictional properties and f, similar to those in the research [14]. The unusual fact is that due to the presence of micron size particles original disperse Aluminum PAP-2 cannot be named as nanopowder [12]. The F_{fr} and f decrease as a result of application of a nanofilm of quaternary ammonium compounds or HSL to a metal surface.

CONCLUSION

Thereby, in the circumstances when concentrations of additives, dispersity of solid-additive, mechanical pressure, the nature of tribological pair, and the temperature of the experiment are equal for all samples; it was found that as a number of T–underlayers included in Al-additives with chemisorpted layer of ethylhydridsiloxane reduces from 3 to 1, the force of friction and coefficient of friction also reduce in heterogeneous systems like oil I-20 with Al-additive. The positive impact of the triamon underlayer on the water-repellent properties of Al-additives and tribosystem with these additives is associated with small molecular size of triamon, steric availability of nitrogen atom, which eases the stabilization of system, as well as adsorptional and anti-frictional properties of the external surface of metal.

REFERENCES

[1] D. S. Bystrov, A. G. Syrkov, I. V. Pantyushin, T. G. Vakhreneva, Anti-frictional properties of industrial oil with additives with nanostructured metals, *Chemical physics and mezoscopy,* Vol. 11, No. 4, p. 462. (2009).

[2] A. G. Syrkov, Synergetic enhancement of reactivity of aluminum in presence of quaternary ammonium compounds on the surface, *Journal of General Chemistry*, Vol. 83, No. 8, p. 1392. (2013).

[3] L. I. Voronchikhina, O. E. Zhuravlev, E. V. Andrianova, N. I. Krotova, Ionic liquids - pyridinium salts, γ- and β- picolinyl, *International journal of applied and fundamental research*, No. 3, p. 139. (2014).

[4] *Surface Phenomena and Surfactants. Reference Book,* edited by A.A. Abramzona, E.D. Shchukina. Leningrad: Chemistry, 1984. p. 392.

[5] A. G. Syrkov, D. V. Fadeev, V. V. Taraban, M. O. Silivanov, Quantification of non-linear effects of the dependence of the integral index of friction of tribosystem on water-repellent properties of the metal filler, *Condensed atter and interphase boundaries,* Vol.16, No. 2, p. 215. (2014).

[6] L. M. Khanashvili, K. A Andrianov, *Technology of organoelemented monomers and polymers*. Moscow: Chemistry, 1983. p. 416.

[7] A. G. Syrkov, From Laboratory to Industry, *Smart Nanoobjects*, Ed. by K. Levine. New York: Nova Science Publishers, Inc., 2013. 214 p.

[8] T. N. Trofimova, The *course of physics.* Moscow: Publishing center "Akademiya," 2010. p. 560.

[9] D. S. Bystrov, *Nanostructured regulation of anti-friction properties and reactivity of the surface of steel and aluminum* Dis. kand. khim. nauk. SPb: SPbGTI(TU), 2009. p. 182.

[10] V. B. Aleskovsky, *Chemistry of supramolecular compounds.* Saint Petersburg: Publishing house of Saint Petersburg State University, 1996. p. 256.

[11] G. Syrkov, Synergetic change of tribochemical properties of copper in the presence of quaternary ammonium compounds at the surface, *Journal of General Chemistry*, Vol. 85, No. 6, p. 1043. (2015).

[12] http://www.icp.ac.ru/conferences/old/Nanochem/Kolesnikova.

[13] A.G. Syrkov, D. S. Bystrov, L. A. Zhurenkova, T. G. Vahreneva, Water-repellent properties of nanostructured aluminum based metal powders, *Russian journal of non-ferrous metals*, No. 2, p. 79. (2009).

[14] Tarasov S., Kolubaev A., Belyaev S., Lerner M. et al., Study of friction reduction by nanocopper additives to motor oil, *Wear.* Vol. 252, p. 63. (2002).

Smart Nanocomposites
Volume 6, Number 2
ISSN: 1949-4823

INVESTIGATION OF COVERED COLLOIDAL QUANTUM DOTS CDSE/ZNS AND CDSEZNS/ ZNS AS A BASIS OF DETECTOR COATING

S. A. Tarasov*, M. O. Gurevich, L. I. Kozlovich, I. I. Mikhailov, E. M. Stepanov, O. S. Vatalev, P. O. Tadtaev, and A. V. Solomonov
Saint Petersburg Electrotechnical University "LETI" (ETU), Russia

ABSTRACT

Covered colloidal quantum dots CdSe/ZnS and CdSeZnS/ZnS were studied. The high efficiency of luminescence in the range of wavelengths from 500 to 700 nm was shown. The CQD`s energy and dimensional properties was modeled; it was shown that particles size varying in diameters in the range from 2 to 5 nm. Using a mixture of CQDs as a basis, detector coating were created; such covers are promising for use in non-contact surface quality diagnostics. Fast and convenient way of topologic features visualization was made, which can be easily introduced everywhere from facilities to field researches of various applications constructions.

Keywords: colloidal quantum dots, luminescence, dimensional parameters

GOALS

Investigation of covered colloidal quantum dots CdSe/ZnS and CdSeZnS/ZnS, measurement and analysis of their main optical and luminescent properties. Modeling of CQDs' energy and dimensional properties. Creating of detector coating on a basis of mixture of CQDs.

INTRODUCTION

Colloidal quantum dots (CQDs) are considered one of the most promising materials of the state-of-the-art electronics. CQDs have all the nanodimensional particles' benefits, such as the good luminescent and photosensitive properties, and can be created by relatively simple and affordable methods of colloidal synthesis.

* SATarasov@mail.ru

Colloidal quantum dots (CQDs) have high efficiency and are able to change the wavelength of output radiation easily by varying echnological parameters of nanoparticles synthesis [1-2].

Sizes of nanoparticles contains in the quantum dots solution vary greatly due to features of their synthesis technology. This leads to significant broading luminescence luminescence spectra of CQD`s, that determines by particle's size dispersion. Half-width of spectral characteristics allows to stimate the amount of this dispersion and to bring out technological factors that are influencing on nanoparticles size. At present technology of QD's colloid synthesis allows to create samples with high degree of monodispersity. It this case the half-width of luminescence peak is about tens nanometers.

The main process exciting the luminescence in CQDs is the exciton energy states transitions which are the result of size quantization effect and electron-hole interaction. Such transitions can be compared with luminescent band-to-band transition in usual semiconductor materials and lead to appearing of narrow radiation peaks, which are often based in visible part of visual spectra Lots of CQDs (especially those which don't have a wide-band coat) have an additional long wave peak [3]. It is considered that its presence on spectrum is connected with defects such as surface states on the edge between core and shell and others. Second peaks half-width exceeds the first ones by too large a margin and should be treated as unwanted exposure for the majority of samples. However, in some samples luminescence peak intensity is essentially increasing what helps to find a positive application for wide-spectrum structures. The problem is the lack of information about this defects nature so their dependence on spectrum can hardly be predicted.

The important advantage of CQDs is the light absorption in a wide wavelength range. It is very convenient because quantum dots with different sizes can be excited by only one radiation source. Also the same dots type can be excited by different pumping sources what demonstrates a high universality of such materials. The other advantage of CQD's is their better photostability comparing with other organic materials what makes them very perspective for creating luminophore and other emitting layers.

Due to their small sizes, CQDs are capable of filling various devices' surface defects including nanopores, nanocracks and other topographic features of the substrate [4]. Besides, CQDs can also interact with nanostructures of the coated device itself. It can be used as a basis of the non-contact luminescent method of surface quality diagnostics or as the source of information about surface nanostuctures' features. From this point or view the research of CQDs optical properties and determination of their size parameters (which are affecting on probability of introduction into surface layers) is topical.

EXPERIMENTAL SECTION

The objects of this chapter are CdSe/ZnS and CdSeZnSe/ZnS colloidal quantum dots [5-6]. The wide-bandgap ZnS covering enhances the stability of CQDs to oxidation and increases quantum efficiency of luminescence because of the smaller quantity of surface defects. Main optical and luminescent properties of CQDs were measured and analyzed. Experiments facility [1] based on double-grating monochromator (SDL-1) were used. Semiconductor laser with peak wavelength 445 nm was used to excite the luminescence. The lock-in amplifier SR-810 was applied to increase the sensibility.

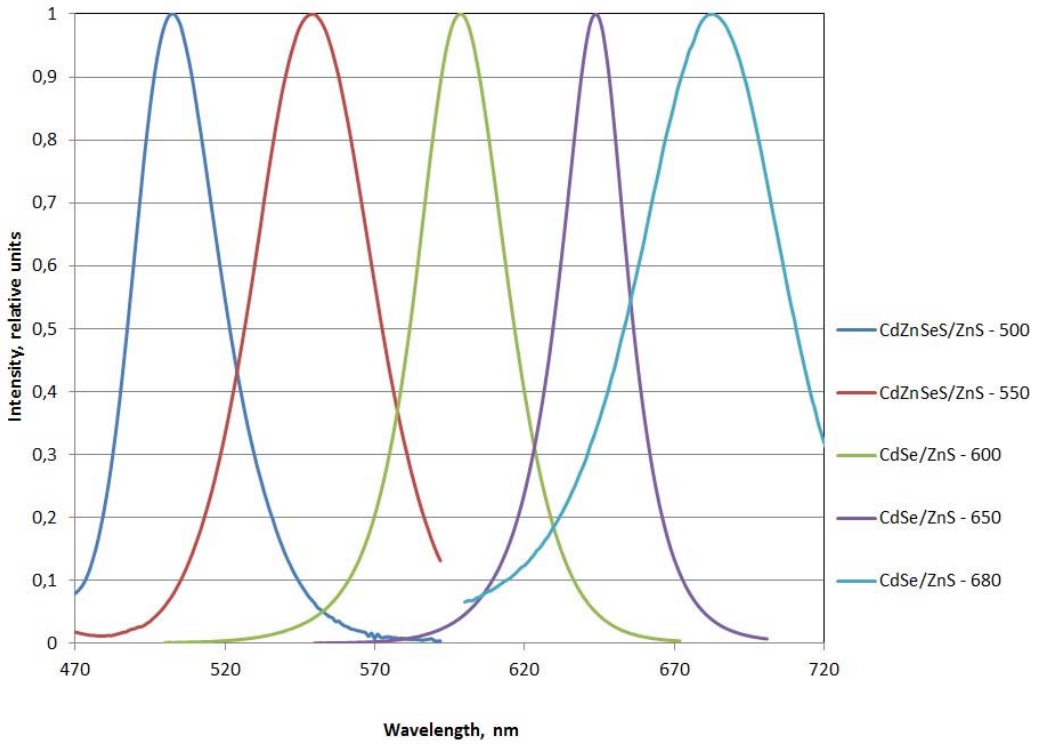

Figure 1. Luminescence spectra of researched CQD's CdSe/ZnS and CdSeZnS/ZnS samples.

Luminescence spectra of researched CQD`s CdSe/ZnS and CdSeZnS/ZnS samples are shown on Figure 1.The study showed that changing the size of CdSe colloidal quantum dots and the composition of CdSeZnS solid solution causes a shift of the spectra from green to red part of the visible range (from 500 to 700 nm). It is obviously that QD's of CdSe covered by wide-band shell of ZnS is the realization basis of dots with characteristic luminescence wavelengths near 600 nm and higher. For getting shorter wavelength spectrums the further increase of band between QD's exciton energy states is necessary. Farther size reduction could lower the characteristic luminescence wavelengths but is nearly impossible due to technological and fundamental reasons. Used resolutions contain CQD`s which nucleuses have an addition of wider-band lead sulphide and such solution leaded to 500 nm luminescence peak shift.

Figure 1 shows that the emission lines of CQD's were narrow and symmetrical, which proves the low size dispersion and the low influence of surface states on luminescence processes. Form and placement of spectral characteristics allow us to conclude that their appearance is dictated by transitions between fundamental exciton states in QD's.

The size parameters of CQDs are very important, because they affect luminescent characteristics and also defines the possibility of inclusion of nanoparticles into nanostructured surfaces. In order to define particles dimensional parameters and energy states in the study samples, the simulation with consideration of excitonic effects was run. In order to define particles' dimensional parameters and energy states in the study samples, the

simulation with consideration of excitonic effects was run. One of the most commonly applied methods of defining quantum dots' dimensions is the one based on the first luminescence and absorption peak analysis. Based on the comparison of photoluminescence spectra with experimental data of transmission electron microscopy (TEM), some formulas for the calculation were suggested [7]:

$$E = 1.7 + \frac{3.73}{R^2} \tag{1}$$

$$E = 1.7 + \frac{0.82}{R} \tag{2}$$

$$E = 1.7 + \frac{1.5}{R^2} \tag{3}$$

$$E = 1.7 + \frac{3.73}{R^2} - \frac{0.26}{R} \tag{4}$$

Among these approximations, formulas (1) and (2) show relatively good correlation with experimental data. Figure 3 contains not only these curves but also some experimental data, obtained from different sources [8-10].

As follows from the analysis, two methods provide the best results. The first one is based on the effective mass approximation and is applicable to the particles no less than 1.6 nm in diameter; the second one accounts for the Coulomb interaction effects which extends its application to the range of 0.6 to 4.2 nm. Nevertheless, there was a substantial divergence in calculated data. The application of the first method resulted in particle dimensions varying from 2.2 to 5.7 nm in the range of peak luminescence wavelengths from 500 to 700 nm; accounting for Coulomb effects yielded 1.5 – 2 times smaller values. The work is underway to adjust methods' accuracy in calculating particles' dimensional parameters.

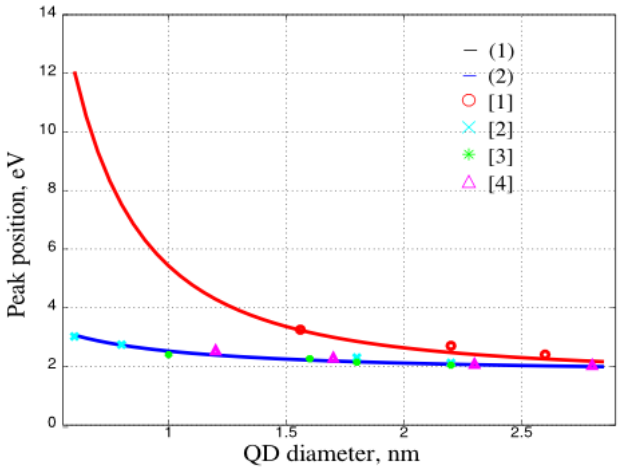

Figure 2. Results of comparison of the approximations (1) and (2) with experimental data from references [8-10].

Experiments were run to deposit examined colloidal quantum dots from the solution to the surfaces of various samples. It was shown that particles retain good luminescent properties and even show some stability augmentation which is explained by lower influence of the solvent's composition and concentration. The research on the characteristics of surface distribution of the particles and related change in luminescence spectrum was conducted. Deposition of the mixture of the various sized CQD's was made for changing chromatic characteristics of their emission.

Work on creation mixtures of CQD's with preset luminescent parameters has been done. These mixers allow detecting the sample surface states in the best way. The process of creation consists of mixing nanoparticles with luminescence spectrums shown on Figure 1 and precipitating them on detecting surface. Particles concentration was previously calculated with the help of special software which allows reaching preset glow color characteristics. The most interesting results were obtained during forming white glow luminophores mixes. As a modulation target and mix realization etalon white glow source based on black body (T = 5400 K) was used. Its spectral characteristics are shown on Figure 3, curve 3. Two types of luminophores mixes were realized. For blue glow improvement a small dose of wide-band CdS CQD's has been added to the mix based on CdSe QD's.

First sample (Figure 3, curve 1) is prepared from mix of CdS CQDs with 440 nm luminescence peak and CdSe CQDs with 500 and 600 nm peaks. Such components set didn't allow reaching an ideal formed spectrum. Ravines on luminescence spectrums near 480 and 550 nm wavelengths are observed. Long-wave spectrum part is also low on intensity. All this factors are decreasing CRI to 85. However, this result can be described as successful because its color rendering is much better than common white LEDs one. Minimum of components amount was used during synthesizing of above-mentioned structures.

Second sample is made of CdS CQDs (440 nm luminescence peak) and CdSe CQDs with 500, 550 and 680 nm peaks mix. The summary spectrum covers almost the whole visible range. Chosen concentrations are so that maximum of summary spectra lies near 500 nm wavelength. Concentrations which are providing side peaks are selected to get an indispensable intensity on appropriate wavelengths. This helped in increasing CRI to 95.

Worked out luminophore mix samples were used for studying the possibility of creation of CQDs-based detector coating with controllable emission parameters. The mixture has been precipitated from the resolution to surfaces with preset topologies and been irradiated by different short-wave sources. As a radiation sources Hg-lamps as well as short-wave (290-360 nm) LEDs were used. Experiments have shown the high applicability of created mixes for detecting a relief presence on the different samples surfaces and visualization of these reliefs form. Typical visualization example is shown on Figure 4. It is apparent that CQDs concentrates on topology features. Cheap and wide-spread mobile short-wave sources could be used for visualization. Thus fast and convenient way of topologic features visualization has been made, which can be easily introduced everywhere from facilities to field researches of various applications constructions.

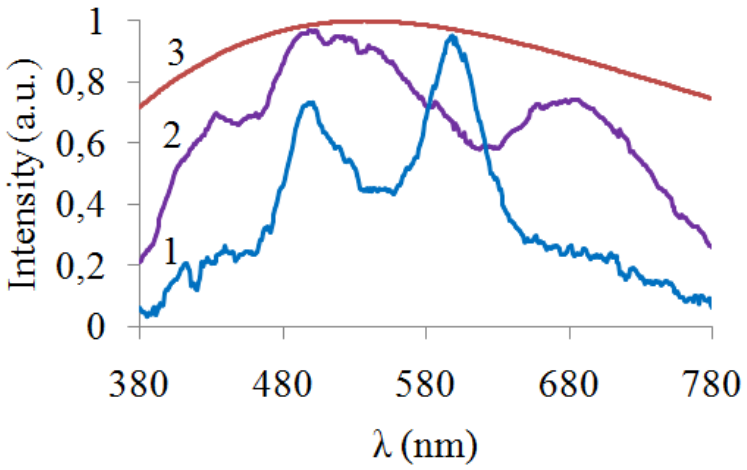

Figure 3. The photoluminescence spectra of the mixture of CQD's deposited on a glass substrate and spectra of black body (T = 5400 K).

Figure 4. Example of topologic features visualization of glass sample surface.

CONCLUSION

Covered colloidal quantum dots CdSe/ZnS and CdSeZnS/ZnS were investigated. Main optical and luminescent properties of CQDs were measured and analyzed. High efficiency of luminescence was shown in the range of wavelengths from 500 to 700 nm. It was shown that the emission lines of CQDs were narrow and symmetrical, which proves the low size dispersion and the low influence of surface states on luminescence processes. Simulation of CQDs' energy and dimensional properties was run; it was shown that particles vary in diameters in the range from 2 to 5 nm. Using a mixture of CQDs as a basis, detector coating were created; such covers are promising for use in non-contact surface quality diagnostics. Fast and convenient way of topologic features visualization has been made, which can be easily introduced everywhere from facilities to field researches of various applications constructions.

REFERENCES

[1] Mikhailov, S. Tarasov, A. Solomonov, L. Matyushkin, D. Mazing, *Function Materials*, vol. 2, N 21, 2014, pp. 142-145, 2014.

[2] Mikhailov, S. Tarasov, I. Lamkin, M. Andreev, A. Solomonov, *Journal of Physics*: *Conference Series* 643, 012080 (2015).

[3] S. Tarasov, O. Aleksandrova, A. Maksimov, E. Maraeva, L. Matyushkin, E. Men'kovich, V. Moshnikov, S. Musikhin. *Semiconductors*, vol. 48, N 13, 2014, pp. 1729–1731.

[4] S. Tarasov, O. Aleksandrova, I. Lamkin, A. Maksimov, E. Maraeva, I. Mikhailov, V. Moshnikov, S. Musikhin, S. Nalimova, N. Permyakov, Yu. Spivak and P. Travkin. *Semiconductors*, vol. 49, N 13, 2015, pp. 1710–1713.

[5] I. Mikhailov, S. A. Tarasov, A. V. Solomonov et al. *J. of Phys.: Conf. Ser.* 572 (2014) 012029.

[6] D Mazing, L Matyushkin, O Aleksandrova, I Mikhailov, V Moshnikov, S Tarasov, Journal of Physics: *Conference Series* 572 , 012028 (2014).

[7] Сюда то, что было [5].

[8] A. L. Rogach, A. Kornowski, M. Gao et al. *J. Phys. Chem*. B 1999, 103, 3065.

[9] V. I. Klimov. *J. Phys. Chem. B* 2000, 104, 6112-6123.2.

[10] X. Peng et al. *J. of the Amer. Chem. Soc*., v. 120, N 21, 1998, pp. 5343-5344.

Smart Nanocomposites
Volume 6, Number 2
ISSN: 1949-4823

INVESTIGATION OF THE DEPENDENCE OF THE DISPERSION FORCES ON THE PROPERTIES OF THE METALLIZATION LAYER IN MDS–STRUCTURES

A. B. Fedortsov[1] and V. A. Yurova[2,*]
[1]Mining University, Saint Petersburg, Russia
[2]The Bonch-Bruevich Saint Petersburg State University of Telecommunications, Saint Petersburg, Russia

ABSTRACT

We presented the new results of calculations dispersion force pressure with different material used as metal layer in metal–dielectric–semiconductor (MDS) structures based on silicon substrate. The calculations are based on the Lifshitz theory at nonzero temperature. We discuss the range of the typical value of the thickness a dielectric layer used in modern electronics. As an example, we show how the value of the dispersion force pressure depends on of changes electro-optical properties of the metal layer in MDS–structures. As the metallization layer we used aluminum, platinum and palladium.

Keywords: metal–dielectric–semiconductor (MDS) structures, Silicon, Metallization, Dispersion forces, Lifshitz theory

INTRODUCTION

The major tendency of the electronics development is the decrease of the weight and overall dimension of elements. It provides a high density of elements on a chip and reduces the power consumption. Currently, the typical distances between the conductive layers of electronic circuits are several ten or one of nanometers. At this scales quantum effects and intermolecular interaction (dispersion forces) becomes commensurable on size with influence of typical electric forces [1]. The interaction of objects is called the dispersion force, which is due to wavelength fluctuation of electromagnetic field (van der Waals forces) and it can take into account effects of the electro-magnetic field lag (Casimir–Polder force). At the same time, efforts are undertaken to develop nanoelectromechanical devices based on dispersion forces. So important is the

* Corresponding author: Valentina A. Yurova, Docent, the Bonch-Bruevich Saint - Petersburg State University of Telecommunications, Saint – Petersburg, Russia, E-mail: va-yurova@mail.ru.

investigation of dispersion forces in the different structures widely used of modern electronics.

OBJECT OF RESEARCH

One of the widely used metal–dielectric–semiconductor (MDS) structure is based on a silicon monocrystal substrate. It is manufacturing apply planar technology. The dielectric layer can be made of the oxide semiconductor substrate. In modern electronics also used the specific type of MDS–structure that is called structures metal–oxide–semiconductor (MOS). Generally, it's the layer of a dioxide that formed on a substrate surface by oxidation of a surface by water steams [2]. A metal layer is formed over it by thermal sprain methods. The electronic equipment generally is based on the structure Si–SiO_2 with different type of metallization.

These metal–dielectric–semiconductor structures are widely used in developing integrated circuits due to its unique electrodynamics and technological properties, and the possibility of integration in electronic chips. Also this kind of structures may be used as a good and simple model for the first calculations of the dispersion pressure in MDS–structures.

The contacts from aluminum have a good electrical properties and high reflectivity. Besides structures Al–Si–SiO_2 the structures with metallization of palladium (Pd) and platinum (Pt) found practical application, for example, in gas sensors [3]. It is possible to measure high and low concentrations of gas, especially hydrogen using MDS–structures Pd–Si–SiO_2 and Pt–Si–SiO_2. The operating principle of the gas sensors based on processes of the adsorption of atoms of different gases (for example, hydrogen, oxygen, nitrogen and others) on the surface of metal and its oxides, as a result the gas atoms act as electron donors.

The aims of our research are: to determine the dispersion pressure on the dielectric layer in the structure metal–dielectric–semiconductor based on a silicon substrate; to estimate the influence of the layers electro-optical properties on the dispersion pressure.

CALCULATIONS

According to the Lifshitz theory the dispersion pressure between layers of metal and semiconductor in MDS-structure in thermal equilibrium at the temperature T is determined by the equation:

$$P(a,T) = -\frac{k_B T}{8\pi a^3}\sum_{l=0}^{\infty}{}'\left(1-\frac{\delta_{l0}}{2}\right)\int_0^{\infty} k_\perp dk_\perp K_l^{(0)} \sum_q \left[\frac{e^{2K_l^{(0)}a}}{r_q^{(0,1)}(i\xi_l,k_\perp)r_q^{(0,2)}(i\xi_l,k_\perp)}-1\right]^{-1},$$

In this equation the notations are used: k_B is the Boltzmann constant; q is the magnetic and electric modes of the electromagnetic field; δ_{l0} is the Kronecker symbol; $k_\perp$ is the magnitude of the electromagnetic wave vector onto the plane of plates; i – the imaginary unit; ξ – frequency.

The expressions for the Fresnel reflection coefficients for two polarizations of the electromagnetic wave are

$$r_{TM}^{(SiO_2,n)}\left(i\xi_l,k_\perp\right)=\frac{\varepsilon_l^{(n)}K_l^{(SiO_2)}-\varepsilon_l^{(SiO_2)}K_l^{(n)}}{\varepsilon_l^{(n)}K_l^{(SiO_2)}+\varepsilon_l^{(SiO_2)}K_l^{(n)}},\ r_{TE}^{(SiO_2,n)}\left(i\xi_l,k_\perp\right)=\frac{K_l^{(SiO_2)}-K_l^{(n)}}{K_l^{(SiO_2)}+K_l^{(n)}},$$

where coefficient

$$K_l^{(SiO_2,n)}\equiv\sqrt{k_\perp^2+\varepsilon_l^{(SiO_2,n)}\frac{\xi_l^2}{c^2}}.$$

Here, index (n) denotes either metallization or silicon layers in the metal–dielectric–semiconductor structure. The value of dispersion pressure mainly depends on the thickness *a* of the dielectric layer and the material's permittivities.

As the typical layers thickness of the MDS–structure and thus characteristic wavelengths of the electromagnetic fluctuations exceeds the typical atomic distance, all properties of these fluctuations and their contribution to the value of the dispersion pressure can be expressed in terms of the macroscopic approach to describe electro-optical properties of these layers.

In our research we used the simplest models of the material permittivities and the experimental data of the refraction coefficient along the imaginary frequency axis [4]. The values of the dielectric permittivity along the imaginary frequency axis can be calculated using the Kramers–Kroning relations applicable to the dielectric permittivity of the plasma model

$$\varepsilon\left(i\xi\right)=1+\frac{2}{\pi}\int_0^\infty\frac{\omega\,Im\varepsilon\left(\omega\right)}{\omega^2+\xi^2}d\omega+\frac{\omega_p^2}{\xi^2}.$$

In this equation the imaginary part of the dielectric permittivity calculated along the real frequency axis

$$\mathrm{Im}\,\omega_D\left(\omega\right)=\frac{\omega_p^2\cdot\gamma}{\omega\left(\omega^2+\gamma^2\right)},$$

where the values of plasma frequency ω_p and relaxation parameter γ for the materials of MDS–structures.

RESULTS AND DISCUSSION

We researched the influence of the electro-optical properties of metal layer on the dispersion pressure in widely structure metal–dielectric–semiconductor based on Si–SiO_2 used in modern electronics. The thickness of the dielectric layer was 50 nm. Received the following inequalities dielectric permittivities of the layers MDS–structures in the whole

frequency range: $\varepsilon^{(\mathrm{Me})}(i\xi) > \varepsilon^{(\mathrm{Si})}(i\xi) > \varepsilon^{(\mathrm{SiO_2})}(i\xi)$. This means that the dispersion interaction between metal layer and Si substrate is attractive for any thickness of an insulating layer SiO_2. As the example, the results of the calculations dielectric permittivities of the layers that consists Si–SiO_2–Al structure are shown in the Figure 1 as function of logarithm of the imaginary frequency described using tabulated optical data extrapolated to lower frequencies.

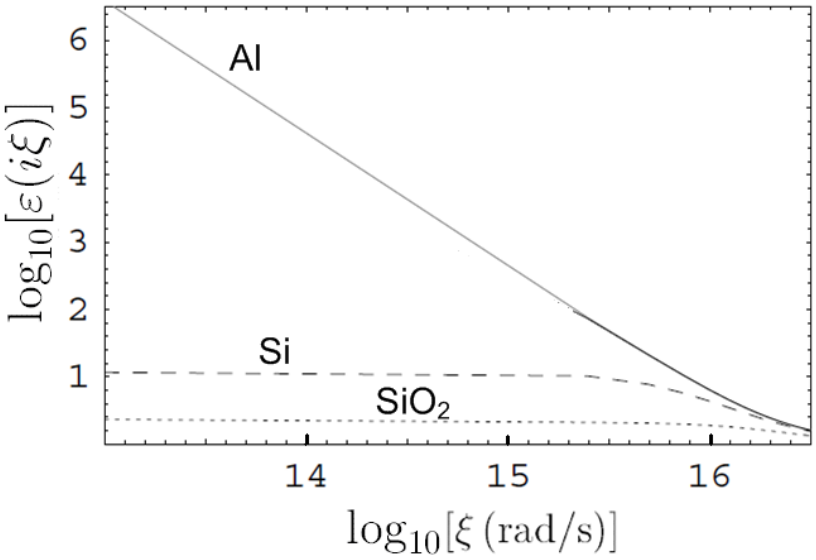

Figure 1. The layers dielectric permittivities in the metal-oxide-semiconductor structure as a function of the imaginary frequency on a logarithmic scale.

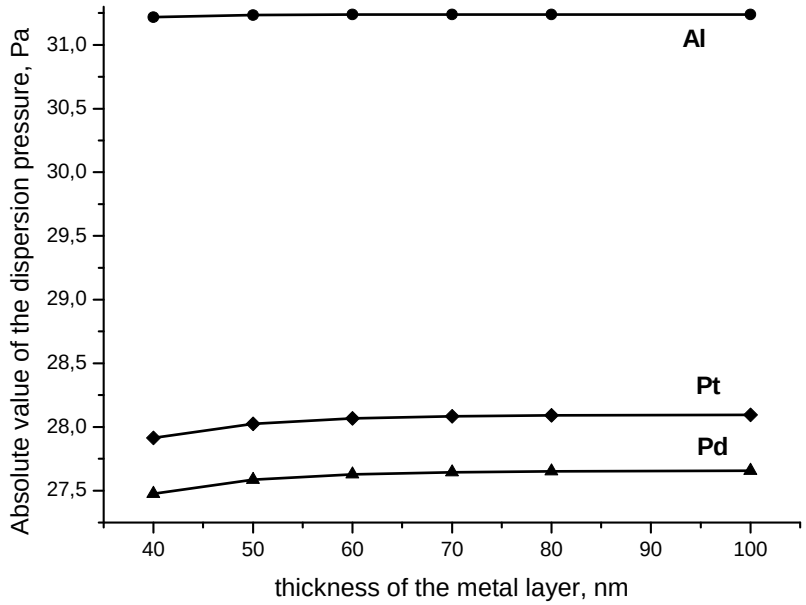

Figure 2. The absolute value of the dispersion pressure in the metal-oxide-semiconductor structure as a function of thickness of the metal layer.

In works [5–6] we obtained the values of the dispersion force pressure with the help of the nonrelativistic theory of the van der Waals forces. It was found that the results, obtained with using the dielectric permittivity to describe the electro-optical properties of layers in the MDS–structure with the thickness of SiO_2 less than 10 nm, in a good agreement with the results of the non-relativistic theory. And, therefore, the macroscopic description of the properties of the interacting layers can be used for investigation the dispersion force acting at the distance of a few atomic layers.

Also it was shown that the type of model used to describe the metallization permittivity doesn't influence on the value of dispersion pressure [6–7].

The Figure 2 shows that the value of the pressure of the dispersion force in the structure metal–dielectric–semiconductor is practically independent on the thickness of metal layer. It varies less than 1% with decreases of metal layer thickness in the range from 100 nm to 40 nm. These values appear into the range of the thickness actually used in electronics.

CONCLUSION

It was theoretical investigated the dispersion force pressure on the dielectric layer in metal–dielectric–semiconductor (MDS) structures using the Lifshitz theory at nonzero temperature. In this investigation the standard parameters of semiconductor devices with a thin dielectric layer are used. The value of the dispersion pressure depends weakly on the electro-optical properties of the metal layer and the model of its permittivity. The analysis shows that the value of the dispersion pressure is mainly depend on the properties of dielectric layer in structures metal–dielectric–semiconductor. Thus the carried-out calculations showed that in metal–dielectric–semiconductor structures based on a silicon monocrystal substrate with aluminum, platinum or palladium metal layer the dispersion pressure, putting on the dielectric layer, amount to considerable value. Apparently, it makes sense to take this value into account when developed the electronically devices with structures metal–dielectric–semiconductor.

REFERENCES

[1] Borgad M., Klimchitskaya G. L., Mohideen U., Mostepanenko V. M. Advances in the Casimir effect. – Oxford: Oxford University Press, 2009. – 768 p.

[2] Burger R. M., Donovan R. P. Fundamentals of silicon integrated device technology. Oxidation, diffusion and epitaxy. USA: Prentice-Hall – 1967 – Vol.1 – 451 p.

[3] Gracheva I. E., Kuznezov V. V., Maximov A. I. Hierarchical nanostructured semiconductor porous materials for gas sensors. *Journal of Non-Crystalline Solids*, 2010, No. 356 – pp. 2020 – 2025.

[4] Palik E. D. (ed.) Handbook of optical constants of solids. USA, NY: Academic Press, 1998. – 999 p.

[5] Klimchitskaya G. L., Yurova V. A., Fedortsov A. B., Churkin Yu. V., Bukina M. N. Casimir pressure in MDS–structures. Intern. *Journ. of Modern Physics: Conference series,* 2012, Vol. 14 – P. 566 – 575.

[6] Fedortsov A. B., Yurova V. A. Dispersion forces in nanoscale structures metal–dielectric–semiconductor. *Smart Nanocomposites*, 2013, Vol. 4, N. 1 – pp. 67 – 70.

[7] Klimchitskaya G. L., Yurova V. A., Fedortsov A. B., Churkin Yu. V. Casimir force pressure on the insulating layer in metal-insulator-semiconductor structures. *Physics of the Solid State*, 2012, Vol. 53, N. 9 – pp. 1921 – 1926.

Smart Nanocomposites
Volume 6, Number 2
ISSN: 1949-4823

SHORT COMMUNICATIONS

PROCEEDINGS OF THE INTERNATIONAL CONFERENCE – "NANOPHYSICS AND NANOMATERIALS" – 2015 ST. PETERSBURG, MINING UNIVERSITY, NOVEMBER 24 – 25, 2015

This Short Communications section of the journal is represented by the selected proceedings of the Symposium NIN-2015, "Nanophysics and Nanomaterials," St. Petersburg, Mining University, November 24-25, 2015.

The section on alloys describes studies in alloys, metal oxides, and metallurgy.

The section on semiconductors covers studies in semiconductor technologies, doping and charge transfer processes, different types of semiconductor structures, structural transformations in thin films and their visualization, oxides with semiconductor properties, and modeling.

The section on electrochemistry and corrosion protection covers nanostructured coatings, electrochemical analytical methods, and corrosion protection of different materials.

The section on nanoporous and nanostructured materials deals with silicon powder nanostructured systems, porous materials and the influence of porosity on properties, shungites, materials with stretchable geometry, and nanoparticle catalytic properties.

The section on optical nanocomposite systems describes nanocrystals optical properties, luminescence, electroluminescence, the effect of synthetic method, and quantum dots.

The section on plasma technologies is a broad section that describes plasma energetics and diagnostics, magnetron scattering, and sintering methods. Fractal structures, terahertz frequency scattering, and electron scattering as analytical tools are also included.

SUBJECTS

Alloy and Oxide Nanometallurgy

Electrochemistry and Corrosion Protection

Nanoporous and Nanostructured Materials

Nanocomposite Systems with Optical Properties

Plasma Technologies, Diagnostical Methods, Fractal Structures, and Nano-Sized Structures

Semiconductors and Thin-Film Technologies

Smart Nanocomposites
Volume 6, Number 2
ISSN: 1949-4823

DEVELOPMENT OF MECHANICAL PROPERTIES OF ALUMINUM-SILICON ALLOYS

S. N. Fedorov and V. Y. Bazhin
Mining University, Faculty of mineral raw materials processing

ABSTRACT

An effect of modification has been studied for the aluminum-silicon alloys. Different types of modifiers have been studied such as sodium, strontium, various phosphides and aluminum-based alloys containing titanium and antimony. Segregation has been investigated during sampling and casting ingots. Carbothermic technology has been proposed for producing aluminum-silicon alloys in a melting furnace. It will produce alloys with finer granularity and improve its mechanical properties.

Keywords: aluminum, silicon, modifying silumin, carbothermic technology, modificator

GOALS

Improving mechanical properties of aluminum-silicon alloys:

1. Choosing of the best modifier element;

2. Increasing the homogeneity of samples.

Improving the mechanical properties of metal products is always relevant. This is especially important for the casting aluminum alloys leading manufacture of Rusal company. According to the general director of Rusal Vladimir Solovyov, the company is going to increase production release with higher added cost [1].

Improving mechanical properties of aluminum-silicon alloys allows us to keep the leading position in sales of this segment of production.

We can get around the problem, using the modification of alloys. Modifying silumin - special treatment of the melt to produce fine granularity eutectic silicon. Such a structure will improve the mechanical properties of the products (elongation, etc.). Typically the modification is carried out by addition of sodium or strontium.

The essence of modification silumin - the effect of a modificator on the possible forms of eutectic silicon in silumin. It is shown in Figures 1 and 2.

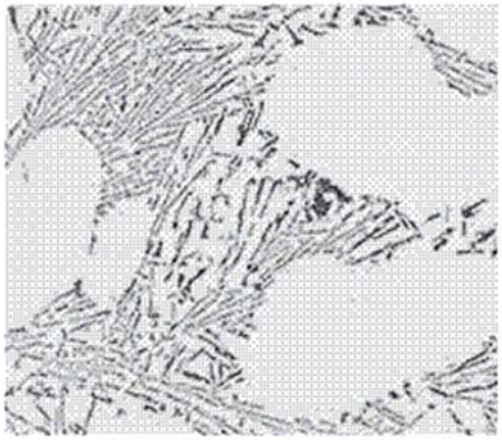

Figure 1. The lamellar structure of the eutectic silicon.

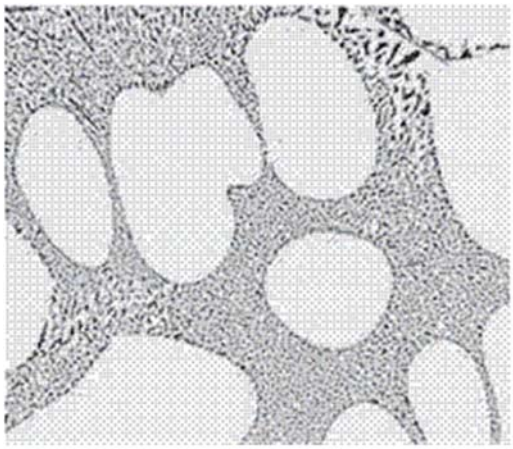

Figure 2. The modifying structure of the eutectic silicon.

REFERENCES

We can see on the figures that the structure of the alloy after modification is a more uniform grain and it becomes fine-grained. Modification was produced by sodium in an amount of 0.1% by weight of the alloy. However, this substance has a significant disadvantage - low boiling point of 880°C, whereby sodium fumes, the melt gases and sodium has a short modifying effect [2].

That's why strontium is more appropriate. It has a number of advantages compared to sodium. Strontium provides a stable modifying effect for several hours and after repeated remelting [3].

Also as a modifier various metal phosphides are used. The most favorable is aluminum phosphide. But we also can recommend copper and zink phosphide if the modificators do not change technical characteristics of the alloy with the introduction of copper and zinc above the limits are setted by Russian state standard or technological instruction of a plant. Copper phosphide is the most technologically convenient modifier. Zinc phosphide is the cheapest

[4]. Using of sodium and phosphides are limited because of the unfavorable effect to the ecology.

Processing will disperse silumin main phase of castings from 2 to 20 times by aluminum-based alloy containing titanium and antimony as a modifier (an amount of 0.5% by weight of the melt) and improve the environmental safety of the casting process [5].

Besides to the modification the attention should be given to sampling and segregation casting ingots. Segregation is influenced by the nature of the alloy crystallization, size and shape of the casting, heat dissipation, gassing and other factors, depending on the specific casting. Zonal segregation divided into direct and inverse. Direct zonal segregation - segregating components in the crystallization are concentrated in the central part of the ingot. Inverse zonal segregation - segregating components are concentrated in the periphery of the ingot. Such segregation is typical for aluminum alloys of copper, silicon, magnesium and zinc. The nature and extent allow us to attribute heterogeneity of the chemical composition of samples to zonal segregation.

A method was defined to increase the homogeneity of samples for spectral analysis on the basis of the survey. It is increasing of the cooling rate of the alloy with a corresponding refinement of the macrostructure and suppressing the zonal segregation. Increasing the cooling rate can be achieved by improving heat storage capacity of a mold and reducing the wall thickness of the casting. Moreover, these molds can significantly heat up.

“Fungal samples” were introduced to increase the cooling rate. The thickness of the cap is 4 mm. It is less than reduced thickness of the cylindrical sample. The specific heat of copper is above an order the heat capacity of steel. Heterogeneity has been reduced to acceptable limits after the introduction of “fungal samples” of the chemical composition of the samples [6, 7].

Production of the alloy is a key pillar in the producing of quality products. According to invention [8] feed and dissolving of aluminum-silicon ligature (as a melt) will provide an alloy having a homogeneous fine-grained structure in liquid aluminum. This gives us reason to believe the production will provide an opportunity to produce high quality silumin with lower cost by carbothermic technology. It will positively affect the marketing of aluminum-silicon alloys [9].

CONCLUSION

Were considered improving mechanical properties of aluminum-silicon alloys to show the production with higher added cost. Among big amount of modificators were chosen the most acceptable modifier element – strontium. Also can be recommended as a modificators titanium and antimony. Increasing the homogeneity of samples let get samples with better structure to analyze it.

REFERENCES

[1] RUSAL is going to increase production release with higher added cost [Electronic resource]//metaprom.ru: METAPROM industrial portal. - URL: http://www. metaprom.ru/news/cvetmet/28-08-15-news22442.html (date of treatment: 10.25.2015)

[2] Modifying silumin [Electronic resource]//aluminium-guide.ru: Aluminium Casting. - URL: http://aluminium-guide.ru/modificirovanie-siluminov/ (date of treatment: 10.25.2015).
[3] Nemenenok B.M. Theory and practice of complex modification silumin. - Minsk: Tehnoprint, 1999. - 272 p.
[4] Gharibyan G.S., Rashupkin V.P., Zyuzyuko I.V. Influence phosphide on the structure and properties of hypereutectic silumin//Omsk Scientific Bulletin №2. OGTU - Omsk. 2010. - P. 64-65.
[5] Stetsenko V.Y. Modifying silumin by crystalline aluminum alloys//Machine Building and Engineering. V.Y. Stetsenko, A.I. Rivkin, A.P. Gutev, R.V. Konovalov. - Mogilev. 2008. P. 21-24.
[6] Kuzmin M.P., Kuzmina M.Y. Segregation and quality of samples cast aluminum alloys//Vestnik ISTU №12. - Irkutsk. 2013. P. 210-213.
[7] Kuzmin M.P., Kuzmina M.Y., Kuzmin P.B. Shrinkage defects of casting small ingots of aluminum and its alloys//Metal Technology .: Moscow - Science and Technology. 2013. P. 21-27.
[8] Pat. 2432411 Russian Federation IPC C22C1/10. A method for producing aluminum-silicon alloy/Kulikov B.P., Nikolaev M.D., Kuznetsov A.A., Filipov V.V., Strelov A.V., Fedorov N.I., Sirotkin D.N. .; applicant and patentee BH “Baikal aluminum” - № 2010104824/02; appl. 11.02.2010; publ. 27.10.2011.
[9] Fedorov S.N., Bazhin V.Y. The concept of development of aluminum alloys from kyanite ores. Theoretical and practical problems of modern science. International scientific-practical conference. 2014. P. 52-55.

PROSPECTS OF NANOMETALURGY APPLICATION IN THE PREPARATION OF MASTER ALLOYS AND COMPOSITE MATERIALS

S. A. Savchenkov, Ya. I. Kosov* and V. Yu. Bazhin
National Mineral Resources University, Saint Petersburg, Russia

ABSTRACT

The prospects of nanometalurgy application in the preparation of master alloys and composite materials with rare earth metals (REM) are covered. In the field of production of master alloys based on aluminum and magnesium the determined results are achieved at the Department of Metallurgy Mining University.
Keywords: aluminium, magnesium, alloys, master alloys

INTRODUCTION

In the past three decades the new direction, which is connected with the production and use of substances in the nanocondition, has been formed. It's when a crystals or particles size is equals to hundreds of nanometers or less (10^{-9} m). For nanostructured materials the crystal lattice parameters change, allowing us to create new composite materials and products with unique properties, in which the sizes of the original objects are on the level of the sizes of atoms and molecules [1]. In recent years the increased attention to the rare-earth metals (REM) and intermetallic compounds thereof is observed. It is known that the use of REM as alloying and modifying additives allows to increase the strength of aluminum and magnesium alloys at room and elevated temperatures significantly [2]. Researching in the field of light alloys is currently focused on the improving of existing ones and on the developing of new alloys with using REM, through the development of technologies for the production of ultrafine powders of metals and nanostructured compounds. There are some achievements in the creation of new construction materials and methods of their treatment, in the aircraft industry, rocket production, mechanical engineering. Therefore, the areas of their applications are expanded; the resource of products for various purposes - for aviation and space, mechanical engineering and other industries - is increased by 3-5 times.

The goal is to reflect the perspectives of nanometallurgy techniques in the preparation of aluminum and magnesium master alloys which contain as major alloying component REM.

In non-ferrous metallurgy the researching of nanotechnologies is widely conducted and the results are achieved in the production of alloys based on aluminum and magnesium.

Methods of synthesis of aluminum and magnesium alloys, which are hardenable with refractory nanometric dimensions particles of REM, can be carried out by vacuum

* aafafka@gmail.com.

metallothermic reduction of REM compounds, as well as the injection with the plasma torch of solid metallic particles in the matrix melt having the predetermined chemical composition and the proper temperature. As a result of chemical interaction in the melt under certain technological parameters the nanoscale particles of intermetallic phases are formed. Obtaining and synthesis of nanostructures by the metallothermic reduction in a matrix of liquid aluminum and magnesium, the studying of size-dependent properties of REM nanostructures intermetallic compounds in the molten alloy is the most promising research topics for the development of new processing methods.

At the Department of Metallurgy Mining University a set of scientific-research works of fundamental and applied character is made [3]. It's about the development of synthesis compositions technologies based on aluminum by the metallothermic reduction of transition metal compounds. The endogenous process's conducted studies of producing aluminum-magnesium master alloys with REM showed that the reduction of yttrium and scandium compounds contributes to the formation of certain intermetallic compounds.

In the case of presence the compounds of yttrium in the mixture the crystal needles, consisting of Al_3Y and Mg_5Y_{24}, synthesize. On the basis of synthesized master alloy Al-Mg-Mn-Sc aluminum alloys are obtained with thin microstructure and high strength characteristics (100 MPa higher than the standard ones). Al_3Sc particles are the secondary and they allocate from primary solid solution crystallized in a large amount after homogenization of alloys. They are disperse (10 nm) and they have a rounded shape conjugated with the substrate. These particles largely block dislocations and subgrain boundaries, they impede the movement of dislocations and grain boundary migration and ultimately they exert hardening effect on the alloys after deformation [4].

Figure 1. The distribution of intermetallics particles in the master alloy.

Nucleation in the liquid metal environment leads to the formation of various structures, reaching initially the size of a few hundred atoms. Then, depending on the conditions, a spontaneous crystal growth can be, or at this stage the process can be interrupted. Introduction the master alloys, containing nanoscale intermetallic compounds, into alloys, will significantly increase the service life, reliability and product designs in various segments of the industry.

Nowadays also the technologies of intensive plastic deformation (equal channel angular extrusion, twisting under hydrostatic pressure, extrusion, etc.) are developed. With their help it is possible to obtain metal sub-microcrystalline materials and nanomaterials with improved mechanical properties. During the processing of materials in high-energy mills are formed the nanostructured powders, and with using of them the dispersion-strengthened alloys and mechanically alloyed composite powders are synthesized [5].

CONCLUSION

The methods for producing master alloys based on aluminum and magnesium in the conditions of controlled temperature regime is promising for industrial applications. Getting the master alloys of aluminum and magnesium with transitional and REM, aluminum and magnesium alloys thereof, and composite materials involving nanostructured compounds in the long term the scientific and technological interest is increased.

REFERENCES

[1] M.K. Roko, R.S. Uil'yams and P. Alivasatos. Nanotekhnologiya v blizhayshem desyatiletii. Prognoz i napravleniya issledovaniy [Nanotechnology in immediate decade. Forecast and research directions] Mir, Moscow 2002, 292 p.

[2] E.A. Luk'yanova. PhD dissertation, “Issledovanie magnievykh splavov s redkozemel'nymi metallami dlya sozdaniya novykh legkikh konstruktsionnykh materialov” [“Research of magnesium alloys with rare-earth metals for creating new light structural materials”], IMET RAN, Moscow, 2014, 130 p.

[3] V. Yu. Bazhin, Ya. I. Kosov, O. L. Lobacheva, and N. V. Dzhevaga, Synthesis of aluminum based scandium–yttrium master alloys, Russian Metallurgy (Metally) No. 7, 2015 pp. 9–14.

[4] S.V. Aleksandrovskii, V.M. Sizyakov, V.G. Gopienko, B.K. Kim et al., Poluchenie dispersnykh poroshkov titana, tsirkoniya i skandiya i sintez ikh tugoplavkikh nanosoedineniy metallotermicheskim vosstanovleniem khloridov [Obtaining of dispersed powders of titanium, zirconium and scandium and synthesis of high-melting nanocompaunds by metallothermic reduction of chlorides], Ruda I Metally, Moscow, 2006. 243 p.

[5] V.F. Teren'tev, A.G. Kolmakov, D.V. Prosvirnin, Fizicheskie svoystva metallov i splavov [Physical properties of metals and alloys]. Proceedings of the Conference UGTU-UPI. Ekaterinburg. 2007. pp.133-134.

THE EFFECT OF SYNTHESIS CONDITIONS ON THE QUANTITATIVE COMPOSITION OF THE NANOSTRUCTURED METAL OXIDES BASED ON SIO2 - SNO2

A. S. Kanaeva, A. U. Limanskaya* and I. A. Averin
Penza State University

Keywords: nanostructured, oxide, concentration, synthesis, Fourier-spectroscopy, Sol-gel, temperature, spectrograms.

INTRODUCTION

The growing interest in nanostructured materials has stimulated considerable activity in the study of their structure. One of the basic and versatile experimental techniques to determine qualitative and quantitative composition of substances are rentgenodiffraction methods and Fourier spectroscopy.

The relevance of this study is determined by scientific and practical interest in the development of new nanocrystalline materials with high catalytic activity, selectivity to analysed gases, thermal stability.

Therefore, the aim of this work is to develop a methodology and research of quantitative structure of nanocomposite materials based on SiO_2-SnO_2 with an infrared Fourier transform spectrometer.

The objects of study are nanocomposite materials based on SiO_2-SnO_2 with different composition obtained by sol-gel technology.

MATERIALS AND METHODS

To obtain experimental samples were used sols based on SiO_2-SnO_2.

For the study of the quantitative composition of the samples of SiO_2-SnO_2 the method of IR – spectroscopy was used. The method is informative and allows to obtain information about the presence the connection between atoms in the materials of and their concentration quickly.

The obtained samples were investigated by Fourier spectrometer FSM 1201. Typical spectrograms of the samples obtained at annealing temperatures of 100 ° C, at 200 º... 600º C, presented in Figure 1.

* nlim92@mail.ru.

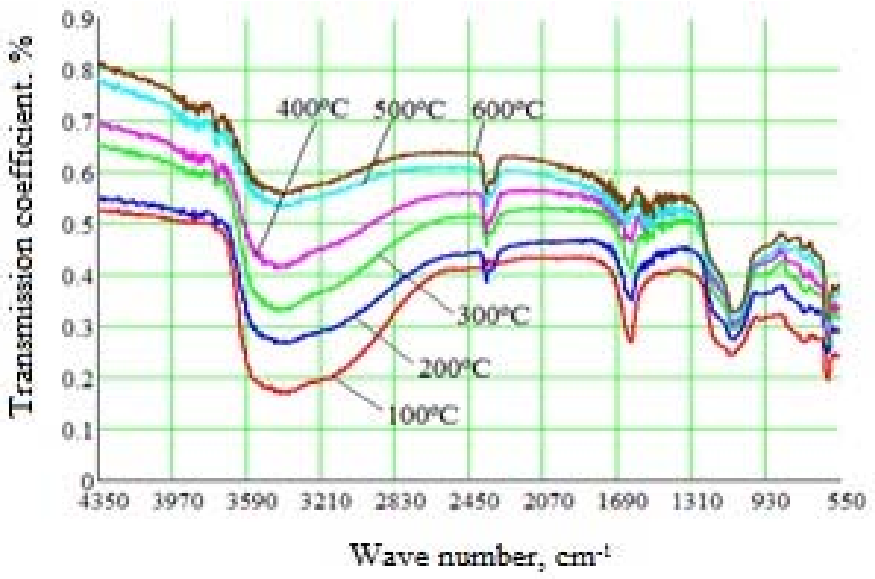

Figure 1. Spectrograms of SiO_2-SnO_2 films at different annealing temperatures.

From the obtained spectra it is seen that the peak on the reverse wavelength (3690 cm^{-1} to 2590 cm^{-1}) corresponds to the O-H links.

QUANTITATIVE ANALYSIS

The integral intensity of link (peak area) is a quantitative characteristic, which is calculated from the spectrum and reflects the changes occurring in the film structure.

A methodology and a universal program for calculating the concentration of components in the samples, studied by means of IR Fourier spectroscopy are developed.

The results of the concentration of O-H calculations depending on the annealing temperature are given in the table.

Data of the concentration of O-H calculations depending on the annealing temperature

Concentration, $C \cdot 10^{-20}$ cm^{-3}	Annealing temperature, ºC
6,3	100
5,5	200
4,9	300
3,3	400
3,2	500
2,9	600

On the basis of statistical processing of experimental data equation relating concentration and the annealing temperature of the samples was found:

$$C = A \cdot e^{-aT} + B \quad (1)$$

where A = 7.35 cm^{-3}; a = 1,88·10^{-3}°C^{-1}; B = 0.332 cm^{-3}.

Calculated and experimental values of link concentration depending on the annealing temperature is shown in Figure 2.

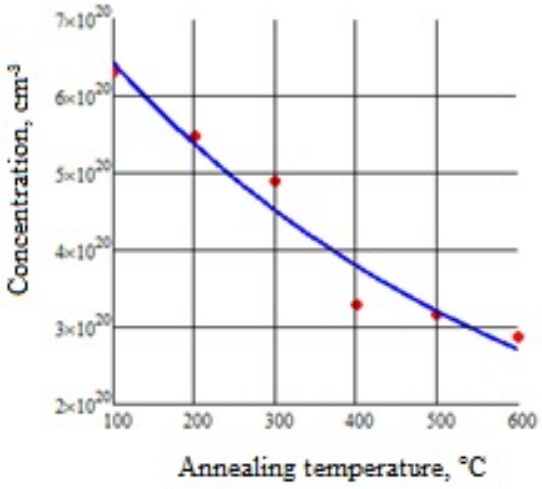

• Experimental data — - calculation by equation (1)

Figure 2. Dependence of the concentration on the annealing temperature.

From Figure 2 it is seen that there is a good correlation between experimental and calculated values, indicating the validity of the developed technique for determining the link concentration

REFERENCES

[1] Kovtonuk N. F. Measurement of parameters of semiconductor materials// Kovtonuk N. F., Kontsevoy U. A. – Moscow: Metallurgy, 1970. – 432 p.

[2] Averin I. A., Karmanov A. A., Pecherskaya R. M., Pronin I.A. Features of the synthesis and study nanocomposition films obtained by sol-gel technology// *University news. Povolzhsky region. Ser. "Physics and mathematics." – 2012.* - №2 (22). – p. 155-162.

[3] Averin I.A., Igoshina S.E., Karmanov A.A., Pronin I.A., Moshnikov V.A., Terukov E.I. Technical Physics. Sensitive elements of vacuum sensors based on porous nanostructured sio2-sno2 sol-gel films. The Russian Journal of Applied Physics. 2015. T. 60. № 6. C. 928-932.

[4] Sigaev A. P., Averin I. A., Karmanov A. A., Igoshina S.E. Definition of the concentration of the adsorbed gases on the surface of the SIO 2-SNO 2 two-component system by the method of IR-spectroscopy. – 2015. – Vol 2. – p. 88-91.

[5] Averin I. A., Sigaev A. P., Pronin I.A., Kudashov A. A., Igoshina S.E. Karmanov A. A. The study of the qualitative composition of nanostructures on the basis of SIO 2, SIO 2-SNO 2, SIO 2-SNO 2-IN2O 3 and its dependence on the annealing temperature. – 2014. – p. 521-523.

INVESTIGATION OF LASER MICROMACHINING OF ZINC OXIDE

D. N. Redka*

Saint Petersburg Electrotechnical University "LETI"
Saint-Petersburg, Russia

ABSTRACT

Big size (~1,4м2) silicon-based thin-film solar module (SM) consists of elements connected between each other in a way to get the maximum efficient solar energy conversion in the output. In solar modules production the technological process of separating elements is realized using laser scribing. As a result, the SM area will consist of "active area," where the photoeffect occurs, providing the current constituent part of the converted energy, and "dead zone," which does not participate in photo-electric current generation, but it is a required element for effective separate elements commutation.

The research includes analysis of possibility to decrease the "dead zone" and to increase the parameters of electrical energy output. This can be achieved both by decreasing the width of scribes and by optimizing the commutative connections of SM elements. In terms of precision and quality of manufacture the shape and type of the scribes depend on laser irradiance parameters used in technological process of division of SM into separate elements.

Keywords: ablation, laser ablation, scribe, transparent conductive thin films of zinc oxide(ZnO), "dead zone," shunting effect, laser beam energy, scribe profile

INTRODUCTION

Thin-film solar module (TFSM) of large square (~ 1.4 m^2) based on silicon consists of separate elements interconnected in a certain way to ensure the most efficient conversion of solar energy into electrical energy. In the production process TFSM separation into individual components is carried out using laser scribing techniques [1].

This technology is described in detail in [2], where the laser scribing advantages are established and evidence given that use of this method of TFSM switching elements based on a-Si (amorphous silicon) can increase power output of the product by 20% as compared to mask using method [3]. Process flow throughout the manufacturing cycle of TFSM includes several stages of scribing, called Pattern (iterative design template). The aim of our work is to study the possibility of improving the electrical characteristics TFSM by increasing the area not occupied by laser marking. One way of solving this problem is to improve the quality of

* dnredka@gmail.com.

cuts, in particular in case Pattern1 (P1), where the segmentation of the front contact from zinc oxide (ZnO), deposited on glass is performed.

EXPERIMENTAL

The glass film with deposited thereon zinc oxide was used as an experimental sample. Processing of the sample was performed by laser radiation with a wavelength of 355 nm, the laser pulse energy ranged from 14 mJ to 21 mJ (measurement error of the laser beam energy of 0.05 mJ). There were seven groups for different cuts of focus distance that vary in increments in 0.1 mm. Each group included five consecutive Scribes obtained with the power of laser pulses of 14 mJ, 16mJ, 18 mJ, 20 mJ, 21mJ, respectively. Pulse repetition rate was 60 kHz and a pulse duration was 30 ns. The intensity of the laser pulse has a shape close to a Gaussian distribution with a maximum at the center of focus of the beam. Data matrix was obtained during the experiment. Primary control Scribe was performed using optical microscopy. Photographing of groups of Scribes was conducted in different coordinates of the sample. There was detected Scribe, which has the following characteristics: a minimum width on the surface of 27 ± 0,5mkm Scribe, Scribe at the bottom (on the side of the glass substrate), the width is 25 ± 0,5 mkm; width of cut on the surface and at the bottom is constant in different coordinates of the cutting length; minimum number of chips and no shunt elements. This Scribe was obtained by defocusing value (the distance from the focus to the treated surface) of the laser beam by 1.5 mm and a laser pulse energy of 20 mJ. When passing by through the glass beam was focused to the treated layer ZnO.

RESULTS AND DISCUSSION

During the experiments it was found that at low energies of the laser pulse (less than 3 mJ) it is impossible to obtain uninterrupted Scribe, as a result there are shunts. The value of the width of the resulting “track” is an important factor. Increasing the width of cut reduces the active area of the solar module, as a consequence, the decrease of the photocurrent values of the solar module (photocurrent depends on the “active area” involved in the generation of charge carriers) [1]. At this stage, the problem is the need to reduce the area of “dead zone.”

One way to reduce the area of “dead zone” is to reduce the width of the Scribe. In [5,6,7] Scribe P1 width is more than 40 microns. With such widths Scribe the area of “dead zones,” which is undesirable increases significantly. In [8] width Scribe is 25-27 microns, the measurement has been carried out in a single coordinate system, in the area of the module, where the thickness of the front contact does not differ. In case of measuring the width Scribe in other areas, where the thickness of ZnO may take other values, the width Scribe will vary.

The power of the laser radiation used in the processing has a direct influence on the cutting depth (Scribe). Scribe depth determined by the equation:

$$h \approx Pt / \left(\pi r_0^2 L_u\right) \tag{1}$$

where P-power of laser beam, t- duration of the laser pulse, r_0 - the radius of the laser spot on the surface to be treated, L_u - hide heat of vaporization.

Laser spot size will also affect the width Scribe. The dependence of the width of the Scribe on the laser spot size is described by equation:

$$l \approx 2\left(r_0 + P\,\mathrm{tg}\,\gamma / \pi r_0 L_u\right) \tag{2}$$

If using equation (1) we determine r_0 and put the value obtained in the equation 2, we obtain the following relation:

$$l \approx 2\left(\sqrt{P t / h \pi L_u} + P\,\mathrm{tg}\,\gamma / \pi r_0 L_u\right) \tag{3}$$

where l - Scribe width - half angle of the focused beam impinges on the sample, h- thickness of ZnO layer in place of the laser beam.

Knowing what values of laser power remove the needed material, Scribe depth can be correlated with the film thickness. Thus, the equation (3) determines Scribe width dependent on the following variable parameters of the laser radiation: P and t. In this paper, the laser pulse duration t remained constant, only the focal length of the optical system and the power of the laser beam changed.

It should be noted that the Scribe widths are also effected by the unevenness of thickness of the substrate (glass). Film ZnO that is processed is deposited directly on the glass. When processing laser beam must be focused on the film itself. When scanning the surface with a laser beam because of the uneven thickness of the glass, the film may periodically fall in defocus area therefore the size of the laser beam in the treated area will vary. When the film is in focus the laser beam, that is minimum. However, the treatment by focused beam Scribe brings more melts and spray the material at the edges. These defects afterwards, with high probability, may become shunt elements that will increase the number of defective SM at this stage of production. The appearance of melts using the laser beam of the minimum radius can be explained by the fact that as a result of focusing of the laser beam at the processing spot film of the beam power density per unit area (W/m^2) increases sharply. These adverse effects can be avoided, on the one hand, by reducing the power laser with an attenuator to energy levels that do not appear melts ZnO. However, this option is not acceptable in view of the fact that the treatment area where it is necessary to ensure the minimum radius of the laser beam oscillates strongly due to variations in thickness of the glass. This in turn leads to oscillation of the beam power density per unit area (W/m^2) .This means that the processing with focused on the film the laser beam quality ZnO scribing occurs only at a fixed thickness over the entire area of the glass but, as the glass has a non-uniform thickness (± 0,06 mm), a laser beam is at different moments focused either in the glass or above film ZnO. As a result, for a given processing mode we obtain unsatisfactory results of treatment, since it does not provide the required level of the laser power, sufficient for removing the material. Based on the foregoing, it is expedient to proceed in the region where the oscillation power of the laser beam per unit area (W/m2) is minimal. This area is the defocusing area where r_0 is more than the minimum. Switching to defocusing provides better and more uniform treatment, but automatically leads to an increase in the width of the Scribe l.

CONCLUSION

Processing with of optimum focus settings allows to obtain correct geometrical form of cuts, the width of which is almost independent of the ZnO film thickness unevenness (in the case cutting width variations differ in less than 0.5 microns), with a minimum number of chips and absence of the shunt elements. Implementation of the results achieved in the TFSM production technology will increase the output current by reducing the area of laser micromachining (compared with typical TFSM produced by this technology).

ACKNOWLEDGMENTS

This study was supported by Russian Science Foundation, project № 14-12-00327.

REFERENCES

[1] Shah Arvind. Thin-film silicon solar cells. Lausanne: EPFL Press, 2010.S. 331-336.

[2] Kuwano Y. et al.: Amorphous Silicon Integrated Cell Modules (I)/1st Photovoltaic Sci. & Engg. Conf. in Japan, (1979) 55.

[3] Kiyama S., Matsuoka T., Hirono Y.et al. Laser Patterning of Integrated-type a-Si Solar Cell Submodules/*Journal of the Japan Society for Precision Engineering*. 1990. № 11, PAGE.2069-2074.

[4] Haas S., Ku V., SchopeG.et al. Patterning of thin-film silicon modules using laser with tailored beam shapes and different wavelengths/23th European Photovoltaic Solar Energy Conference Valencia, Spain, 2008. Pages 2383-2387.

[5] Schoonderbeek A., Schuts V., Haupt Oliver, and Stute U. Laser Processing of Thin Films for Photovoltaic Applications//*JLMN Vol*. 5, No.3, 2010.Pages 248-254.

[6] Buzas A., Geretovsky Zs., NemethA. et al. Selective cutting of ZnO: Al contact layers/24th European Photovoltaic Solar Energy Conference. 2009 Pages 3004-3006.

[7] Canteil D., Fernandez S., Molpeceres C. et al. Nanosecond laser ablation processes in aluminum-doped zinc-oxide for photovoltaic devices/Applied Surface Science15 September 2012, Pages 9447–9451.

[8] Booth H. Laser Processing in Industrial Solar Module Manufacturing//JLMN Vol. 5, No. 3, 2010.

INFLUENCE OF THE TRIAMON UNDERLAYERS ADSORPTED ON THE INTERFACE ON TRIBOCHEMICAL CHARACTERISTICS OF THE METAL-LUBRICANT SYSTEM

A. G. Syrkov[1,*], T. G. Kamalova[1], V. R. Kabirov[1], V. S. Kavun[2] and K. L. Levine[1]

[1]Mining University, St. Petersburg, Russia
[2]Lappeenranta University of Technology, Finland

ABSTRACT

In this research the influence of mixed and consistent chemisorption of differently sized molecules of quaternary ammonium compounds (alkamon and triamon) on disperse aluminum on its properties. As a part of the research the lubricants containing modified aluminum were tested. It was discovered that as the hydrophobicity of Al-additives increases, the force of friction (F_{fr}) and coefficient of friction (f) decrease. It was discovered that Al-additives with external layer of ethylhydridesiloxane and only one underlayer of triamon has the best anti-frictional effect. The addition more T-underlayers (from 1 to 3) did not give a significant improvement. The force of friction (F_{fr}) and coefficient of friction (f) were measured for tribosystems, containing ten types of differently modified Al-additives.

Keywords: chemisorption of quaternary ammonium compounds, aluminum, anti-frictional effect, influence of the triamon underlayers, ethylhydridesiloxane on surface of metal, Al-containing lubricants

INTRODUCTION

Consistent (mixed) chemisorption of quaternary ammonium compounds such as alkamon (A) and triamon (T) proved to be a potentially successful method of regulation of tribochemical properties of modified metals [1-3]. As a result of this research, sample based on aluminum powder (PAP-2) with external layer of hydrophobic silicone liquid (HSL) above the underlayer of triamon was obtained. The influence of the presence of T-underlayer on the force and coefficient of friction of the heterogeneous system with oil I-20 with the Al-additives was studied. The sample with external layer of HSL was obtained by the adsorption of HSL from its vapors on Al-powder with already applied underlayer of triamon.

* Corresponding author: syrkovandrey@spmi.ru.

EXPERIMENT AND RESULTS

Methods of modification of powder were fully described in prior researches [2, 3]. Force of friction (F_{fr}) and coefficient of friction of system with oil I-20 with Al-additives was determined by using friction testing machine (DM-29M). The tribological pair was Steel 45 (GOST 1050-88) – Bronze Br Aj 9-4 (GOST 18175-78).

In prior researches, the influence of different modes of modifications, using alkamon and triamon on hydrophobicity and integral index of friction (D), was described. The integral index of friction (D) is proportional to the coefficient of friction. Fundamental tribological characteristics (F_{fr} and f) of systems with oil I-20 with different additives were measured.

Additives modified in a mixture of vapors of A and T (Al/(A+T)) and additives with T-underlayer (Al/T/A, Al/T/HSL) improve the anti-frictional properties of oil I-20 the most. As it is shown in the table the reduction of force of friction in comparison with initial oil I-20 can be up to 16%. Measurement error of F_{fr} is less than 1.5%. Al/HSL sample does not improve the anti-frictional properties of oil I-20, but after the addition of T-underlayer, Al/T/HSL sample improves the anti-frictional properties significantly. The application of 2 or 3 T-underlayers does not improve anti-frictional properties (samples 7, 8). The most efficient out of all Al-additives are the additives which have under the layer of alkamon or HSL a layer of triamon with the small (C_1–C_2) organic substituents on the nitrogen atom. We have concluded that this is due to the steric availability of the nitrogen atoms in the triamon, which eases the forming of heteroatomic interaction between nitrogen and metal and between triamon and external layer of A or HSL. High level of adhesion between metal and a layer of surfactant is necessary to obtain good anti-frictional properties of the sample at high load pressure [1, 4].

Table. The influence of type of Al - additive (0,5 % by mass) on $F_{fr} = \Phi(N)$ equation, the change of F_{fr} (ΔF_{fr}) and coefficient of friction (f) in comparison with the initial lubricant (I-20)

№	Al - additive (lubricant)	$F_{fr} = \Phi(N)$ equation	R^2	ΔF_{fr} (average), %	ΔF_{fr} (N = 5 кN), %	f (N = 3.5 кN)
1	Al/(A+T)	y = 0.037x + 12.47	0.991	-11.41	-15.92	0.0075
2	Al/T/HSL	y = 0.043x + 12.15	0.986	-7.42	-5.99	0.0075
3	Al/T/A	y = 0.048x + 10.81	0.992	-7.75	-3.69	0.0079
4	Al/A	y = 0.050x + 12.05	0.997	-1.05	-1.40	0.0089
5	I-20 (no additives)	y = 0.050x + 12.29	0.994	0	0	0.0089
6	Al/T	y = 0.050x + 11.86	0.999	-1.52	0.13	0.0087
7	Al/T/T/HSL	y = 0.049x + 12.49	0.993	-0.21	0.89	0.0085
8	Al/T/T/T/HSL	y = 0.048x + 12.50	0.995	-0.20	0.88	0.0086
9	Al/T/T	y = 0.051x + 11.59	0.994	-1.59	0.89	0.0086
10	Al/HSL	y = 0.048x + 13.22	0.994	2.32	3.80	0.0086
11	Al/A/T	y = 0.050x + 12.68	0.992	1.96	3.95	0.0085
12	Al (PAP-2)	y = 0.065x + 11.74	0.997	12.61	20	0.0101

CONCLUSION

Due to the small size of molecules of triamon and steric availability of the nitrogen atoms application of underlayer of triamon eases the stabilization of structure and properties of the surface of the metal. Obtained results show that application of T-underlayer is a potentially successful way of improvement of anti-friction properties of Al-additives. The linearity of the boundary friction equation can be changed by the addition of T-underlayer. Also, the value of summand (from 10.8 to 13.2 N) which stands for the amount of intermolecular forces in the boundary friction equation can be regulated in Al – additives by adding low-molecular T – underlayer.

ACKNOWLEDGMENTS

The authors thank M.O. Silivanov for the adjustment the method of measuring the friction force and for carrying out some of the measurements. This work was partially financed by Ministry of Education and Science of the Russian Federation in the frame of the governmental contract (projects 5279, 8635 and 10.1392.2014/K).

REFERENCES

[1] D.S. Bystrov, A.G. Syrkov, I.V. Pantyushin, T.G.Vakhreneva, Anti-frictional properties of industrial oil with additives with nanostructured metals, *Chemical physics and mezoscopy,* Vol. 11, No.4, pp. 462-466 (2009)

[2] A.G. Syrkov, Synergetic enhancement of reactivity of aluminum in presence of quaternary ammonium compounds on the surface, *Journal of General Chemistry*, Vol. 83, No.8, pp. 1392-1393. (2013)

[3] A.G. Syrkov, D.V. Fadeev, V.V. Taraban, M.O. Silivanov, Quantification of non-linear effects of the dependence of the integral index of friction of tribosystem on water-repellent properties of the metal filler, *Condensed matter and Interphase boundaries,* Vol.16, No. 2, pp. 215-219. (2014)

[4] *Surface Phenomena and Surfactants. Reference Book,* A.A. Abramzon, E.D. Shchukina. Leningrad: Chemistry, 1984. p.392.

INFLUENCE OF CHROME-OXIDE NANOSTRUCTURES ON THE CONDITION OF THE DISPERSE BORON NITRIDE SURFACE AND HEAT CONDUCTIVITY OF THE POLYMERIC COMPOSITE

A. A. Malkov[1], M. A. Alekseev[1], N. V. Zakharova[1,*] and A. E. Verstakov[2]

[1]Saint-Petersburg State Institute of Technology (Technical University);
[2]Federal Unitary Enterprise SCTB "Technologist"

Keywords: heat conductivity, composite materials, surface modification

INTRODUCTION

The solution of the problem of creation of the high-heat-conducting materials possessing good dielectric properties is an actual problem of materials science. One of the solutions of this task is using of the polymers which have high insulating properties, simplicity of receiving, light weight and low cost. However low thermal conductivity of polymers is their essential disadvantage. For improvement of the heat exchange the fillers with rather high heat conductivity are entered into polymeric material composition. But there are some limiting factors during the exploitation of such composites and the main one is the limit of phase boundary between a matrix and a filler, which reduces conductivity of composites [1]. It is possible to reduce the influence of phase boundary on composite's heat conductivity by increasing of the adhesion between two phases (filler and polymer matrix). The most perspective way of increasing of the adhesion is the modification of a filler's surface, which allows to form strong and homogeneous bonding with a matrix [2].

Among variety of methods of regulation of phase boundary character in polymeric composites is the method of the molecular layering (ML), which is known in foreign works as atomic layer deposition (ALD), can be used. This method is based on the realization of cyclic chemical reactions between the active centers of a solid-phase matrix's surface and low-molecular reagents from a gas or liquid phase in the conditions of the maximum removal from the balance [3].

In this work the changes of a hexagonal boron nitride surface state, which are caused by carrying out the synthesis of chrome-oxide nanostructures by the ML method is considered. The assessment of influence of filler's surface modifying on heat conductivity of composite material has been carried out.

* zakharova@lti-gti.ru.

The objects of research are the hexagonal BN with a specific surface area is 8,4 sq.m/g, the low-molecular reagents CrO_2Cl_2 and C_2H_5OH, which have been chosen for modifying of a surface, and epoxy polymer EP-9150 (TU 16-504.054-84), which has been chosen for creation of composite material.

The synthesis of chrome-oxide nanostructures has been carrying out on the facility with the reactor of flowing type by the way of the serial processing (1 – 4 times) of the disperse BN by vapors of CrO_2Cl_2 and C_2H_5OH at 180°C. The character of formation of the nanostructures has been studied by chemical analysis, IK-spectroscopy of diffusion reflection (DRIK), spectroscopy of diffusion reflection in UF and visible area. Registration and differentiation of the donor-acceptor centers of the boron nitride sample's and the products of its modifying surface have been carried out by use of the acid- base indicators with pKa values in the range of –4,4 ÷ 12,8.

Assessment of the original sample of BN by the indicator method shows the presence of the Lewis's base centers on the surface and the Bronsted's acid centers with pKa = -4,4; 2,5; 12,0 and 12,8, which are relevant, according to the results of IK-spectroscopy, to functional N-H and B-ON groups, which are capable to take part in synthesis process. The increase of the content of chrome as a part of the modified filler from 1,7 μmol/sq.m to 10,9 μmol/sq.m is registered during of the synthesis process after carrying out one and four cycles ML respectively. It is shown, that the main active centers on the original BN surface, which take part in interaction with molecules of CrO_2Cl_2, are the Bronsted's centers with pKa = 2,5.

The received polymeric compositions possess the increased heat conductivity (1,08 W/m*K) in comparison by the composition containing not modified filler (1,01 W/m*K).

Work has been done with partial support of a grant of RSF (demand No. 14-13-00597) and the Ministry of Education and Science (the state task for No. 601 SRW)

REFERENCES

[1] Karnthidaporn Wattanakul, Sittisak Satasit. The Versatile Method to Control the Orientation of BN Particles in Thermoset Matrix//*J. Chem. Chem. Eng*. 6 (2012) 769-773.

[2] Thermal Conductivity of Polymeric Composites: A Review. I.A. Tsekmes, R. Kochetov, P.H.F. Morshuis, J.J Smit//*IEEE International Conference on Solid Dielectrics,* Bologna, Italy, June 30 – July 4, 2013. – P. 678 - 681.

[3] Malygin A.A. The Molecular Layering Nanotechnology: Basis and Application.// *J. Ind. Eng. Chem.*- 2006.- V. 12, No 1.- P.1-11.

NANOSTRUCTURED FUNCTIONALLY GRADIENT COATING FOR THE PROTECTION OF STRUCTURAL ELEMENTS FROM CORROSION AND WEAR

T. I. Bobkova* and B. V. Farmakovsky
Federal state unitary enterprise Central research institute of
structural materials "Prometey"

ABSTRACT

A technology for creating nanostructured composite powders for spraying was developed.. Studies on the development and application of thermal spraying methods for functionally graded coatings production have been conducted. A hardness gradient over the cross section of the coating was investigated. The present study shows the possibility of the formation of thick coatings with controlled hardness.

Keywords: nanostructured composite powders, coating, functionally gradient coating, hardness gradient, combining methods of spraying

INTRODUCTION

In the world practice technologies based on the manufacture of products from low-cost , well- processed material and following coating formation the coated to provide the required surface properties are widely used. The direction of technology for repair and restoration of worn parts and units of equipment is also highly relevant. Analysis of published data shows that the further development of such areas as thermal spray coating deposition techniques is on the way of improving the properties by using nanostructured raw powders [1, 2, 3]. Nanostructure is conditioned by bringing nanopowders into conventional powder for spraying, followed by fixing it with an adhesive agent or by a partial implementation [4]. The practice shows that the introduction of nanopowders allows to obtain much better properties than by spraying traditional powders [5]. On the base of the data concerned to implemented nanopowder quality it also allows to predict accurately the properties such as hardness, porosity and adhesion. It is also important not only to achieve high properties of sprayed coatings , but also to ensure their uniformity throughout the entire volume of the coating. Introduction of nanoparticles of superhard materials increases the sprayed coating hardness, and its isotropy in the coating will directly depend on the uniform distribution of the nanoparticles and the strength of their adhesion to the matrix. Therefore it is very important to achieve uniform content of nanoscale components in the powder for spraying at the stage of nanostructure formation in it.

* taby87@mail.ru.

DESCRIPTION OF THE METHOD

In the Federal State Unitary Enterprise “Central Research Institute “ Prometey “ several technologies for creating nanostructured composite powders for thermal spraying has been developed .The most efficient and economical method of creating composite powders with a surface nanostructure, based on the joint processing of matrix and reinforcing powders mixture in a high speed cup attritor .During the short (no more than 3 minutes at a rotational speed of cups 1400-2000 rev/min) process of mechanosynthesis the introduction of nanoparticles in the surface of micron-sized powder matrix takes place and a bond between the matrix material nanopowder is formed. That provides strong adhesion and prevents the removal and displacement of the reinforcing phase during subsequent spraying.

As In this method the matrix powders are conventional metal powders (Fe, Al, Mg, Mn, Cr, Co, Ni, Ti, Zn, Cu,) and their alloys, and the reinforcing component are nanopowders of carbides oxides , nitrides, borides , carbonitrides, etc obtained by plasma method [6]. Reinforcement with various nanopowders effects on the properties of the sprayed coating in various ways, so reinforcing with MgO, NbB_2 increases coating thermostability, additions of WC, TiN, Al_2O_3, TiCN increase the coating hardness. In general, the use of the composite surface- reinforced powders for spraying enhances the stability of the process running due to the configuration and spheroidal shape of the powder particles. Nanostructured powder materials synthesized in the Federal State Unitary Enterprise “Central Research Institute “Prometey,” are sprayed with supersonic “cold“ gas-dynamic and microplasma methods. Layer-specific alternating of materials during spraying can create a gradient of properties , such as hardness , porosity , etc. along the cross section of the coating The most interesting directions in creating wear-resistant coatings for the protection and recovery of critical parts and components of modern engineering is creating a gradient of the coating hardness. In addition to the alternating materials during the functionally graded coatings spraying combination of technological methods of spraying are successfully used. Application of the technology of functionally graded coatings (FGC) creation provides obtaining a thick coating with high adhesive and cohesive properties, with a uniform increase in the hardness from the substrate to the surface layers. In the course of the work a comprehensive study of the FGC properties both cross-sectional and layer by layer were carried out. A method of layer wise determining of the friction coefficient in the coating was developed. Also, Experiments with magnetron sputtering deposition of FGC TiN layer onto the surface to improve corrosion resistance in fresh and sea water were also conducted.

CONCLUSION

The studies have shown that the combination of technological options during spraying of layers of composite powders of various systems provides the FGC with recurrent layers including plastic and reinforcing components, whereby high values of hardness and corrosion resistance of the surface layers in combination with high adhesive properties are achieved.

It was established experimentally that the application of such technological options for creating a properties gradient increases significantly the performance capabilities of the coatings: toughness, corrosion resistance, wear resistance. This approach is promising for the

creation of new ship fitting parts and reconstruction of worn ones, as well as of the critical parts and components of modern engineering, which have to meet high requirements to hardness and wear resistance.

REFERENCES

[1] Siegmann, S. The role of nano-particles in the field of thermal spray coating technology/S.Siegmann, M. Leparoux, L. Rohr/*Proc. of SPIE Nanotechnology and Nanophotonics,* Dublin, Ireland, 2005-2005.-p. 224-231.

[2] Chawla V. Performance of plasma sprayed nanostructured and converntional coatings/ V. Chawla, B.S. Sidhu, D. Puri, S. Prakash/*Journal of the Australian Ceramic Society*.-2008.-Vol. 44.-№2.-p.56-62.

[3] Gell, M. Development and implementation of plasma sprayed nanostructured ceramic coatings/ M. Gell et al./ Surface and Coatings Technology.-2001.-Vol. 146.-p.48-49.

[4] Kerber M.L. *Polymer composite materials Structure Properties. Technologies.* - SPb .: Professia (2008) – 560.

[5] Grigoriev MV Influence of ultrafine Al_2O_3 additives on physical and mechanical properties of alumina ceramics/M. Grigoriev, EI Stepanov , Kirko VI/Journal of the NSU . -2008 .-№1.from. 162-167.

[6] Alekseev N.V. Physical chemistry and technology of plasma-chemical synthesis of nanopowders of elements and compounds/Y. V. Tsvetkov, A.V.Samokhin, N.V. Alekseev , Y.V.Blagoveschensky/II- th International Nanotechnology Forum , Moscow, October 6-8 , 2009 , at s.498-500.

NANO- AND THE MICRO-DIMENSIONAL COATS POLYCRYSTAL TITANIUM-CONTAINING THE BASES A METHOD OF ELECTROCHEMICAL BORONIZING

E. S. Gorlanov[1,*] and V. Yu. Bazhin[2,#]
[1]Expert-Al Ltd., Saint Petersburg, Russia,
[2]Gorniy University, Saint Petersburg, Russia,

ABSTRACT

The technology for the production of wettable aluminium coating was implemented using the method of electro-chemical borating of the carbon-titanium cathode directly at the electrolytic reduction of cryolite-alumina melts in laboratory conditions.

TiC and TiB_2, responsible for the wetting effect, were detected by X-ray phase analysis of cathode surface layer. The mechanism of electro-chemical and chemical processes of Ti-B-C compound formation in the subsurface cathode volume is proposed for the discussion.

Keywords: electro-chemical deposition, borating, carbon-titanium cathode, wettable coating

INTRODUCTION

Attempts to create coatings by an electrochemical technique often undertaken on graphitized carbon items, is more exact on a surface of cathode blocks in the conditions of an electrolysis a cryolite-alumina melts [1–5]. But, from the physical, hence, energetic and electro-chemical point of view the non-uniform surface of composite materials represents a main restriction for the creation of coherent layer of double and triple compounds in the system Ti–B–C.

The possibility to avoid this restriction and chances for the formation of even and uniform wettable coat in the subsurface layer of the cathode appear when reduced elements (i.e., boron) interact not only with cathode material but with its specially inserted impurities as well (with titanium, in our case). Thus, the essence of the proposed method consists in the electrochemical borating of carbon-titanium cathode.

EXPERIMENT AND DISCUSSION

All experiments were performed at 970÷990°C in an electrolyte with CR = 2.5 at the electrolysis unit. The installation was connected to the electrolysis with a

* gorlanove@yandex.ru.
# bazhin-alfoil@mail.ru,

constant purging of the cell atmosphere with argon. Intrinsically the joint electrical deposition of aluminium and boron onto cathode took place in galvanostatic conditions.

After their removal from the melt the pictures of the specimen were taken, then the specimen were mechanically treated against electrolyte to be sampled for the X-ray phase analysis and for the preparation of metallographic sections to be used in the electronic microscopy.

In this chapter we discuss the results of some from more than 30 experiments that were obtained at the current densities of 0.4–1.3 A/cm^2. After electrolysis on the cathode surface was formed a layer of aluminum 3÷5 mm with good adhesion to carbon (Figure 1).

Thus, the SEM-EDS analysis founds the surface 500 μm layer of titanium carbo-boride with rather good wetting properties in respect with aluminium (Figure 2). After separation of the aluminum from the cathode layer SEM-EDS analysis of the exposed areas is fully preserved surface boundaries of the aluminum-carbon reverse previously inaccessible. Figure 3 shows the segment with indication of some points where the analysis was carried out.

On closer examination in compositional contrast, the field of dark color represents a textured mixture of carbon particles, adjacent to the light field that is located below (between the layer of aluminium and carbon surface). As EDS-analysis shown, this light field represents the layer of borides, generated during the 42-hour experiment. Points 2 and 4 represent boride-titanium compositions of $TiB_{2.8}$ and $TiB_{3.2}$ accordingly.

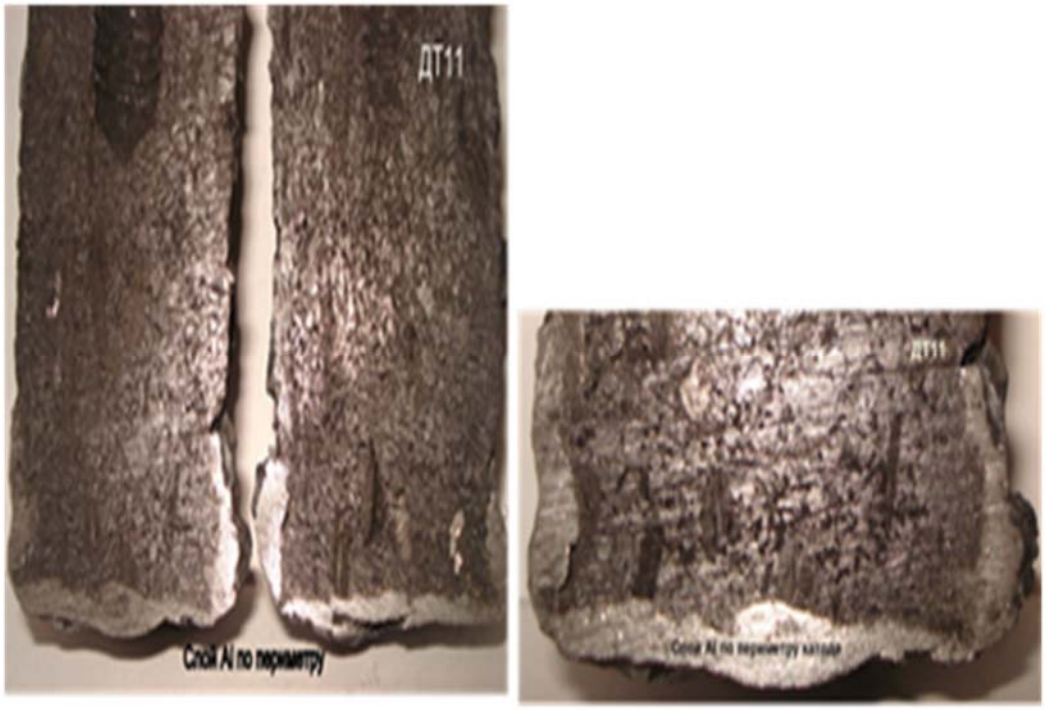

Figure 1. Longitudinal section of DT11 specimens.

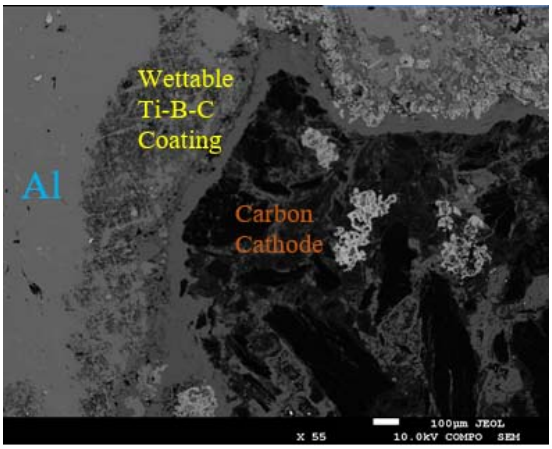

Figure 2. Microstructure of the DT11B specimen (x55). The cross-section.

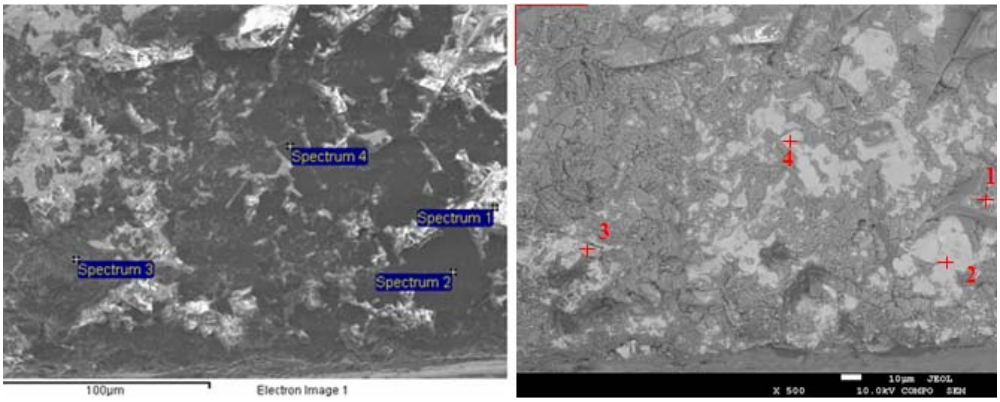

Figure 3. View of microstructure DT11T from reverse side (x500): a) in secondary electrons; b) in back-scattered electrons.

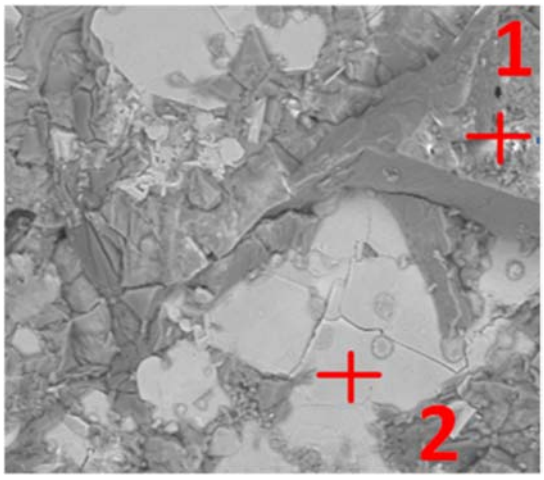

Figure 4. Enlarged field at the area of points 1 and 2.

In order to illustrate the mentioned above, we enlarged one of the field of the segment under examination (Figure 4). In fact, this is the first time when we visually observe the boride-titanium buildup – fragment of wettable coating (field with point 2) not in profile, but fullface.

What stands out on the aluminium map is bright nodal points; they being concentrated in the field of titanium diborides. On Figure 5 is clearly visible that nodal points on the aluminium map correspond to the 2 μm circular buildups. We suppose that these nodular buildups belong to the aluminium layer, situated below, that has penetrated into 2 μm pores of boride-titanium coating and was stopped by carbon surface of the cathode.

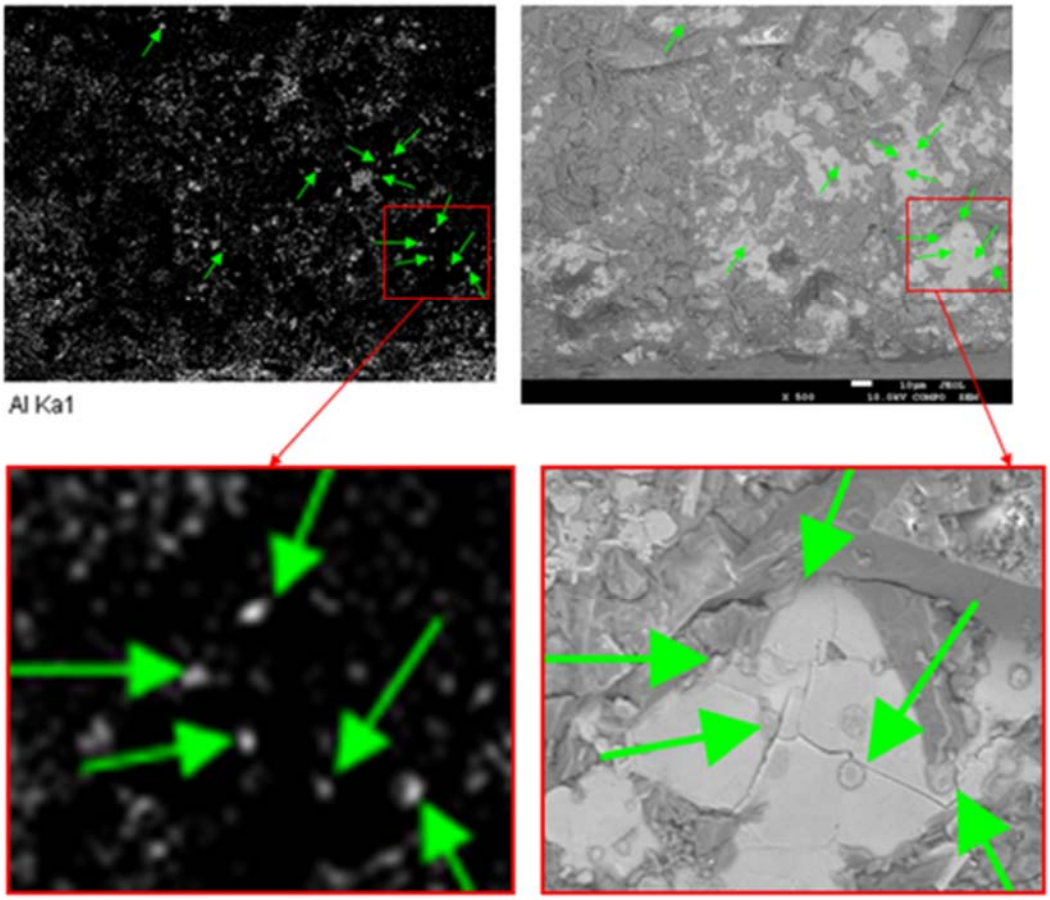

Figure 5. Microstructure of the segment DT11T. Highlighted fields.

Data obtained allow assuming that the transfer of titanium in liquid phase takes place in parallel with the solid-phase diffusion. During the electrolysis the titanium-bearing buildups of Ti, Ti_xO_y and $Ti_xO_yC_z$ in the cathode body are subjected to the impregnation and dissolution with filtrate of electrolyte. As a result the conditions appear for the quick and efficient distribution of titanium in its atomic and ionic states, in elementary form and in form of oxides. Thus, titanium would be evenly distributed in any form within the carbon body to the depth of cathode impregnation with electrolyte if the exposure time would be rather sufficient.

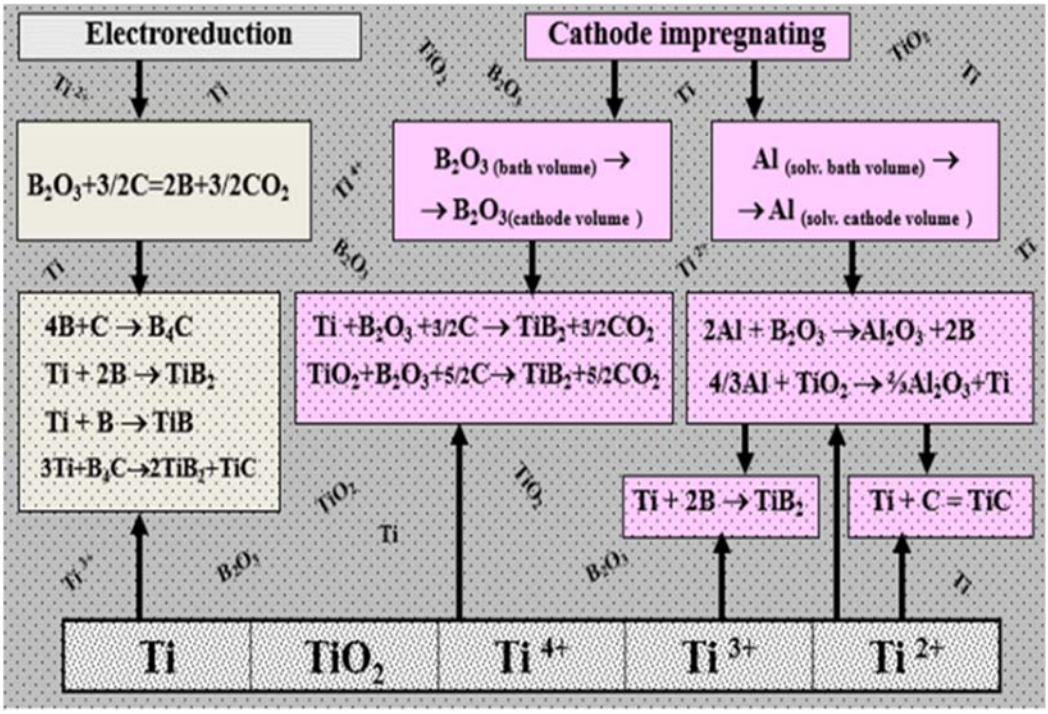

Figure 6. Formation mechanism of the Aluminium-Wettable Coating.

When arranging the opposite flow of boron and aluminium solutions in their elementary form or in form of compounds the conditions would be created for direct interaction of main components of the wettable coating and preliminary stage of boron and titanium reduction from oxides by dissolved aluminum. These active forms would finally interact to the generation of titanium borides $Ti+2B = TiB_2$.

Graphically, discussing the mechanism can be represented by the scheme 6.

The reactions under discussion go with high heat emission. Therefore, it is quite possible that the temperature within the reaction zone would drastically increase to the initialization of endoergic reactions:

$$TiO_2 + 2C \leftrightarrows TiC + CO_2$$

$$TiO_2 + 2C \leftrightarrows TiC + 2CO$$

The further development of solid phase processes could create conditions for the formation of complex compounds in the system Ti–B–C, e.g., $xTiB_2 + yTiC \rightarrow xTiB_2 \cdot yTiC$.

So, at the electrochemical borating of the cathode to the depth of electrolyte penetration into the carbon-titanium array the aluminium-wettable layer of titanium borides Ti_xB_y and carbo-borides $Ti_xB_yC_z$ would be generated. As the opposite flows of boron and titanium are determined by their transfer in liquid phase, i.e., these transfers have a relatively high rate, the generation of these compounds occurs within the subsurface impregnated volume of the cathode without forming any laminar structure and composition.

CONCLUSION

Thus, in laboratory conditions the process of producing Al-wettable subsurface layer was developed and carried out by method of electrochemical borating of carbon-titanium cathode. Visual inspections of the specimen after electrolytic experiments show obvious wetting of the carbon surface with aluminium, having a good adhesion of the metal to the cathode. The cause of carbon cathode wetting with aluminium was found – the presence of 100-500 μm subsurface layer of carbide-boride compounds that were synthesized during the 20-42-hour electrolytic cycle. The results of XRD and SEM-EDS analyses of cathode specimens obviously discover the presence of compounds of the system Ti-B-C, including TiB_2 and TiC.

Developed in the laboratory, the technology is ready for pilot testing in an industrial environment, which will bring to the development of aluminum cell new generation with a drained cathode.

REFERENCES

[1] Devyatkin S.V., Kaptay G., Boutellion J., Poignet J.-C. Electrochemical synthesis of titanium diboride coatings from cryolite melts//*Molten Salts Forum. Trans Tech Publications*.- 1998.- Vols. 5-6.- P. 331-334.

[2] Makyta M., Danek V., Haarberg G.M., Thonstad J. Electrodeposition of titanium diboride from fused salts//*Journal of Applied Electrochemistry*.- 1996.- Vol. 26.- P. 319-324.

[3] James B.J., Welch B.J., et al. *Interfacial Processes and the Performance of Cathode Linings in Aluminum Smelters*.//JOM, №47, №2, 1995, pp. 22-25.

[4] McClung M. et al. Plant Experience with an Experimental Titanium Diborid Cell.//*Light Metals*, 2004, pp. 399-404.

[5] Gorlanov E. S., Nikiforov S. A., Alternative technology to create wettable protective coating on the surface of the carbon bottom aluminum cell. In proc. reports of the International Conference “Aluminum of Siberia,” Krasnoyarsk, 2006.

MICROCRYSTALLINE CELLUSE ADDITIVE FOR MODIFICATION OF PROPERTIES OF POLYMER FILMS

Kirill L. Levine[1,3,*], Brian R. Hindderlitter[2], Albert K. Khripunov[3], Peter Y. Krauinsh[4], Tatyana E. Shtyrlyaeva[1] and Andrey G. Syrkov[1]

[1]National Mining Resources University,
Russia, St. Petersburg, Vasil'evsky Island
[2]University of Minnesota – Duluth, Duluth, MN
[3]Institute of Macromolecular Compounds Russian Academy of Sciences,
Russia, St.-Petersburg, Vasil'evsky Island
[4]Tomsk Polytechnic University, Russia, Tomsk

ABSTRACT

In this study, polymer coating was modified with microcrystalline cellulose (MCC). The progress of water uptake inside the coating was studied by electrochemical impedance spectroscopy (EIS). Observed results show morphological changes related to swelling in ions and channels during ions propagation.

Conducted study allows more justified approach in the formulation of composition of coatings for medical and technical application.

Keywords: coatings, electrochemical impedance spectroscopy, microcrystalline cellulose, polymethylmethacrylate, moisture uptake, thin films

INTRODUCTION

Electrochemical impedance spectroscopy (EIS) is a non-destructive method of thin films characterization. Different porous structure can be emphasized. Impedance spectra encrypt valuable information regarding physical properties of polymer films. Decrypting this information is an important task which requires approach uniting modeling and carefully advanced physical experiment.

MC as biocompatible ecologically safe material attracts serious attention in during few recent decades [1]. Cellulose-based composites can be used in flexible polymer displays [2], biocompatible and biodegradable optical diodes [3],electro-optical properties of cellulose are investigated for application in sensors [4], such as nanocomposite with silver is studied for applications for Plasmon-base sensor [5]. In the very recent past the special attention has been drawn to biocompatible nano-cellulose for using in wet nan0-cellulose membranes, artificial blood containers, materials for reconstructing bone tissue and stent coatings [6, 7, 8]. Microcrystalline cellulose is a polymer with straightened polysaccharide chain suitable for all the mentioned applications.

* levinkl@hotmail.com.

In this work processes of moisture uptake of a composite of MC with PMMA were studied in a solution close to physiological. The work was directed to establish whether biodegradable MC properties will be present ion the composite at small MC amounts, by other words, by other words, whether possible modification of properties of polymer films based on non-biopolymer by biopolymer, and how properties of non-biopolymer matrix of the composite coating will be changing.

Figure shows the example EIS plot typical for studied samples. Initially samples demonstrate lower impedance, that slightly increases.

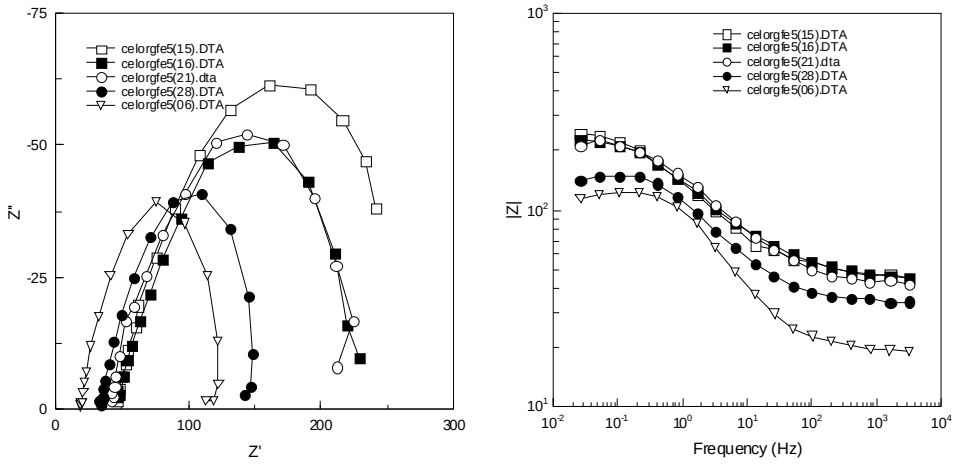

Figure 1. EIS data for PMMA with MCC film.

Similarity of plots shape is the evidence of corrosion products transport through the film rather than their storage inside film, which can be due to the presence of MCC providing micro channels for draining of those products. Those micro-channels likely to remain unchanged during corrosion that can be concluded from keeping plots shape during the entire of the experiment. Such behavior of samples containing MC allows suggesting additional mechanism of changing in the media containing ions than for classical barrier coating without MC. The properties of a barrier coting seem to be modified by the presence of MC. After the initial period of moisture uptake followed by slight impedance increasing for both barrier and modified coatings, further process of films damage for modified coatings occurs at a lowered rate and in more controlled manner, followed by keeping barrier properties longer, until decomposition.

CONCLUSION

Changes in the properties of coatings containing microcrystalline cellulose (MCC) were studied by electrochemical impedance spectroscopy. Barrier properties of films change with time depending on the amount of MCC. Observed behavior can be explained by morphological changes related to swelling in voids and channels during ions diffusion. Obtained results allow more justified approach in the formulation of composition of coatings formed for medical and technical application.

Financing

The project was funded by Russian Academy of Sciences.

REFERENCES

[1] D.A. Serqueira, A.J.M. Valente, G.R. Fihlo, H.D. Burrows, *Carbohydr. Polym*. 78 (2009) 402–408.
[2] Shah, R.M. Brown Jr., *Appl. Microbiol. Biotechnol*. 66 (2005) 352–355.
[3] C. Legnani, C. Vilani, V.L. Calil, H.S. Barud, W.G. Quirino, C.A. Achete, S.J.L. Ribeiro, M. Cremona, *Thin Solid Films* 517 (2008) 1016–1020.
[4] Andrey N. Aleshin, Alexander S. Berestennikov, Pavel S. Krylov, Igor P. Shcherbakov, Vasily N. Petrov, Irina N. Trapeznikova, Rustam I. Mamalimov, Albert K. Khripunov, Albina A. Tkachenko, *Synthetic Metals* 199 (2015) 147–151.
[5] Nahid Pourreza, Hamed Golmohammadi, Tina Naghdi, Hossein Yousefi, *Biosensors and Bioelectronics*, 74, (2015), 353–359.
[6] W.K. Czaja, D.J. Yuong, M. Kawecki, R.M. Brown Jr., *Biomacromolecules* 8 (2007) 1–12.
[7] D. Klemm, D. Schumann, U. Udhardt, S. Marsch, *Progr. Polym. Sci*. 26 (2001) 1561–1603.
[8] S. Kalia, A. Dufresne, B.M. Cherian, B.S. Kaith, L. Averous, J. Njuguna, E. Nassiopoulos, *Int. J. Polym. Sci*. (2011) 1–35.

THE USE OF NANO-COATING TO PROTECT PARTS OF MINING MACHINES FROM FRETTING-CORROSION

V. A. Krasnyy*, PhD in eng.sc, associate professor
and V. V. Maksarov*, Dr. in eng.sc, professor
National Mineral Resources University (Mining University), Saint Petersburg

ABSTRACT

The application of nano-coatings based on fluorocarbon polymer composition, friction-mechanical brass, fullerene C_{60} and surface treatment of vibroroling with the regular roughness for the protection of heavily loaded mating parts of machines, working in conditions of fretting-corrosion. Studied the mechanisms of friction of nano-coating, which will considerably reduce the fretting-wear mechanisms of friction in engineering products.

Keywords: nano-coating, fretting corrosion, vibroroling, fullerene C_{60}

GOALS

The aim of this work was to study the effect of nano-coatings based on fluorocarbon polymer composition,friction-mechanical brass, fullerene C_{60} and surface treatment of vibroroling with the regular roughness on the wear of highly loaded compounds mechanisms of mining machines working in the conditions of fretting-corrosion.

INTRODUCTION

Fretting is often the cause of failure of some critical components of mining machines, in particular engines of heavy-haul trucks and locomotives, parts and other drilling equipment, working in conditions of vibration and high contact loads. The fretting characteristic of nominally stationary joints of structures (for example, in places of fastening parts, etc.) and occurs typically during vibration, leading to different kinds of oscillatory relative displacements and deformations. Often frothing is accompanied by chemical processes on the friction surfaces (fretting-corrosion). Wear when fretting is manifested in the "grazing" material in places of fastening of details of the design. A characteristic feature of fretting, unlike other types of sliding friction, is small amplitude relative displacement of the components, comparable to the distance between the tops of microroughnesses on the surface

* vikras1955@yandex.ru.
* maks78.54@mail.ru.

friction, which complicates the removal of wear products from the contact zone. Products wear often start to play the role of the abrasive, which leads to additional wear. These also occur the phenomenon of fretting-fatigue, reinforcing the damaged parts.The fretting-corrosion damage are observed, in particular in such conjugation, as the support surface clamps the cylinder linings, the rear surface ("head") crankshaft bearings, the bearing surface of the main bearing caps and the block truck engines and locomotives, threaded connections and other.

MATERIALS AND METHODS

When selecting materials for protective coatings of parts of high load of mates from fretting-corrosion it is necessary to pay attention not only to their durability but also sensitivity to the shift, i.e., the ability of a material to assume deformation without shear initiation process of fatigue damage. It is known that this property have a sufficiently thin coating, handy, that do not violate the maintainability of the nodes and ensure the operation fits When carrying out model tests of samples from cast iron and steel in conditions of high contact loads studied a wide range of protective coatings, such as coatings electroplated and sputtered copper, molybdenum, friction-mechanical brass, bronze, PTFE coating; thin-layer ($40A^0$) fluorocarbon coating; samples were used with solid-lubricant coating thickness of 25 μm; the samples processed by laser in the solid phase, and samples treated with vibroroling, provided during assembly and fullerene C_{60}. The tests were carried out using a special installation that allows users to create a reciprocating rotational movement of samples along the circular contact in a wide range of loads and amplitudes at a frequency of 250 to 900 cycles per minute.A mechanism of fretting on the friction surfaces was studied by scanning electron microscopy.

RESULTS AND DISCUSSION

Studies have shown that the thickness of the coatings, their hardness and the presence of oil environments are not always optimal ways of reducing fretting-wear. In some cases, thin-layer nano-coating is able to exert more influence on the resistance to fretting-corrosion. A number of thin-layer coatings (friction-mechanical brass with a thickness of 3-5 μm, the solid-lubricant coating with a thickness of 25 μm, thin polymer film $40A^0$) showed high efficiency in reducing fretting wear. Positive results were obtained for the case of surface treatment of vibroroling with the formation of a regular roughness, which allows making a conclusion about the wave nature of the development process and fretting corrosion, as confirmed by studies of the friction surfaces using scanning electron microscopy.

Test of fullerene C_{60}as a material that prevents the fretting-wear on samples of steel and brass with lubricant industrial oil, showed that adding grease to the fullerene C_{60} (2.5%) in powder form and its use in the form of a coating on the brass sample is promising and reduces wear in 1,5-2 times.

CONCLUSION

It is established that in all studied for the protection of heavily loaded mating parts of machines with the use of nano-coating is a single mechanism of increasing wear resistance when fretting in the area of the contact layer of the fine particles through the use of thin-layer coatings. Their presence may be due to either structural self-organization material, or forming of composite structures with small wear particles when using the polymeric composition. At that the protective coating virtually eliminates component corrosion mechanism of fretting - wear.Positive results were obtained for the case of surface treatment of vibroroling with the formation of a regular roughness.

REFERENCES

[1] Bulatov V.P., Krasnyy V.A., Kireyenko O.F., Popov I.N. The study of fretting-corrosion under conditions of high contact loads. *Friction and wear*, vol. 15 (1994), No. 1, pp. 101-108.

[2] Ginzburg B. M., Krasnyy V. A., Kozyrev Y. P. , Bulatov V. P. Effect of fullerene C60 on the wear of metals under fretting. *Russian journal of theoretical physics*, vol. 23 (1997), No. 15, pp. 1-6.

[3] Bulatov V.P., Krasnyy V.A., Shneider Y.G. Basics of machining methods to yield wear- and fretting-resistive surfaces, having regular roughness pattern. *Wear*, 208 (1997). pp. 132-137.

[4] Ginzburg B.M., Krasnyy V.A., Kozyrev Y.P., Bulatov V.P. The decrease in the fretting-wear of metals under the action of fullerene C60. *Friction and wear*, vol. 18(1997), No. 4, pp. 523-526.

[5] Krasnyy V.A., Maksarov V.V., Viushin R.V. The effect of thin nano-coatings on the fretting corrosion high load of mates of large machine parts. *Metalworking*, No. 5-6 (2013), pp. 63-67.

[6] Maksarov V.V., Krasnyy V.A. The mechanisms of friction of thin-layer nano-coatingsunder conditions of fretting.Scientific and technical Gazette of St. Petersburg GPU. 226, (2015),№3, pp. 111-120.

INVESTIGATION INTERNAL STRUCTURE OF NANOPARTICLES BASED ON POROUS SILICON POWDERS

A. O. Belorus[1,*], Yu. M. Spivak[1] and V. A. Moshnikov[1,2]

[1]Saint Petersburg Electrotechnical University "LETI"
Saint-Petersburg, Russian Federation
[2]Peter the Great St. Petersburg Polytechnic University
Saint-Petersburg, Russian Federation

ABSTRACT

Nanoparticles of porous silicon were obtained by electrochemical anodic etching. Morphology and structure of the particles was investigated with using atomic force and scanning electron microscopy and methods of sorbometrii such as measurement of specific surface area BET and capillary condensation. The influence of technological conditions of preparation on geometrical parameters of the porous silicon particles (particle size distribution, pore shape and size, the specific surface area of the porous silicon) is discussed.

Keywords: Porous silicon nanoparticles, electrochemical etching, capillary condensation

INTRODUCTION

Porous silicon is used in different fields such as micro and optoelectronics, photonics, alternative energy, nanoelectronics, and many others, because this material has specific properties such as photoluminescence, large specific surface area and as consequently high chemical activity, good antireflection properties. For biomedicine applications particles of porous silicon powders have such important properties as biocompatibility, biodegradability and easy technology of obtaining, that does this material one of the most perspective in this area [1-5].

THE EXPERIMENTAL PART

Por-Si powders were obtained in one-chamber electrochemical cell in an aqueous solution of hydrofluoric acid and isopropanol mixture with the addition of hydrogen peroxide [5-8]. The choice of process conditions is due the requirement to obtain mesopores and based on the experience of previous studies. As a raw material, single crystal n and p types were

* E-mail: mop_92@mail.ru.

used. Thus obtained por-Si samples were then subjected to sonication, and thus yields a powder of por-Si.

Gas adsorption and capillary condensation measurements were carried by means of SORBI MS ("META," Novosibirsk), software SoftSorbi II. As the carrier gas, helium was used, and as the adsorbate gas - nitrogen while created gas mixture of given composition. The results of measured volumes of gas sorbed on the test sample at the four values of the partial pressure using the BET equation calculated value of the specific surface. Before the measurements the samples were heat treated for removal of the adsorbate from the surface using SorbiPrep station. Additional experiments were performed on the choice of heat treatment time and temperature so as to remove as much of the adsorbate from the surface, but does not lead to a change in the porous structure (pore coalescence) [8].

EXPERIMENTAL RESULTS

Thus, the measured specific surface area of the porous silicon powders by gas adsorption. It is shown that under the chosen conditions produce a decrease in resistance of the n-silicon substrate results in a substantial increase in the specific surface area of the porous silicon powder (201 and 104 m^2/g respectively for Si wafer with 0.3 and 1.0 Ω·cm specific resistance respectively). For porous silicon powder prepared from silicon (1.0 Ω·cm) defined pore size distribution. In the selected process conditions in por-Si is mainly pore size of 5 nm or less, there is also a small fraction of pores with a size of 10-20 nm and about 50 nm. It was shown that the capillary condensation method enables to determine the pore sizes in the porous silicon with a complex porous structure (2 or more types of pores, micro-and mesopores).

The specific features of storage conditions of por-Si powders in the different kinds of mediums and the effect of post-processing terms on morphology and internal structure of particles were revealed. The experimental results of the changes of simples' mass and specific surface area were discussed.

ACKNOWLEDGMENTS

The reported study was this work was supported by project "Preparation and study of porous systems, functionalized nanomaterials, applications in photonics, sensor technology and medicine" (under the Russian Ministry of Education state task № 16.2112.2014/K.

REFERENCES

[1] Moshnikov V.A., Gracheva I. E., Lenshin A.S. (2012) Porous silicon with embedded metal oxides for gas sensing applications. *J. of Non-Cryst. Sol*. Vol. 358, is. 3, 2012, Pages 590–595 pp.

[2] Nalimova S.S., Spivak Yu. M., Moshnikov V.A., etc. (2014) Morphological Feature Analysis of the Prospective Combined Gas Sensitive Sensor Elements. *Smart Nanocompos.* 2014. Vol. 5, N. 1., 5 p.

[3] Patel p. N., Mishra v., Panchal a. K. (2012)Synthesis and characterization of nano scale porous silicon photonic crystals for optical device and sensing applications. *Journal of Optoelectronics and Biomedical Materials*. 2012. Vol. 4, is. 1., 19 – 28 pp.

[4] Lenshin A.S., Kashkarov V.M., Spivak Yu. M., Moshnikov V.A. (2012) Investigations of nanoreactors on the basis of p-type porous silicon: Electron structure and phase composition *Materials Chemistry and Physics*. 2012, Vol. 135, is. 2–3, 293-297 pp.

[5] Chufarov A Yu, Ermakov A N, Samigulina R F, Zainulin Yu G, Forostyanaya N A, Maskaeva L N and Markov V F (2013) *Russian J. of Inorganic Chem*. 2013, V. 58, 1362–1369 pp.

[6] Spivak Yu M, Maraeva E V, Belorus A O, Molchanova A V, Nigmadzyanova N R (2013) Preparation and investigation of porous silicon nanoparticles for targeted drug delivery *Smart Nanocomsite*, 2013,V. 4, pp. 115-118.

[7] Belorus A. O., Spivak Yu. M., Moshnikov V. A. (2014)The research of behavior of powder porosilicon nanoparticles using the method “drop projection The 9th International Conf. on European Science and Technology. Publ. Munich: Vela-Verlag, Waldkraiburg, 2014. Vol. II. P. 268–277.

[8] Belorus A O, Maraeva E V, Spivak Yu M, Moshnikov (2015) *Journal of Physics*: *Conference Series* 2015 , V. 586, 012017pp.

EVOLUTION OF COPPER(II) OXIDE NANOSTRUCTURES IN POROUS GLASS MATRIX

Vyacheslav N. Pak* and Oleg V. Golovin
Herzen State Pedagogical University of Russia, Saint-Petersburg, Russia

ABSTRACT

Controllable accumulation of copper(II) oxide in porous glass was carried out by repeated impregnation of the carrier by $Cu(NO_3)_2$ aqueous solutions with subsequent thermal decomposition of the salt. The results of measuring electric conductivity of a series of modified plates make it possible to characterize the trend in the oxide distribution on a silica surface. In the case of its cyclic accumulation by small portions, a two-dimensional structure of monolayer filling the surface is presumably formed in a narrow range of CuO concentration.

Keywords: porous glass, CuO, monolayer, electrical conductivity

INTRODUCTION

Porous glasses (PG), in which the pore radius can be reliably controlled in the range r = 2–100 nm offer wide possibilities for the investigation of substances in the nanodimensional state [1-3]. It is important that PGs with highly developed pore structure and surface area allow the compounds to be introduced in amounts sufficient for the experimental investigation. The nanoparticles and monolayers of transition metal oxides in PG are promising materials in which dimensional features of the optical and electrical properties are well manifested. However, peculiarities of the electric conductivity in such systems with small number of atoms (10^{15}–10^{16} cm^{-2}) of d –elements in the oxides formed at the initial stage of filling of the silica surface remain unstudied. The results reported here demonstrate a specific stepwise increase and unusual temperature dependencies of the electric conductivity in the course of copper(II) oxide deposition in PG.

The experiments were performed on PG plates with dimensions 1·1·0.1 cm, predominant pore radius of r = 70 nm and specific surface area of S = 22 m^2/g [4]. The PG was modified by adding copper(II) oxide through diffusion impregnation of the plates with an aqueous solution of $Cu(NO_3)_2$ with a concentration of 0.15 M, followed by dehydration at 120^0C and thermal decomposition of the intercalated salt by heating in air at 400^0C. Repeated cycles of this treatment allowed the oxide step-by-step growth on the walls of through channels in PG to be performed in a controlled way and reliably monitored by weighing. *X*-ray diffraction measurements confirmed the amorphous nature of all CuO/PG samples examined. The d. c. electric resistance was measured in dry atmosphere across the CuO/PG samples.

* E-mail: pakviacheslav@mail.ru.

The conductivity (σ) dependence on the content of CuO (Q) in PG exhibits a monotonic increase at the first steps of oxide deposition followed by a sharp jump in the region of Q = 2.95–3.38 % mass indicating a percolation threshold (Table). The temperature dependencies of σ in the modest range investigated show a drastic difference between the CuO/PG samples "before" and "after" percolation threshold. The samples *1-9* listed in Table demonstrate unusual change from low-activated to metal-like conductivity accompanied by gradual shift of smooth maximum to high temperature. Those maxima in turn become less pronounced as the amount of CuO increases. By contrast, the plots of log σ(1/T) in case of samples *10-14* ($Q \geq 3.38$ % mass) turns out to be linear in all temperature range. Attention must be given to the low values of the electrical activation energies (Table) calculated from the slopes of log σ(1/T) dependencies *10-14* and from their initial linear parts in case of samples *1-9*.

Based on the results obtained, a probable model of step filling of PG surface may be suggested. As far as PG conductivity is low ($\sigma < 10^{-9}$ Ω^{-1} cm^{-1}) we can assume that values of 10^{-8} Ω^{-1} cm^{-1} obtained at the initial steps of CuO deposition owes to the formation of some percolating chains of conjugated copper oxide polyhedrons. Indeed, being reduced to a specific surface area of S = 22 m^2/g, the oxide content in PG Q ~ 0.35% mass (sample *1*) corresponds to ~ one CuO formula unit per 10 nm^2. In case of such a small "surface density" the most reasonable way for σ–level explanation implies some conducting chains organization at the first step of the oxide deposition.

This guess also provides a first explanation for the peculiarities of the electrical T-dependencies. Low values of the activation energies (Table) are associated with excitation of the heat oscillations within conducting chains, thus enhancing a $3d_\pi$–$2p_\pi$ conjugation of Cu–O–Cu bonds (and possibly, a direct $3d\cdots3d$ overlap). The increase of the oscillations amplitude can gradually provoke a metal-like conductivity resulting in its inverse T-dependence. In the course of CuO monotonous growth in PG the lateral Cu–O–Cu bonds are formed and gradually prevail, which adds to the oxide structure rigidity and reduces the oscillations amplitudes. That's why the dependencies log σ(1/T) maxima become smoother and shift to a high temperature while the activation energy values steadily rise up (Table). Thus, T-dependencies of the electric conductivity demonstrate a counteraction of activated and metal-like behavior of CuO/PG system.

Sample	CuO content (% mass)	σ_{20} (Ω^{-1} cm^{-1})	Activation energy (eV)
1	0.35	$1.1\cdot10^{-8}$	0.07
2	0.67	$1.2\cdot10^{-8}$	0.07
3	1.06	$1.2\cdot10^{-8}$	0.08
4	1.42	$1.3\cdot10^{-8}$	0.09
5	1.73	$1.5\cdot10^{-8}$	0.10
6	2.00	$2.0\cdot10^{-8}$	0.11
7	2.36	$2.4\cdot10^{-8}$	0.13
8	2.72	$3.0\cdot10^{-8}$	0.15
9	2.95	$4.0\cdot10^{-8}$	0.18
10	3.38	$1.3\cdot10^{-6}$	0.23
11	3.70	$1.4\cdot10^{-6}$	0.25
12	4.01	$2.0\cdot10^{-6}$	0.27
13	4.33	$2.5\cdot10^{-6}$	0.29
14	4.60	$3.2\cdot10^{-6}$	0.33

CONCLUSION

Progressive increase in the copper(II) oxide content in porous glass is accompanied by a monotonic increase in electrical conductivity, which subsequently exhibits an abrupt jump within a narrow composition range corresponding to monolayer coverage of the support surface. Based on the results obtained, a model was proposed which states that the porous glass surface is covered in a stepwise manner, via predominant formation of extended copper(II)-oxygen chains as the first step and subsequent change to 2D structures, eventually leading to oxide monolayer.

ACKNOWLEDGMENTS

This work was supported by the Ministry of Education and Science of Russia within the base part of the Government Instruction.

REFERENCES

[1] Pak V.N., Gavronskaya Yu.Yu., Burkat T.M. Porous glass and nanostructured materials, N.Y.: Nova Science Publishers, Inc., 2015.

[2] Pak V.N., Gavronskaya Yu.Yu., Shilov S.M. Optical and electrical properties of low dimensional forms of substances in porous glass//*Glass Physics and Chemistry*, 41(1), (2015), 68–72.

[3] Enke D., Janowski F., Schwieger W. Porous glasses in the 21st century – a short review//*Microporous and Mesoporous Materials*, 60(1), (2003), 19–30.

[4] Lyubavin M. V., Burkat T. M., Pak V. N. Fabrication of silica structures with controlled pore structure//*Inorganic Materials*, 44(2), (2008), 203-206.

STUDY OF THE DEPOSITION PROCESS OF VINPOCETINE ON THE SURFACE OF POROUS SILICON FOR THE PURPOSE OF ESTABLISHMENT OF THE TARGETED DRUG DELIVERY SYSTEMS

Yu. A .Polkovnikova*, P. V. Seredin and A. S. Lenshin
Voronezh State University, Russia

ABSTRACT

Currently the most prospective way in pharmacotherapy is the obtaining of nanoparticles involving pharmaceutical substances. Application of porous inorganic materials on the basis of silicon is among the main tendencies in solving of this problem. The present work is concerned with the problem of the deposition of pharmaceutical drug with nootropic activity – vinpocetine – into porous silicon. Silicon nanoparticles were obtained by electrochemical anodic etching of Si plates. The process of vinpocetine deposition was studied in a dependence of the deposition time. As a result of the investigations it was found that infrared transmission spectra of porous silicon with the deposited vinpocetine revealed the absorption bands characteristic of vinpocetine substance.

Keywords: nanoparticles, porous silicon, vinpocetine

INTRODUCTION

The purpose of this work was the study of sorption process of vinpocetine onto porous silicon in a dependence on the deposition time.

At present the idea concerning the use of nanostructured containers for targeted drug delivery is of a great interest for specialists in medicine and pharmacy. The reason for such interest is not only in successes in production of the new nanomaterials but also rather low efficiency in conventional ways of the drug delivery. It is well known that only a small part of the introduced medical preparation gets just into the nidus. A perspective trend in solution of this problem is the application of porous inorganic materials on the basis of silicon [1]. A possibility of the point targeted delivery of such drugs as ibuprofen, folic acid, triclosan and so on with the use of porous silicon nanoparticles is actively investigated by the experts [2].

Diagnostics and treatment of disorders in the cognitive functions is one of the most intensively studied problems in up-to-date neurology. For the treatment of these disorders medical preparation known as vinpocetine is routinely prescribed. Vinpocetine is characterized by a broad range of pharmacological activity [3-4]. It provides an adequate

* E-mail: juli-polk@mail.ru.

blood supply and improves microcirculation in the brain tissue, reduces thrombocyte aggregation, facilitates normalization of the rheological properties of blood, activates hypoxia tolerance of the brain cells by facilitating of the oxygen transport to the tissues due to the decrease of erythrocyte sensitivity to oxygen and enhancing of the uptake and metabolism of glucose [5].

Now vinpocetine is produced in the form of tablets with the content of drug 5 and 10 mg. This drug formulation is rather efficient for the treatment but it does not provide the desired sustained action. Chemical structure of vinpocetine can cause the instability of its tableted drug formulation. Thus, it seems appropriate to elaborate the sustained-release drug formulation.

Porous silicon was obtained by electrochemical etching of single-crystalline silicon with n-type conductivity in the alcohol solution of hydrofluoric acid according to the standard technique described in [6]. Maximum pore size of por-Si was less than 100-150 nm, specific surface area of these samples was of about 250 m^2/g. Deposition of vinpocetine on the surface of porous silicon was performed from the solution prepared by solving of 0,005 g of vinpocetine in 1 ml of water for 20 and 60 minutes. Scanned images of the sample surface cleavages were obtained with electron scanning microscope JEOL-JSM 6380LV. The features of the sample's composition were investigated by IR-spectroscopy with the use of IR-Fourier spectrometer VERTEX 70 (BRUKER) within the range of 400–4000 cm^{-1}.

Analysis of the obtained data indicated at the increase of vinpocetine concentration on the deposition time that was observed as an increase of intensity of the absorption peaks related to vinpocetine. No chemical bonds between silicon and vinpocetine molecules were detected. Porous silicon composition did not considerably change as compared with the original samples. It means that physical adsorption of the drug preparation on porous silicon is a prevailing process in the investigated system.

REFERENCES

[1] O.I.Ksenofontova et al. Porous silicon and its application in biology and medicine//*Zhurnal tekhnicheskoi fiziki,* 2014, v. 84, Iss. 1 , P. 67-78.

[2] Leigh Canham Handbook of Porous Silicon /Springer International Publishing Switzerland 2014 1016 p.

[3] Ogunrin A. Effect of vinpocetine (cognitol™) on cognitive performances of a nigerian population. *Ann Med Health Sci Res* 2014; 4:654-61.

[4] Szakács T, Veres Z, Vereczkey L. In vitro –in vivo correlation of the pharmacokinetics of vinpocetine, *Pol. J. Pharmacol* 2001; 53: 623–628.

[5] Lobzin V.Yu. et al. Modern approaches to the diagnostics, prevention and therapy of the cognitive disorders under discirculatory encephalopathy. *Neurology,* neuropsychiatry, psychosomatics, 2014; 2: 51–56.

[6] Levitskiy V.S. Study of the degradation processes of the optical processes in meso- and macroporous silicon under the impact of solar radiation simulator/V.S. Levitskiy, A.S. Lenshin, P.V. Seredin, E.I. Terukov//*Fizika I technika poluprovodnikov*. 2015. v. 49. Iss. 11. P. 1540-1545.

GRAPHENES, STACKS AND GLOBULES IN NANOPARTICLES OF SHUNGITE CARBON AND NEW MATERIALS

N. N. Rozhkova*, S. S. Rozhkov and R. V. Sadovnichi
Institute of Geology Karelian Research Center RAS, Petrozavodsk, Russia

ABSTRACT

Shungite carbon (ShC) is considered as the natural carbon allotrope of a multi-level fractal structure produced by the consecutive aggregation of ~ 1 nm graphene fragments. Turbostratic stacks of ~ 1.5 x 2.5 nm and the globular composition of the stacks ~ 6 nm are responsible for the secondary and tertiary levels of the structure. Aggregates of globules, measuring tens of nanometres, form 3D-nets and complete the structure. All structural levels could be released through stable aqueous dispersion of ShC nanoparticles. Each level is important for obtaining special properties in new materials with ShC nanoparticles.

Keywords*:* Nanocarbon, shungite carbon, graphene, nanotechnology

INTRODUCTION

Great attention is now given to the development of technological processes of synthesis and purification of nanosized carbons. Nanocarbons are commonly purified (fullerenes or nanodiamonds) or exfoliated (graphite to produce graphene oxide (GO) using "wet chemistry" methods, its interaction with water and solutions should be studied. Nanostructurized carbonaceous materials are typically highly homogeneous in terms of the size and structure of primary carbon particles. These nanoparticles are packed in certain order to form a secondary particle (aggregate). Examples of such nanostructurized materials are ultradisperse diamonds, produced by detonation synthesis, and shungite carbon (ShC) [1]. In spite of graphene (Gr) layers with superior electron transport characteristics are synthesized using dry methods its mass production is connected with preparation of multilayered GO flakes in suspensions and further reduction of GO. Since the electronic, photonic, and mechanical properties of Gr depend on the number of layers and its crystalline structure the controlled synthesis of reduced GO with defined layers and degree of GO reduction is very important [2].

* rozhkova@krc.karelia.ru.

GRAPHENE FLAXES IN SHC

New concept of ShC exhibits this natural material as a multi-level fractal structure of nanosize fragments of reduced graphene oxide (rGO) ~ 1 nm that are easy dispersible in water and other polar solvents [3]. The natural rGO deposits turn out to be quite challenging for the current graphene technology. Two direct justifications of the concept have been obtained.The first one is related to the study of photoluminescence of ShC aqueous and organic dispersions that exhibits properties similar to those of synthetic Gr quantum dots of the rGO origin [4]. The second was obtained in the course of the neutron scattering study that was profoundly discussed in [5]. The study was initiated because ShC according to geological data was formed in aqueous environment. Being porous due to its fractal structure, ShC provides favorable conditions for water confining and the confined water can say much about the space in which it is kept. Both graphene-like configuration and chemical composition of basic structural elements of ShC attributing the latter to rGO nanosize sheets. The experimental data were supplemented with quantum chemical calculations suggesting a clear vision of the ShC structure at its first fractal levels.

GLOBULES AND STACKS

The conditions, required for obtaining the various structural types of ShC nanoclusters and their aggregates, have been determined [4]. Globular clusters were identified and stabilized in aqueous dispersion under normal conditions. Nanoparticles in the films produced from the dispersions lie at net sites formed upon condensing dispersions. The size of the nodes in the 3D-nets in the films coincides with that of globular clusters (~ 100 nm). This supports the essential contribution of water to the formation of ShC in nature and its texture and electronic structures. Upon replacement of water by non-polar solvents, globular clusters at 3D-net nodes are deformed and the net is broken up. Connection between the structural levels disappears in non-polar organic solvents. Ellipsoid clusters and chains as well as stacks and plate aggregates were obtained dominantly in films from different organic solvents.

The stacks were released demonstrating homogeneous distribution in the liquid crystals (LC) environment and further introduction into the cholesteric mesogenic LC matrix. This combination of LC and ShC nanoparticles revealed a decrease in the viscosity of the composites over the ranges of high strain rates and is claimed in lubricating coolant a dditives [6].

ACKNOWLEDGMENT

The work was supported by the RFBI grant 13-03-00422.

REFERENCES

[1] N.N. Rozhkova, L.E. Gorlenko, G.I. Yemel'yanova, A. Jankowska, M.V. Korobov, V.V. Lunin, E. Osawa. The effect of ozone on the structure and physico-chemical

properties of UDA and shungite nanocarbon elements. *Pure and Appl. Chem*. 2009; 81 (11): 2093-2105.

[2] Y. Zhu, S. Murali, W. Cai, X. Li, J. W. Suk, J. R. Potts, R. S. Ruoff, Graphene and Graphene Oxide: Synthesis, Properties and Applications. *Adv.Mater.*2010; 22, 3906−3924.

[3] E.F. Sheka, N.N. Rozhkova, Shungite as the natural pantry of nanoscale reduced graphene oxide. *Int. J. Smart Nano Mater*. 2014; 5: 1–16.

[4] B.S. Razbirin, N.N. Rozhkova, E.F. Sheka, D.K. Nelson, A.N. Starukhin, Fractals of graphene quantum dots in photoluminescence of shungite. *JETP*. 2014;145 (5) : 838–850.

[5] E.F. Sheka, I. Natkaniec, N.N. Rozhkova, K. Holderna-Natkaniec, Neutron scattering study ofreduced graphene oxide of natural origin. *JETP Lett.* 2014; 118: 735–746.

[6] N.V. Usol'tseva, M.V. Smirnova, A.V. Kazak, A.I. Smirnova, N.V. Bumbina, S.O. Il'in, N.N. Rozhkova, Rheological Characteristics of Different Carbon Nanoparticles in Cholesteric Mesogen Dispersions as Lubricant Coolant Additives. *Journ.of Friction and Wear. 2015; 36 (5): 380–385.*

FORMATION AND OPTICAL PROPERTIES OF CuCl NANOCRYSTALS IN FLUOROPHOSPHATE GLASS

M. Abdelghany*, E. V. Kolobkova and M. M. Sychov
Theory of Materials Science Department, St. Petersburg State Technological Institute (Technical University), 26 Moskovsky Prospect, Saint-Petersburg, Russia

ABSTRACT

We study the possibility of formation of CuCl nanocrystals in fluorophosphate glass ($NaPO_3$-$Ba(PO_3)_2$-AlF_3) by heat treatment technique. Using the optical absorption technique, the position of the CuCl nanocrystal exciton absorption band was studied as a function of heat treatment time and the radius of CuCl nanocrystals increased from 3 to 9 nm.

Keywords: Fluorophosphate Glass, CuCl nanocrystals, excitons

INTRODUCTION

In recent years, the formation of a semiconductor nanocrystalline phase in a glass matrix and the control of properties of this phase constitute important problems in the technology of preparation of nano-structured materials [1, 2]. Figure 1 illustrates the absorption spectra at room temperature of fluorophosphates glass as prepared and after 1 hour of heat treatment at 400 ^oC. After the sample of fluorophosphate glass has been subjected to a temperature of 400 ^oC for 1 hour, the two main absorption peaks of $Z_{1,2}$ exciton and Z_3 exciton in CuCl nanocrystals [associated with the doubly degenerate hole band Γ_7 and the quadruply degenerate spin–orbit splitoff subband Γ_8, respectively [3] appear in range 350-380 nm.

Increase of the intensity of optical absorption in range 350-380 nm is caused by the increase of the content of CuCl nanocrystals, where the intensity of the optical absorption may be indication of the amount of the CuCl nanocrystals with different radii formed in the glass matrix [4]. With increased time of heat treatment $Z_{1,2}$ exciton maximum peak exhibit an energy shift (to longer wavelength) and broadening of the excitons peak due to the quantization of the energy spectrum of excitons and can be related for the steady-state size distribution of nanocrystals formed during growth process [5]. The maximum of the absorption peak of $Z_{1,2}$ exciton was used to derive the average radius of CuCl nanocrystals in fluorophosphate glass using the approximate relationship as in [10]. Analyzing of the $Z_{1,2}$ exciton peak show that the maximum of peak shifted from 370 to 372 nm corresponding to a radius distribution of CuCl nanocrystals from 3 to 9 nm in the fluorophosphate glass matrix. Figure 2 shows the growth of CuCl nanocrystals during increased treatment time, in addition to the rate of change in nanocrystals radius have nearly the same rate of change in CuCl nanocrystals content.

* E-mail: ph_abdelghany@yahoo.com.

In this work, we prepared fluorophosphate glass and formed CuCl nanocrystals by H.T. at 400ºC. The displacement of the $Z_{1,2}$ exciton peak position of CuCl is due to the quantum confinement effect. The analysis of the absorption spectra of glass at different time H.T. showed an increase in the amount of CuCl nanocrystals and also increases in the radius of CuCl nanocrystals from 3 to 9 nm during 18 hours H.T.

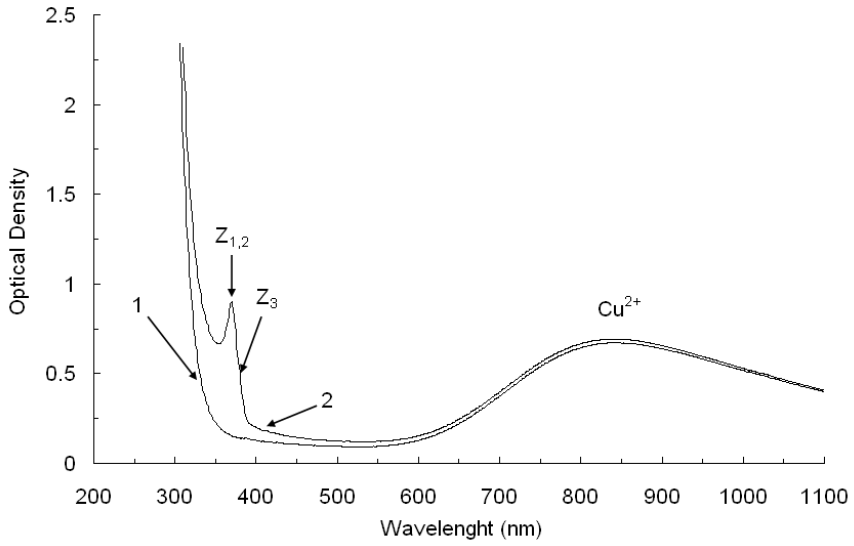

Figure 1. Absorption spectra of fluorophosphates glass before heat treatment (1) and after heat treatment at 400ºC for 1 hour (2).

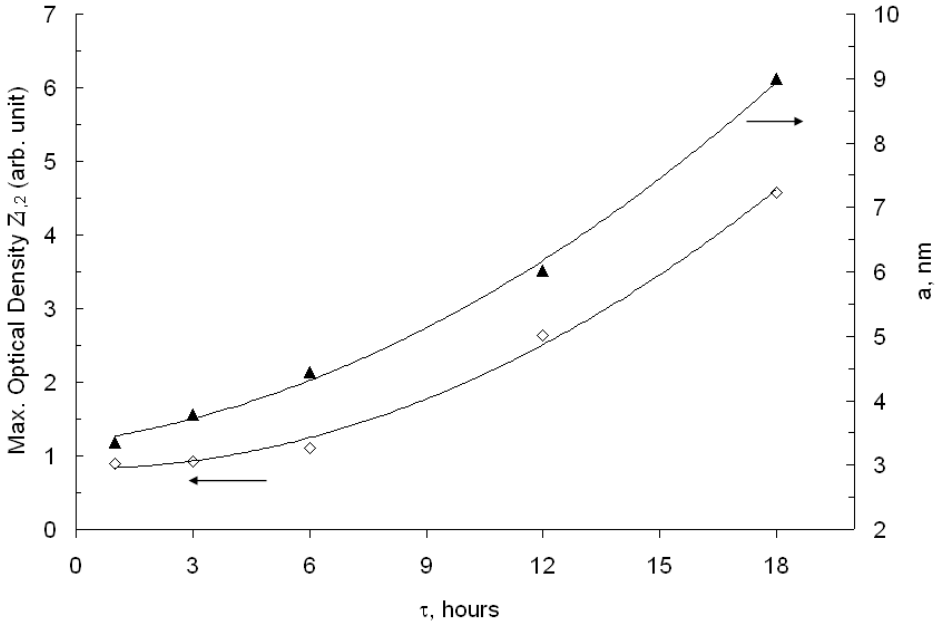

Figure 2. Max. optical density of $Z_{1,2}$ peak at different times of H.T. at 400ºC and average radius of CuCl nanocrystals as calculated.

REFERENCES

[1] V. G. Melekhin, E. V. Kolobkova, A. A. Lipovskii, V. D. Petrikov, A. M. Malyarevich, and V. G. Savitskii, Fiz. Khim. Stekla, 34 (4), 462 (2008).

[2] N. Babkina, N. V. Nikonorov, V. A. Tsekhomskii, and P. S. Shirshnev, Fiz. Khim. Stekla, 41(1), 113 (2015).

[3] I. Ekimov, A. A. Onushchenko, F. G. Plyukhin, and Al. L. Efros, The Quantum Confinement of Excitons and Determination of Parameters of Their Energy Spectrum in CuCl, Zh. Eksp. Teor. Fiz. 1985, vol. 88, no.4, pp.1490–1501.

[4] P. M. Valov, V. I. Leiman, and K. S. Semenov, Initial Nucleation Stages and Properties of CuCl Nanoparticles in Glasses//Physics of the Solid State, Vol. 43, No. 9, 2001, pp. 1770–1773.

[5] A I. Ekimov, A. A. Onushchenko, A.G. Plyukhin and Al.L. Efros//Sov. Phys.-JETP, 61, pp. 991 (1985).

FORMATION OF NANO-DIMENSIONAL STRUCTURES IN AMORPHOUS AND NON-CRYSTALLINE MATERIALS FOR DEVELOPMENT OF MODERN OPTOELECTRONIC SYSTEMS

K. G. Karapetian and O. V. Denisova*

The national mineral resources university "Gorni," St. Petersburg, Russia

ABSTRACT

In accordance with modern understanding of the role of micro- and nano-inhomogenuities in the processes of formation of surface micro relief the problems of the synthesis of materials with pre-defined properties are discussed. The formation of nanoscale structures in the photosensitive glass opens up new possibilities in the preparation of glasses for special purposes. Change in the conditions of synthesis of glasses, their composition, the introduction of activators demonstrates the ability to create modern optoelectronic systems. As model systems, well-known compositions of photosensitive silicate and germanate glasses are investigated. The silver ions are introduced into the test glass by ion exchange diffusion.

Keywords: nanoscale structures, photosensitive glass, ion exchange processes, optoelectronic devices

GOALS

The aim of this research was testing processes of formation of nanoscale structures in photosensitive silicate and germanate glasses. The study of processes of forming silver colloid particles in glass based on the analysis of changes in physico-chemical and spectral characteristics of glasses.

EXPERIMENT AND DISCUSSION

Nanoscale structures and conditions of their formation influence the properties amorphous and non-cristalline materials.

The most known example of non-crystalline material is the glassy one. The glass is a thermodynamically non-stable state of matter and its' inhomogeneous disordered structure naturally demonstrates principles of nanotechnology. A number of papers show that it is the

* e-mail: denisovaov @ list.ru.

presence of micro- and nano- inhomogenuities may be the source of special properties of glass materials [1, 2, 3].

The formation of nanoscale structures in the photosensitive glass that opens up new possibilities in the preparation of glasses for special purposes. Change in the conditions of synthesis of glasses, their composition, the introduction of activators demonstrated the ability to create modern optoelectronic systems [3].

As model systems are investigated well-known compositions of photosensitive silicate and germanate glasses. The introducing of silver ions into the surface layer of photosensible glasses is the effective technique [4]. The silver ions are introduced into the test glass by ion exchange diffusion [5]. The diffusion coefficient of silver use are estimated . The dependences of the differential refractive index and the effective depth of the diffusion annealing temperature. The influence of the concentration of silver in the equilibrium melt to changes refraction during low-temperature diffusion. Ultra violet light exposure of ion-exchanged samples and subsequent annealing lead to appearance of "colloid" color in the surface layer which evidence the formation of silver colloid particles and proved spectroscopically. The interpretation of the optical absorption spectra for glasses obtained in different conditions, as well as after the ion exchange processing and heat treatment was carried out.

Possible technological impact: the introduction of activators, primary and secondary heat treatment, the effect of radiation - have a significant impact on the formation of nano-sized areas in the glass structure. This opens up broad prospects for the use of the formation of nano-objects in the technology of light filters, in the synthesis of glasses for laser systems, radioresistant, photoluminescent and photosensitive glass for optoelectronic devices.

The introducing of activators and secondary thermal treatment influences processes of formation of nano-dimensional structures of various properties in glass systems.

CONCLUSION

Changing the conditions of synthesis of glasses, their composition, introducing of activators shows the ability to adjust formation of nano-dimensional structures in glass systems. That processes have a grate significance during the synthesis of glass doped by ions of rare-earth elements for development of modern active laser elements, radio-resistant, luminescent and photo-sensible glassworks for optoelectronic devices.

REFERENCES

[1] Denisova O.V, Karapetian K.G.//*Abstracts of the Fifth All-Russian conf. "Surface chemistry and nanotechnology*," 24-30 Sept. 2012 - Khilovo Pskov.obl.- P.299-300.

[2] Karapetian K.G, Senichenkov V.A, Zorin G.S, Ryabova M.N//*Journal of Applied Chemistry*, 2005.- T.75, no. 9, p. 1409-1412.

[3] Karapetian K.G, Kuznetsov A.P, Nikitina S.I.//*Glass Physics and Chemistry*, 1996, T.16, № 5.- P.16-19.

[4] Stepanov A.L, Valeev V.F., Nuzhdin E.V., Popok V.N. Features synthesis of silver nanoparticles in silica glass at a low-energy ion implantation, *Russian Nanotechnologies*, 2011.- T. 6, №. 7-8, p. 60-63.
[5] Bocharova T.V.//*Glass Physics and Chemistry*, 2005, T.31, № 2.- P.161-173.

STUDY OF LUMINESCENCE AND SURFACE PROPERTIES OF Y1-XEUXV1-YPYO4 PHOSPHORS

L. A. Lebedev*, S. V. Mjakin, A. A. Nikandrova,
V. V. Bakhmetyev amd M. M. Sychov
Saint-Petersburg State Technological Institute (Technical University)
Saint-Petersburg, Russia

ABSTRACT

The composition of Y1-xEuxV1-yPyO4 phosphors is optimized to provide the highest luminescence brightness achieved for samples with P and Eu contents 10 and 7 mol.%, respectively. The observed brightness growth prominently correlates with the content of specific centers on the phosphor surface reflecting the formation of species responsible for the luminescence efficiency.

Keywords: luminescence, phosphors, yttrium vanadate, surface functional groups

INTRODUCTION

YVO_4 based phosphors doped with europium (substituting for Y) and phosphorous (substituting for V) are promising as red light emitting components in various light sources to "warmer" white light, in field emission displays and medical applications. The efficiency of these phosphors largely depends on the ratio between their components responsible for the optimal composition, substitution degree and formation of luminescence centers, particularly in the surface layer of the phosphor particles. In our earlier studies [1-3] the content of specific surface centers was found to strongly correlate with the luminescence brightness for ZnS based phosphors with different dopants and activators (Cu, Al, Cl, Mn) that is useful for the prediction of luminescence efficiency for various materials.

EXPERIMENTAL

$Y_{1-x}Eu_xV_{1-y}P_yO_4$ phosphors were prepared by solution-combustion (SC) technique from commercial analytical grade materials without further purification. Y_2O_3 and Eu_2O_3 were dissolved in 35% nitric acid followed by diluting with water, consecutive addition of glycine (upon heating) and a mixed solution of NH_4VO_3, $NH_4H_2PO_4$ and NH_4NO_3, evaporation, heating at 600°C to initiate the reaction and annealing of the resulting porous material at 800°C. The prepared phosphors of various composition (1 – 10 mol. % Eu, 0 – 20 mol. % P) were characterized by the study of surface functional groups by adsorption of acid-base

* Corresponding author: 1595lion@gmail.com.

indicators, XRD using a Diffray diffractometer, luminescence spectra analysis using a AvaSpec-3648 spectrometer and measuring the brightness using IL-1700 brightness meter.

RESULTS AND DISCUSSION

According to XRD data, all the prepared samples correspond to YVO4 structure and their luminescence spectra are intrinsic to yttrium vanadate (Figure 1). Their surface characterization indicates that the content of centers with various acid-base properties (pKa values) strongly depends on the sample composition (P and Eu contents) and obviously correlates with the luminescence performances. Particularly, brightness of the samples with 10 mol. % P correlates with the contents of centers with pKa 1.3, 7.3 and -4.4 with the correlation coefficients 0.97-0.99 and a prominent maximum at 7 mol. % Eu (Figure 2). Furthermore, the maximum contents of centers with pKa 1.3 and pKa 7.3 are equal to each other that suggests their interrelated nature, probably reflecting the most efficient P and Eu incorporation into the vanadate structure and formation of both acidic (pKa 1.3) and neutral (pKa 7.3) Broensted centers represented by hydroxyls connected with simultansously displaced V and Y ions, accordingly. Lewis basic centers with pKa -4.4 probably correspond to oxygen atoms connecting ions as bridging groups and stabilizing the desirable surface species responsible for the luminescence efficiency.

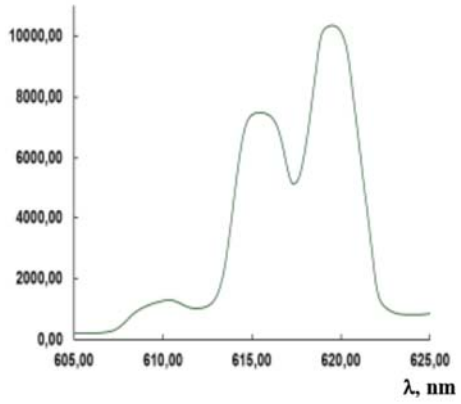

Figure 1. Luminescence spectrum of the synthesized phosphors.

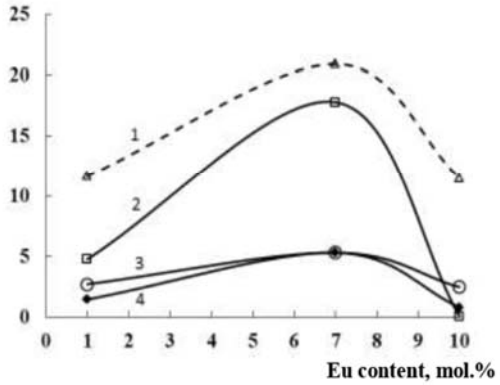

Figure 2. Luminescence brightness of the samples with P content 10% (1) and content of centers with pKa -4.4 (2), 7.3 (3) and 1.3 (4) on their surface as a function of Eu content.

The increase of P and Eu contents above 10 and 7% respectively leads to the deterioration of the considered surface functional composition and significant decrease in the luminescence brightness.

Thus, the obtained data allowed us to optimize the composition of $Y_{1-x}Eu_xV_{1-y}P_yO_4$ phosphors and clarify their surface features reflecting the desired structural modification upon doping with Eu and P.

This work was supported by Ministry of Education and Science of the Russian Federation (Agreement 14.574.21.0002, identifier RFMEFI57414X0002)

REFERENCES

[1] Sychov, M.M., Mjakin, S.V., Nakanishi, Y., Korsakov, V.G., Vasiljeva, I.V., Bakhmetjev, V.V., Solovjeva, O.V., Komarov, E.V., Study of active surface centers in electroluminescent ZnS:Cu, Cl phosphors, *Applied Surface Science,* 2005, 44, 461-464.

[2] Bakhmetjev, V.V., Sychov, M.M., Korsakov, V.G., A model of active acid-base surface sites for zinc sulfide electroluminescent phosphors, *Russian J. Appl. Chem.* , 2010, 83, 1903-1910.

[3] Bakhmetyev, V.V., Mjakin, S.V., Korsakov, V.G., Abyzov, A. M., Sychov, M.M, A study of the surface and luminescence properties of ZnS: Mn^{2+} nanosized phosphors, *Glass Physics and Chemistry*, 2011, 37, 549-554.

EFFECT OF ZNS: CU, CL PHOSPHOR SURFACE MODIFICATION WITH SHUNGITE CARBONON ELECTROLUMINESCENT LIGHT SOURCE PERFORMANCES

P. V. Matveichikova[1,*], S. V. Myakin[1], M. M. Sychov[1], K. A. Ogurtsov[1], and N. N. Rozhkova[2]

[1]St. Petersburg, Russia, St. Petersburg State Technological Institute (Technical University), Department of Theory of Materials Science

[2]Institute of Geology, Karelian Research Centre of RAS, Petrozavodsk, Russia

ABSTRACT

The deposition of shungite carbon micro-additive onto the surface of a commercial ZnS:Cu,Cl phosphor surface provides an adjustable modification of its luminescence spectrum, particularly the control over the ratio between the intensities of "blue" and "green" luminescence bands depending on the deposited additive content.

Keywords: Zinc sulfide, phosphors, electroluminescence spectra, shungite

INTRODUCTION

EL phosphors of AIIBVI composition are widely used in economically efficient and safe electroluminescent light sources (ELS) for displays, flexible luminescent panels, aircraft construction, instrumentation and other industries. The luminescence performances of these materials can be improved using different approaches, including the introduction of activators, co-activators and dopants as well as specific modification.

In our earlier studies [1, 2] the content of specific surface centers (functional groups) on was found to either promote or hinder the luminescent electronic transitions and a precise surface modification was effectively used to improve the target properties of the phosphors.

In this work the surface of a commercial ZnS:Cu,Cl phosphor (EL455 brand) was modified by shungite carbon (natural nanostructured material with a high surface activity) in order to change the surface functional composition.

* matveychikovapolina@gmail.com.

EXPERIMENTAL

The deposition of SC nanoparticles onto the phosphor surface was carried as described in [3] from stable aqueous dispersions with a concentration SC from 0.01 to 0.64 mg/mL. Then ELS (Figure 1) were prepared from the modified phosphors and characterized by measuring electroluminescence brightness at the frequency 400 Hz using a brightness meter IL 1700.

The luminescence spectra of the prepared ELS excited by AC alternator GZ-123 at 180 V and 400 Hz were measured in the range of wavelengths 350-700 nm with 2 nm step using a Avantes AvaSpec-3648 spectrofluorimeter.

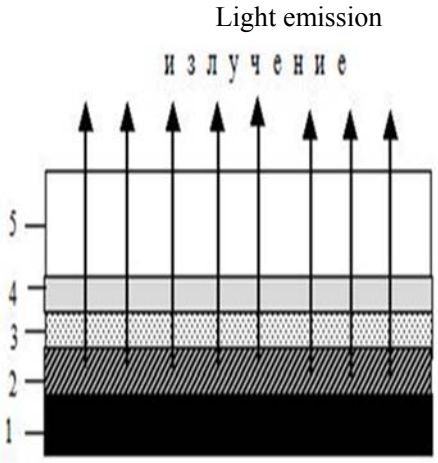

Figure 1. ELS structure: 1 - non-transparent electrode; 2- protective dielectric layer; 3 - electroluminescent layer; 4 - transparent electrode; 5 - substrate.

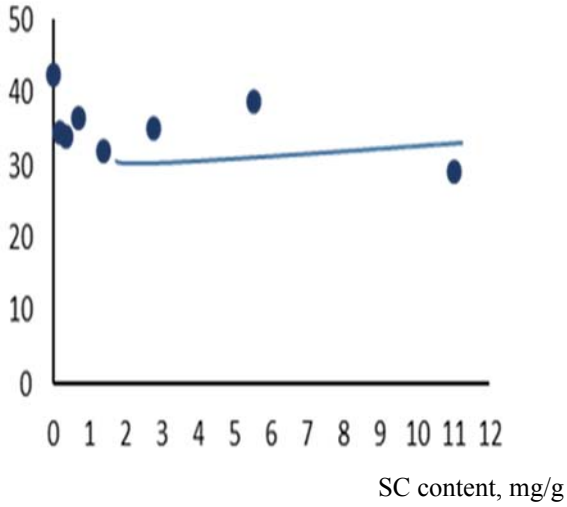

Figure 2. ELS brightness as a function of SC content.

RESULTS AND DISCUSSION

Although the introduction of SC was expected to promote the brightness growth due to electric field concentration on the phosphor particles, the increase of deposited SC amount resulted in a certain decrease in the integral luminescence brightness (Figure 2) probably due to the formation of an opaque SC layer on the surface of phosphor particles.

However, SC deposition is found to significantly affect the luminescence spectra shown in Figure 3. Particularly, the intensities of “blue” luminescence band at 455 nm (corresponding to Cu-Cu associates including one interstitial Cu atom in the crystal lattice) and a “green” band at 490 - 510 nm (corresponding to Cu_{Zn} in combination with V_s and Cl admixture) undergo opposite changes with the added SC amount reflecting specific changes in the phosphor layer structure caused by the interaction with SC.

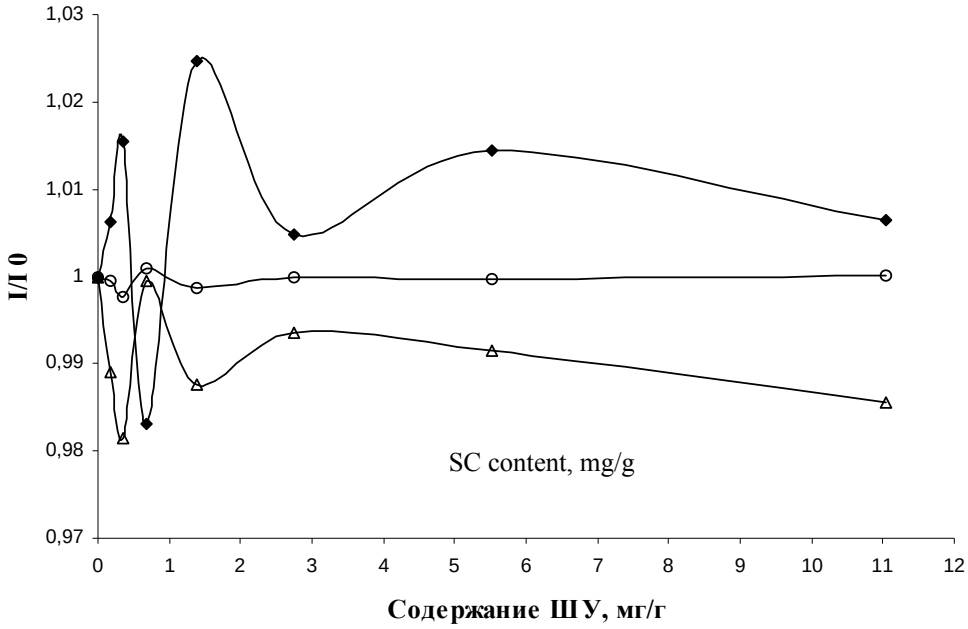

Figure 3. Normalized (relating to the non-modified phosphor) intensity of luminescence bands at 455 (♦), 490 (O) and 510 nm (Δ) as a function of deposited SC amount on the phosphor surface

CONCLUSION

Generally, the obtained results indicating a possibility for the control over spectral characteristics of the studied electroluminescent phosphors due to the introduction shungite carbon as an available micro-additive are promising in respect of adjusting the luminescence spectra of commercial phosphors.

This work was supported by grant RFFI 14-07-00277 and the Russian Ministry of Education (state. 14.VVV.21.0008 contract).

REFERENCES

[1] Sychov, M.M., Mjakin, S.V., Nakanishi, Y., Korsakov, V.G., Vasiljeva, I.V., Bakhmetjev, V.V., Solovjeva, O.V., Komarov, E.V., Study of active surface centers in electroluminescent ZnS:Cu, Cl phosphors, *Applied Surface Science,* 2005, 44, 461-464.

[2] Bakhmetyev, V.V., Mjakin, S.V., Korsakov, V.G., Abyzov, A. M., Sychov, M.M, A study of the surface and luminescence properties of ZnS : Mn^{2+} nanosized phosphors, *Glass Physics and Chemistry*, 2011, 37, 549-554.

[3] Rozhkova, N.N. *Shungite nanocarbon.* Karelian Research Centre of RAS, Petrozavodsk, 2011 (in Russian).

EFFECT OF THE SYNTHESIS METHODS ON THE CRYSTAL STRUCTURE AND LUMINESCENCE OF ZNAL2O4:EU3+ PHOSPHORS

N. S. Podsypanina*, L. A. Lebedev and M. M. Sychov
Saint-Petersburg State Technological Institute (Technical University)

ABSTRACT

$ZnAl_2O_4:Eu^{3+}$ phosphors powders were synthesized with different concentration of activator ions by using sol-gel (SG) method and solution combustion (SC) technique. The effect of the method of synthesis and concentration of Eu^{3+} ions on the structure and luminescence properties of zinc aluminate phosphor were investigated. X-ray diffraction pattern confirmed that the fibers were composed of the cubic $ZnAl_2O_4$ phase. The calculation of the crystallite size according to Scherrer formula and the maximum were for obtained 0.12% of Eu^{3+} ions by using SG and for samples prepared by SC was 0.15%. Luminescence spectra shown peaks at 612 and 618 nm. The intensity of all the emission bands reached at 0.12% and 0.24% depending on activator concentration by using SG and SC techniques, respectively. So the crystallinity, luminescence spectrum profiles and luminescence of phosphors can be effectively adjusted by the variation of method and dopant (activator) concentration.

Keywords: zinc aluminate phosphor, zinc aluminate spinel, phosphor, XRD, luminescence

INTRODUCTION

Field emission displays (FED) is an advanced direction in display technologies providing flat screens with large diagonal size. In contrast to cathode ray technology (CRT) also based on electron beam impact to excite a phosphor layer on the screen, FED are more compact because they do not require a huge deflection yoke for electron beam control[1]. Furthermore, advantageous features of such screens also include low power consumption, wide viewing angle, high image quality and small response time.

In this work $ZnAl_2O_4$: Eu^{3+} phosphors were synthesized as a red emitting component of pixel. Two series of samples prepared using sol-gel (SG) and solution combustion (SC) methods.

EXPERIMENT

The sol-gel technique involves the following steps: preparing of precursor solution in distilled water, neutralizing of solution by NH_4OH with precipitate formation, precipitate

* podsypaninanataly@gmail.com.

filtration on Buchner funnel, drying in vacuum cabinet and annealing at 800°C for two hours [2].

SC technique involves evaporation of the reaction mixture including zinc nitrate, aluminum nitrate and urea as a fuel, introducing the prepared viscous solution in a muffle furnace preheated to 600°C to initiate the reaction, yielding large amount of gases and forming white voluminous product that was annealed at 800°C for two hours.

RESULT AND DISCUSSION

X-ray diffraction (XRD) analysis of prepared samples showed that the samples of both series contain zinc aluminate spinel phase. The samples synthesized via sol-gel method have amorphous structure [3]. However, samples obtained by SC route are featured with higher crystallinity, but it contains an admixture of $AlEuO_3$ phase, which content grows with the increase of Eu^{3+} concentration up to 22 mol %.

The calculation of the crystallite size according to Scherrer formula from the obtained XRD data [Table 1] indicates that the increase of the dopant concentration results in decrease of crystallite size for samples prepared by SG method, while for samples synthesized using a SC technique an opposite trend is observed and the crystallite size grows with the dopant content [4].

Table 1. Crystal properties of $ZnAl_2O_4$ phosphors

	Eu 5%	Eu 10%	Eu 12%	Eu 15%	Eu 22%	Eu 24%
SG	12.2 nm	13.3 nm	6,2 nm	-	-	-
SC	9.0 nm	14.9 nm	15,5 nm	15 nm	14,4 nm	6,9 nm

The photoluminescence spectra of the studied samples are found to strongly depend on both Eu^{3+} ions concentration and synthesis method. The luminescence peaks at 612 and 618 nm. The samples prepared by SG method are featured with much higher intensity of the peak at λ = 618 nm compared with that at 612 nm suggesting that Eu^{3+} ions get into sites with low symmetry because this synthetic procedure yields samples with a significantly amorphous structure[5]. On the contrary, for the phosphors obtained using SC technique the intensities of both bands are comparable and the band at λ = 612 nm becomes narrower with the increase of Eu concentration indicating the improved crystallinity of these samples.

CONCLUSION

Zinc aluminate phosphor prepared by sol-gel technique, increase in Eu^{3+} concentration leads to amorphization of structure. For $ZnAl_2O_4$:Eu^{3+} prepared by SC increase in Eu concentration does not significantly affect crystallinity and leads to formation of admixture $EuAlO_3$ phase. So the crystallinity, luminescence spectrum profiles and luminescence of phosphors can be effectively adjusted by the variation of method and dopant (activator) concentration.

ACKNOWLEDGMENTS

This work was supported by Ministry of Education and Science of the Russian Federation (Agreement 14.574.21.0002, identifier RFMEFI57414X0002).

REFERENCES

[1] Chong Peng, Guogang Li, Dongling Geng, Mengmeng Shang, Zhiyao Hou, Jun Lin, Materials Research Bulletin, Vol 47, I 11, November 2012, Pages 3592–3599.

[2] V.L. Volkov, *Methods for producing nanoscale materials*, 2007, 79.

[3] V.V. Bakhmetyev, L. A. Lebedev, N. S Podsypanina, M. M. Sychov, V. V. Malygin, Effect of Composition and Synthesis Route on Structure and Luminescence of $NaBaPO_4:Eu^{2+}$ and $ZnAl_2O_4:Eu^{3+}$, 2015.

[4] S.V. Motloung, F.B.Dejene, R.E.Kroon, H.C.Swart, O.M.Ntwaeaborwa, Physica B, vol 11, I 20, November 2015, pages 468-469.

[5] Fernández-Osorio, C.E. Rivera, J. Chávez, Proceedings of the World Congress on New Technologies (NewTech 2015), p-p 360.

INVESTIGATION OF COVERED COLLOIDAL QUANTUM DOTS CDSE/ZNS AND CDSEZNS/ZNS AS A BASIS OF DETECTOR COATING

S. A. Tarasov*, M. O. Gurevich, L. I. Kozlovich, I. I. Mikhailov, E. M. Stepanov, P. O. Tadtaev and A. V. Solomonov
Saint-Petersburg Electrotechnical University "LETI" (ETU)

ABSTRACT

Covered colloidal quantum dots CdSe/ZnS and CdSeZnS/ZnS were examined. High efficiency of luminescence was shown in the range of wavelengths from 500 to 700 nm. Simulation of CQDs' energy and dimensional properties was run; it was shown that particles vary in diameters in the range from 2 to 5 nm. Using a mixture of CQDs as a basis, detector coating were created; such covers are promising for use in non-contact surface quality diagnostics.

Keywords: colloidal quantum dots, luminescence, dimensional parameters

GOALS

Investigation of covered colloidal quantum dots CdSe/ZnS and CdSeZnS/ZnS, measurement and analysis of their main optical and luminescent properties. Simulation of CQDs' energy and dimensional properties. Creating of detector coating on a basis of mixture of CQDs

INTRODUCTION

Colloidal quantum dots (CQDs) are considered one of the most promising materials of the state-of-the-art electronics. CQDs have all the nanodimensional particles' benefits, such as the good luminescent and photosensitive properties, and can be created through relatively simple and affordable methods of colloidal synthesis. Due to their small sizes, CQDs are capable of filling various devices' surface defects including nanopores, nanocracks and other topographic features of the substrate. Besides, CQDs can also interact with nanostructures of the coated device itself. It can be used as a basis of the non-contact luminescent method of surface quality diagnostics or as the source of information about surface nanostuctures' features.

* SATarasov@mail.ru.

The objects of this study were CdSe/ZnS and CdSeZnSe/ZnS colloidal quantum dots. The wide-bandgap ZnS covering enhances the stability of CQDs to oxidation and increases quantum efficiency of luminescence because of the smaller quantity of surface defects. Main optical and luminescent properties of CQDs were measured and analyzed. Experiments facility [1] based on double-grating monochromator (SDL-1) were used. Semiconductor laser with peak wavelength 445 nm was used to excite the luminescence. The lock-in amplifier SR-810 was applied to increase the sensibility.

The study showed that changing the size of CdSe colloidal quantum dots and the composition of CdSeZnS solid solution causes a shift of the spectra from green to red part of the visible range (from 500 to 700 nm). It was shown that the emission lines of CQDs were narrow and symmetrical, which proves the low size dispersion and the low influence of surface states on luminescence processes.

The size parameters of CQDs are very important, because they affect luminescent characteristics and also defines the possibility of inclusion of nanoparticles into nanostructured surfaces. In order to define particles dimensional parameters and energy states in the study samples, the simulation with consideration of excitonic effects was run. One of the most commonly applied methods of defining quantum dots' dimensions is the one based on the first luminescence and absorption peak analysis. Approximations built upon the comparison of spectra to experimental data provided by transmission electron microscopy were applied. As follows from the analysis, two methods provide the best results. The first one is based on the effective mass approximation and is applicable to the particles no less than 1.6 nm in diameter; the second one accounts for the Coulomb interaction effects which extends its application to the range of 0.6 to 4.2 nm. Nevertheless, there was a substantial divergence in calculated data. The application of the first method resulted in particle dimensions varying from 2.2 to 5.7 nm in the range of peak luminescence wavelengths from 500 to 700 nm; accounting for Coulomb effects yielded 1.5 – 2 times smaller values. The work is underway to adjust methods' accuracy in calculating particles' dimensional parameters.

Experiments were run to deposit examined colloidal quantum dots from the solution to the surfaces of various samples. It was shown that particles retain good luminescent properties and even show some stability augmentation which is explained by lower influence of the solvent's composition and concentration. The research on the characteristics of surface distribution of the particles and related change in luminescence spectrum was conducted. Deposition of the mixture of the various sized CQDs were made for changing chromatic characteristics of their emission. The possibility of creation of CQDs-based detector coating with controllable emission parameters was shown.

CONCLUSION

Covered colloidal quantum dots CdSe/ZnS and CdSeZnS/ZnS were investigated. Main optical and luminescent properties of CQDs were measured and analyzed. High efficiency of luminescence was shown in the range of wavelengths from 500 to 700 nm. It was shown that the emission lines of CQDs were narrow and symmetrical, which proves the low size dispersion and the low influence of surface states on luminescence processes. Simulation of CQDs' energy and dimensional properties was run; it was shown that particles vary in

diameters in the range from 2 to 5 nm. Using a mixture of CQDs as a basis, detector coating were created; such covers are promising for use in non-contact surface quality diagnostics.

REFERENCES

[1] I. Mikhailov, S. A. Tarasov, A. V. Solomonov et al. *J. of Phys.: Conf. Ser*. 572 (2014) 012029.
[2] A.L. Rogach, A. Kornowski, M. Gao et al. *J. Phys. Chem*. B 1999, 103, 3065.
[3] V.I. Klimov. *J. Phys. Chem. B* 2000, 104, 6112-6123.2.
[4] X. Peng et al. *J. of the Amer. Chem. Soc*., v. 120, N 21, 1998, pp. 5343-5344.

WATER TREATMENT SYSTEMS WITH THE USE OF MAGNETRON NANOSTRUCTURED COATINGS I-RU-O

E. N. Eshmemeteva*, P. A. Kuznetcov, B. V. Farmakovskiy, R. Yu. Bystrov, A. N. Beliakov and A. F. Vasiliev
FSUE "CRISM "Prometey," Saint-Petersburg, Russia

ABSTRACT

The feasibility of making a dimensionally stable anode (DSA) with an active coating Ti-Ru-O prepared by reactive magnetron sputtering was demonstrated through the present work. In addition, it was shown a utilization efficiency of water treatment systems the main element of which is the developed anode.

Keywords: dimensionally stable anodes, magnetron sputtering, nanostructured coating, water treatment

INTRODUCTION

Recently, the use of dimensionally stable anodes (DSA) with an active coating Ti-Ru-O has become technologically and economically preferred for many electrolytic processes. The dimensionally stable anodes composed of electrochemically active coating Ti-Ru-O deposited on a base metal, usually titanium. Previously used as anodes graphite, iron, lead had satisfactory characteristics, however, corrosion and mechanical wear occurred during operation led to contamination of the electrolyte, reduction of the geometric dimensions of the anode and its subsequent replacement. The success of the dimensionally stable anodes is caused by their very low wear rate. Thus the wear is limited by electroactive surface layer which can be easily restored.

DISCUSSION

Based on the unique properties of nanomaterials, a deposition technology of nanostructured active coating Ti-Ru-O by reactive magnetron sputtering has been developed in FSUE "CRISM "Prometey," which allows to get coatings of better quality in comparison with the technology of thermal decomposition of titanium and ruthenium salts, used in the production today. The developed coatings have a smooth surface without cracks and have a high adhesion to the substrate. While the method of thermal decomposition has a negative impact on the environment such as volatile organic compounds and wastewater effluence, the

* prometey_35otdel@mail.ru.

method of magnetron sputtering is the environmental friendly and does not have waste products.

As a result of complex research mutually realized with consortium "ElectroEcoTechnologies" a water treatment system "Kaskad" was created, the main element of which is the anode with an active coating Ti-Ru-O. An absence of necessity of replacement cartridges applying is a feature of this water purification equipment based on the method of electrosorbtion. These water purification systems using the anode with the active nanostructured coating Ti-Ru-O can perform a complete treatment of water containing different types of organic and inorganic microparticles such as protozoa, bacteria, viruses and their waste products, mineral particles, indecomposable petroleum products, as well as soften and purge water of such toxic mineral and organic contaminations as the ions of heavy metals and manganese, phosphates, nitrites, sulfides, cyanides, mercaptans, phenols and others while preserving an important for human body the ions of calcium and natrium. Purification equipments provide effective treatment of water according to sanitary regulations and standards on the maximum permissible concentration of impurities and do not require special maintenance for 5 years.

CONCLUSION

The developed water treatment system "Kaskad," the main element of which is the anode with an active coating Ti-Ru-O, can be used in domestic buildings, hospitals, hotels and cottage complexes, remote settlements, as well as it is possible to create mobile water treatment systems for using in places with the lacking of pure water such as scientific stations, expeditions, field hospitals. In addition, the utilization of these systems is effective for wastewater treatment (including wastewaters of heavy industry).

REFERENCES

[1] C. Comninellis, G.P. Vercesi, *J. Appl. Electrochem*. 21 (1991) 136.
[2] S. Trasatti. *Electrochim. Acta* 45 (2000) 2377.
[3] E.N. Eshmemeteva, R.Yu. Bystrov, A.N. Beliakov, B.V. Farmakovskiy, A.F. Vasiliev, A.V. Krasikov. *Voprosy Materialovedeniya* 3 (79) (2014) 90.
[4] M.R.V. Lanza, R. Bertazzoli. *J. Braz. Chem. Soc*. 13 (2002) 345.
[5] I.C.P. Gusmão, P.B. Moraes, E.D. Bidoia. *Braz. J. Microbiol*. 40 (2009) 649.

FRACTAL STRUCTURE AND ELECTRICAL PROPERTIES OF PERCOLATION SENSOR LAYERS

A. A. Bobkov, S. S. Nalimova* and V. A. Moshnikov
Saint-Petersburg Electrotechnical University "LETI," Russia

ABSTRACT

A model of percolation sensor layers with fractal structure near percolation threshold based on Mandelbrot-Given curve was proposed. Sensitivity values of these layers to reducing gases exceeding the typical values by several orders of magnitude were explained using developed model. The peculiarities of electrical properties of percolation sensor layers were studied by impedance spectroscopy in air and in the presence of reducing gases.

Keywords: gas sensors, percolation cluster, Mandelbrot-Given fractal, impedance spectroscopy

GOALS OF THE STUDY

Nowadays the development of new devices based on the theory of fractals and percolation is of great interest. The important task in this area is to achieve the conditions of transition through the percolation threshold. One of the most promising applications of these effects is the gas sensor technology. The aims of this study were synthesis and investigation of gas-sensitive metal oxide layer with a fractal structure, working at the percolation threshold.

EXPERIMENTAL AND DISCUSSION

ZnO, Fe_2O_3 and $ZnFe_2O_4$ layers were obtained by chemical co-precipitation. The greatest sensitivity to acetone and ethanol vapors in these samples reached 10^5 [1, 2]. Calculation of gas sensitivity was carried out according to the formula $S = (R_{air} - R_{gas})/R_{gas}$, where R_{air} is resistance of the sample in air, R_{gas} is resistance of the sample in the presence of a detectable gas.

Growth processes in the chemical co-precipitation leads to the formation of pores, whose surface has a fractal structure. The experimental results agree well with the fractal nature of the object being analyzed and can be explained qualitatively using the model of Mandelbrot-Given with the dimension of Hausdorff-Besicovitch equal to 1.89 which corresponding to

* sskarpova@list.ru.

fractal properties of infinite cluster in two-dimensional space. Electrical properties of percolation clusters near the percolation threshold determine the fractal properties of its core.

Electrical properties of the samples were studied by impedance spectroscopy [3, 4]. It was found that in the presence of reducing gases inductive component appears in the low-frequency region of Nyquist diagrams, which affects the impedance hodograph in the IV quarter of the trigonometric circle. According to the model of Mandelbrot-Given, fractal structure contains loops of different diameters near the percolation threshold. At high frequencies the loops do not participate in the transport of charge carriers as equivalent to a certain inductance. At low frequencies, on the contrary, the shunt effect occurs. The transport of charge carriers through loops is more profitable as compared to the capacitance which corresponding a dielectric layer between two conductive semiconductor grains. Thus, inductive characteristics of impedance spectroscopy at low frequencies follow from the described model [5].

CONCLUSION

Thus, the obtained metal oxide layers have the structure of percolation cluster on the percolation threshold and high sensitivity to acetone and ethanol vapors. Transition through percolation threshold in the presence of reducing gases results in the appearance of inductive component on Nyquist diagrams.

The investigation was performed within the project part of the state task №16.2112.2014/K in the scientific research.

REFERENCES

[1] Surface functional composition and sensor properties of ZnO, Fe_2O_3, and $ZnFe_2O_4$/Karpova S. S., Moshnikov V. A., Mjakin S. V., Kolovangina E. S.//*Semiconductors.* 2013. V. 47. N. 3. P. 369-372.

[2] Study of the effect of the acid–base surface properties of ZnO, Fe_2O_3 and $ZnFe_2O_4$ oxides on their gas sensitivity to ethanol vapor/Karpova S. S., Moshnikov V. A., Maksimov A. I., Mjakin S. V., Kazantseva N. E.//*Semiconductors.* 2013. V. 47. N. 8. P. 1022-1026.

[3] Hierarchical nanostructured semiconductor porous materials for gas sensors/Moshnikov V.A., Gracheva I.E.,·Kuznezov V.V.,·Maximov A.I.,·Karpova S.S.,·Ponomareva A.A.//*Journal of Non-Crystalline Solids*. 2010. V. 356. N. 37. P. 2020-2025.

[4] Net-like structured materials for gas sensors/Gracheva I.E., Moshnikov V.A., Karpova S.S.,·Maraeva E.V.//*Journal of Physics Conference Series*. 2011. V. 291. N. 1. P. 012017.

[5] Gas-sensitive layers based on fractal-percolation structures/Moshnikov V. A., Nalimova S. S., Seleznev B. I.//*Semiconductors*. 2014. V. 48. N. 11. P. 1535-1539.

ANALYTICAL CAPABILITIES OF REM IN THE MODE OF SCATTERED ELECTRON REGISTRATION WITH ENERGY SELECTION FOR DIAGNOSTICS OF NANOSTRUCTURES

D. M. Dolgintsev*, V. P. Pronin, V. A. Polischuk, A. S. Losev and I. V. Ryzhov

Herzen University, Russian Federation, Saint-Petersburg, Russia
ITMO University, Russian Federation, Saint-Petersburg, Russia
SPSU, 199034, Russian Federation, Saint-Petersburg, Russia

ABSTRACT

The report encompasses capabilities of scanning electron microscopy for quantitative diagnostics of morphology and ultimate composition of soft matter nanostructures in the mode of scattered electron registration with energy selection.

Keywords: scanning electron microscopy, scattering electrons, imaging contrast

ABSTRACT

Advanced REM modifications besides traditional analysis methods – secondary electrons registration method, scattered electrons registration method, fluorescent X radiation registration method and others – allow registration of scattered electrons flows with energy selection which enables registration of scattered electrons with low energy loss or quasielastic reflected electrons [1,2].

The advantage of quasi-elastic reflected electrons registration mode is primarily in relative simplicity of the interpretation of results which could be provided either analytically (based on the models of multiple or, in the simplest case, quasi-single elastic reflection) or by the statistic test method [3, 4].

Unlike other methods this one is almost free from such an effect as "scattering group" allowing X and Y space resolution which is dependent only upon primary electron beam size.

The electrons' energy variation allows gently changing the depth of diagnostic area from fractions to dozens of nanometers thus ensuring three-dimensional reconstruction of the object of investigation.

The experimental investigations were conducted on ESB detector of SEM "Zeiss Merlin" with "GEMINI" column.

The problem of image contrast separation coming from the surface morphology and the contrast associated with the variation of the elemental composition of the target is discussed. The effects of contrast reversal when detecting different energy groups of electrons are shown. As an example, Figure 1 shows an images of Si pyramidal structures (test sample for AFM - TGX1) received by the ESB detector.

* thphys@herzen.spb.ru.

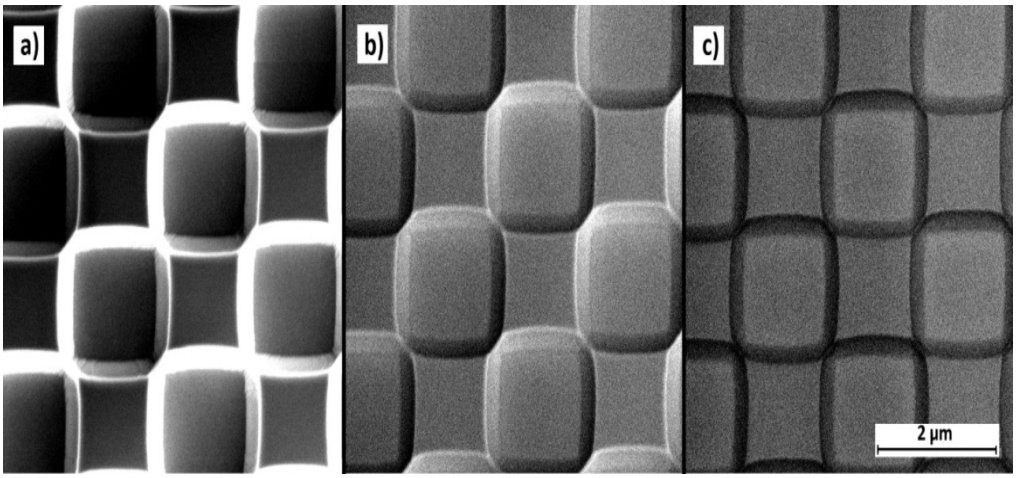

Figure 1. Images of the pyramidal silicon structures (sample 1 TGX) received by ESB detector beam. Energy of primary electrons – E_p=1.5 keV and the potential on the grid of the detector: a) U = 0 V b) U = 357 V c) U = 1000 V.

The problem of image contrast separation is discussed. According to the phenomenological model of change of image contrast in the SEM during the registration backscattered electrons with different energies associated with variation of the electron escape depth and the depth of the inhomogeneity of the elemental composition of a target.

REFERENCES

[1] Barchenko V.T., Pronin V.P., Polishuk V.A., Losev A.S. Elastically scattered electrons in a scanning electron microscope//Coll. works of the 12th All-Russia with international participation scientific conference "Rapidly materials and coatings," 26–27 November 2013, 101–103.

[2] Pronin V.P., Polishuk V.A., Losev A.S., Kanareykin A.G., Pronin I.P., Barchenko V.T. Diagnosis of the elemental composition of the ferroelectric thin multilayer structures with nanoscale resolution in SEM mode recording backscattered electrons with energy selection. Vacuum equipment and technology. 2014, 23, 1, 187-188.

[3] Pronin V.P., Barchenko V.T., Luchinin V.V., Grebnev O.I., Ryzhov I.V. Angular-resolved elastic peak electron spectroscopy for analysis of nanoscale solids. 1-st international conference. Nanomaterials: Applications & properties. NAP – 2011, Alushta, Crimea, 27-30 sept. Proceedings. Vol. 1, Part II. Sumy, Sumy State University. 2011 – P. 339–342

[4] Pronin V.P., Khinich I.I., Chistotin I.A. Elastic Peak Electron Spectroscopy for Quantitative Elemental Analysis of Solids//Technical Physics Letters. 2008, 34, 10, 825-827.

INVESTIGATION OF THE DEPENDENCE OF THE DISPERSION FORCES ON THE PROPERTIES OF THE METALLIZATION LAYER IN MDS–STRUCTURES

A. B. Fedortsov[1] and V. A. Yurova[2,*]

[1]Mining University, Saint Petersburg, Russia

[2]The Bonch-Bruevich Saint Petersburg State University of Telecommunications, Saint Petersburg, Russia

ABSTRACT

We presented the new results of calculations dispersion force pressure with different material used as metal layer in metal–dielectric–semiconductor (MDS) structures. The calculations are based on the Lifshitz theory at nonzero temperature. We discuss the range of the typical value of the thickness a dielectric layer used in modern electronics. As an example, we show how the value of the dispersion force pressure depends on of changes electro-optical properties of the metal layer in MDS-structures.

Keywords: metal–dielectric–semiconductor (MDS) structures, Silicon, Metallization, Dispersion forces, Lifshitz theory

INTRODUCTION

The major tendency of the electronics development is the decrease of the weight and overall dimension of elements. It provides a high density of elements on a chip and reduces the power consumption. Currently, the typical distances between the conductive layers of electronic circuits are several ten or one of nanometers. At this scales quantum effects and intermolecular interaction (dispersion forces) becomes commensurable on size with influence of typical electric forces [1]. So important is the investigation of dispersion forces in the different structures widely used of modern electronics.

OBJECT OF RESEARCH

The electronic equipment generally is based on the structure $Si–SiO_2$ with different type of metallization. These metal–dielectric–semiconductor (MDS) structures are widely used in developing integrated circuits due to its unique electrodynamics and technological properties, and the possibility of integration in electronic chips. Also this kind of structures may be used

* Corresponding author: Valentina A. Yurova, Docent, the Bonch-Bruevich Saint - Petersburg State University of Telecommunications, Saint – Petersburg, Russia, E-mail: va-yurova@mail.ru.

as a good and simple model for the first calculations of the dispersion pressure in MDS–structures.

The contacts from aluminum have a good electrical properties and high reflectivity. Besides structures Al–Si–SiO_2 the structures with metallization of Pd and Pt found practical application, for example, in gas sensors.

The aims of our research are: to determine the dispersion pressure on the dielectric layer in the MDS–structure based on a silicon substrate; to estimate the influence of the layers electro-optical properties on the dispersion pressure.

CALCULATIONS

According to the Lifshitz theory the dispersion pressure between layers of metal and semiconductor in MDS-structure in thermal equilibrium predominantly depends on the thickness of the dielectric layer and the material's permittivities. As the typical layers thickness of the MDS-structure and thus characteristic wavelengths of the electromagnetic fluctuations exceeds the typical atomic distance, all properties of these fluctuations and their contribution to the value of the dispersion pressure can be expressed in terms of the macroscopic approach to describe electro-optical properties of these layers.

In our research we used the simplest models of the material permittivities and the experimental data of the refraction coefficient along the imaginary frequency axis [2].

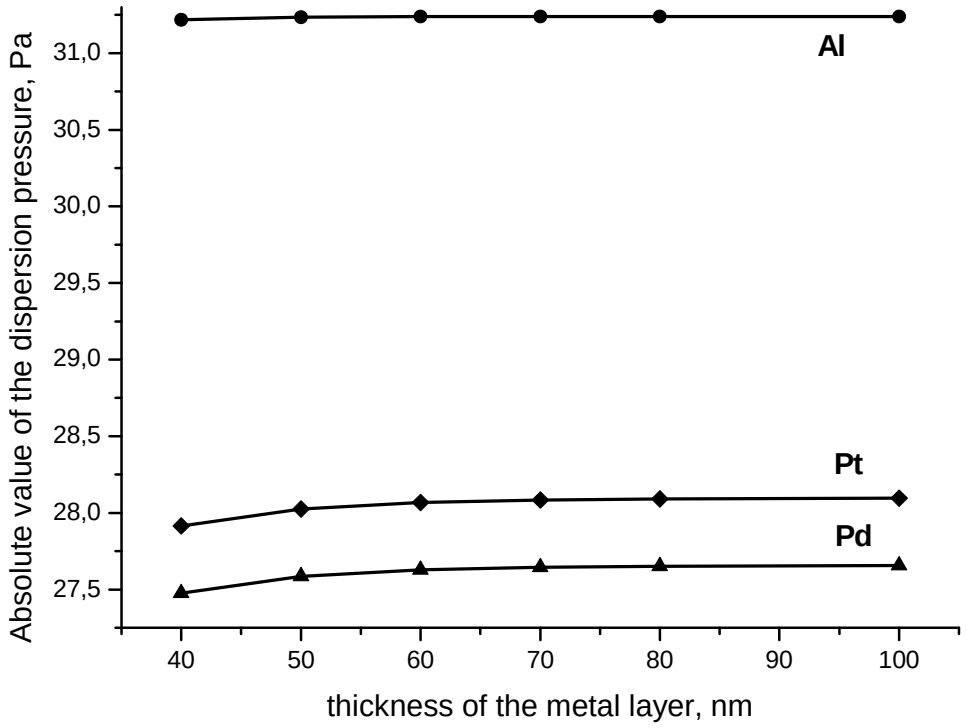

Figure 1. The absolute value of the dispersion pressure in the metal-oxide-semiconductor structure as a function of thickness of the metal layer.

RESULTS AND DISCUSSION

We researched the influence of the electro-optical properties of metal layer on the dispersion pressure in widely used in electronics MDS–structure based on Si–SiO_2. The thickness of the dielectric layer was 50 nm. Received the following ratio dielectric permittivities of the layers MDS–structures in the whole frequency range: $\varepsilon^{(\mathrm{Me})}(i\xi) > \varepsilon^{(\mathrm{Si})}(i\xi) > \varepsilon^{(\mathrm{SiO_2})}(i\xi)$. This means that the dispersion interaction between metal layer and Si substrate is attractive for any thickness of an insulating layer SiO_2.

The Figure 1 shows that the value of the pressure of dispersion force in the MDS–structure is practically independent on the thickness of metal layer. It varies less than 1% with decreases of metal layer thickness in the range from 100 nm to 40 nm. These values appear into the range of the thickness actually used in electronics. We had previously [3–4] found that the type of permittivity model doesn't influence this value too.

CONCLUSION

It was theoretical investigated the dispersion force pressure on the dielectric layer in metal–dielectric–semiconductor (MDS) structures using the Lifshitz theory at nonzero temperature. In this investigation the standard parameters of semiconductor devices with a thin dielectric layer are used. The value of the dispersion pressure depends weakly on the electro-optical properties of the metal layer and the model of its permittivity. The analysis shows that the value of the dispersion pressure is mainly depend on the properties of dielectric layer in MDS–structures. Thus the carried-out calculations showed that in metal–dielectric–semiconductor structures based on a silicon monocrystal substrate with aluminum, platinum or palladium metal layer the dispersion pressure, putting on the dielectric layer, amount to considerable value. Apparently, it makes sense to consider it when designing devices. Apparently, it makes sense to take this value into account when developed the electronically devices with MDS-structures.

REFERENCES

[1] Borgad M., Klimchitskaya G.L., Mohideen U., Mostepanenko V.M. Advances in the Casimir effect. – Oxford: Oxford University Press, 2009. – 768 p.

[2] Palik E.D. (ed.) Handbook of optical constants of solids. USA, NY: Academic Press, 1998. – 999 p.

[3] Klimchitskaya G.L., Yurova V.A., Fedortsov A.B., Churkin Yu. V. Casimir force pressure on the insulating layer in metal-insulator-semiconductor structures. Physics of the Solid State, 2012, Vol. 53, N. 9 – pp. 1921 – 1926.

[4] Klimchitskaya G.L., Yurova V.A., Fedortsov A.B., Churkin Yu. V., Bukina M.N. Casimir pressure in MDS–structures. Intern. Journ. of Modern Physics: Conference series, 2012, Vol. 14 – P. 566 – 575.

CHARGE TRANSFER PROCESSES IN BI12SIO20 SINGLE CRYSTAL

M. P. Sevryugina[1], N. S. Pshchelko[1,*] and V. A. Moshnikov[2]

[1]National University of Mineral Resources "The University of Mines," St. Petersburg, Russia

[2]Saint-Petersburg State Electrotechnical University, St.Petersburg, Russia

ABSTRACT

Charge transfer in $Bi_{12}SiO_{20}$ structures is investigated. Electric current dependences on time at temperature of 300 K in the dc electric field strength of the $2 \cdot 10^5 - 10^6$ V/m range are measured. Flowing of relaxation polarizing current is shown to result in charge accumulation in the sample surface area. Experimental regularities coordinate with provisions of the relay mechanism of transfer of a charge with the participation of deep local levels.

Keywords: electric field, charge transfer, charge accumulation, conductivity, polarization, local states

INTRODUCTION

Sillenite possess electrooptical and magnetooptical properties that in combination with photoconductivity puts them forward in number of perspective materials for creation electro - and the magnetooptical modulators of laser radiation, memory units and other devices. Keen interest to these chemical compounds is caused by their use in instrument making, first of all, in devices of spatial temporary modulation of light as an active element, and also in the electrician and the electronic engineering. Thanks to similarity of electronic structure of all undoped sillenite, it is possible to state that they are materials with the wide energy gap, high specific resistance and low mobility of charge carriers.

Further improvement of devices operating quality based of materials with a sillenite structure is connected with need of obtaining information about the probable defective structure defining distribution of energy levels in the semiconductor energy gap. The specified data can be received, in particular, by studying of the mechanism of conductivity and currents of polarization kinetics in crystals of BSO doped by various impurities. Charge relaxation in semiconductor bulk can be assumed as one of the factors that determine the stability of characteristics of electronic elements. The investigation of temporal dependence of the currents of isothermal relaxation makes it possible to acquire information on the population kinetics of capture centers arranged nonuniformly over the semiconductor thickness as well as on the capture processes in near-electrode regions [1, 2]. In the following,

* nikolsp@mail.ru.

the results of the study of the polarization relaxation in photoconductive $Bi_{12}SiO_{20}$ single crystals are presented.

Kinetic dependences of polarization currents were measured for the $Bi_{12}SiO_{20}$ single crystals. Currents of isothermal polarization were detected using a Keithley 6517A electrometric amplifier. The electric field strength was varied in the range $E = 2 \times 10^5$–10^6 V/m. The furnace was dc-supplied by a stabilized current source. Conductivity measurements in the frequencies range of $f = 10^3 \ldots 10^5$ Hz of the measuring field were performed when using the precision immitance measuring instrument E7-20 at the room temperature.

The data on the kinetics of the isothermal relaxationn currents was interpreted within a model according to which the transfer of an electric charge injected into a crystal occurs through the relay-race mechanism [1, 2]. The charge transfer from the contact into the sample occurs through the mechanism of hopping conduction over the trap centers, which are located in the band gap and have deep trapping levels of free charge carriers. This process is also accompanied by the formation of an energy barrier at the boundary with the anode, which hinders the transfer of electrons (injected from the cathode) to the anode. The energy barrier at the boundary with the anode arises from the energy difference between the electron affinity for the local center and the work function of the anode metal. Thus, the electric current is limited by both the space charge in the bulk of the semiconductor and the energy barrier at the boundary with the anode, which leads to a redistribution of the voltage across the crystal and decrease of electric current passing through the crystal. The current relaxation decay observed for the structure is accompanied by the accumulation of charge whose value can be determined from the area lying under the curve of the time dependence of the current.

Thus, for the studied BSO monocrystals with Germany impurity it was revealed that in all studied interval of temperatures multiplet jumps of charge carriers with $i = 7$ takes place ($T < 340$ K) and $i = 2$ ($T > 340$ K). The behavior of main characteristics of the charge transfer processes occurring in $Bi_{12}SiO_{20}$ single crystals are in agreement with the theory of the relay mechanism of charge transport under the conditions of nonuniform distribution of local centers in metal–(high-resistivity semiconductor)–metal structures. The results of $Bi_{12}SiO_{20}$:Ge monocrystals conductivity research found out in this work are well coordinated with the data obtained earlier for the crystals of similar structure doped by various impurities (Rh, Re, Ru, Os, Cr etc. [3, 4]).

REFERENCES

[1] Sevryugina M.P., Pshchelko N.S.,.Kadi Ya.S., Relaxation phenomena in a naturally disordered Pb3O4 semiconductor//*Journal of Physics: Conference Series*, 586 (2015) 1-6.

[2] Mustafayeva S.N., Hasanov A.I., Relaxation phenomena in $TlGa_{0.99}Fe_{0.01}Se_2$ single crystals//*Physics of the Solid State*, 46 (11), (2004), 1937-1941.

[3] Milenov T.I., Veleva M.N., Petrova D.P., Gospodinov M.M.,Skorikov V.M., Egorysheva A.V., Kargin Yu.F., Electrical conductivity of Bi12SiO20 single crystals doped with Os, Re, Ru, Rh//*Inorganic materials,* 41 (2), (2005), 152-155.

[4] Panchenko T.V., Karpova L.M., Duda V.M. Dielectric relaxation in $Bi_{12}SiO_{20}$:Cr single crystals//*Physics of the Solid State*, 42 (4), (2000), 671-675.

STRUCTURAL TRANSFORMATIONS IN IRON THIN FILMS ON SILICON SUBSTRATE

S. N. Saltykov[1,*] and A. M. Khoviv[2]
[1]Lipetsk State Technical University (LSTU), Russia
[2]Voronezh State University (VSU), Russia

ABSTRACT

During annealing of iron films (20-270 nm) on silicon substrate phase-formation process consists of two stages. Under temperature less than 130^0C the increasing of iron lattice parameter from 2.8663 (traditional bcc lattice) A up to 2.8737 A is observed and solid solution Fe(Si) is formed. The width of transition region (Fe/Si) is increasing up to 30 nm. Under temperature 180^0C the phase Fe_5Si_3 which is an ordered solid solution and which exists under 800^0C only is formed and stabilized in thin film state. The forming of Fe(Si)-phase is initiated by polygonization process of iron structure. Recrystallization process of iron structure is observed only at film thickness more than 100 nm.

Keywords: iron thin film, structure, polygonization, recrystallization

INTRODUCTION

The new way for improving of corrosion and mechanical steel properties is the using of copper as alloying element when added of it to low carbon steel instead of expensive triad of expensive elements (Nb, Ti, V) leads to the formation of precipitates in the Fe-Cu [1]. The precipitates are nano-size particles of saturated solid solution (more 1%) of copper in iron. However the mechanism and conditions of forming of Fe-Cu precipitates remain poorly understood [2]. A new approach to the problem is creation of thin layer containing precipitates on steel surface by forming a thin copper film with subsequent heat treatment to obtain a desired structure. So, "bulk" material properties are function of "near-surface" transition states. The object for their researching is thin film system Fe-Cu. However, for such researching the preliminary systematic study of phase transitions, chemical reactions and structure transformation of iron thin films is required.

The object of the research is the iron films with thicknesses from 20 up to 270 nm, obtained by magnetron sputtering on monocrystalline silicon (100) substrate. Sputtering parameters are: the content of impurities in the target is less than 0.01%, a residual vacuum of $5 \cdot 10^{-4}$ Pa, the voltage and current are 500V and 0.5 A respectively. Phase composition and structure of films were studied by XRD (ARL X'TRA), the surface topography was investigated by AFM (Solver P47 Pro). Concentration elements profiles along the depth of

* saltsn@mail.ru.

film were obtained by Rutherford back scattering (RBS), and temperature dependence of electrical resistance was studied using four-probe method.

The results showed the differences between average grain size found according to the results of AFM and XRD. In our opinion, it due to the globular structure of the film, where the globule should be understand as structural unit which is grains conglomerate. The oxide phases in the film are not detected, so the oxygen atoms found in low concentration by RBS, are located in grain boundaries as closed capsules. During heating the changes of the films structure and temperature intervals have been established. At temperatures below 130^0C the lattice iron parameter is increased, what in complex with RBS results indicated the formation of solid solution Fe(Si) [3]. When the temperature reached 180^0C silicide iron phase Fe_5Si_3 is formed although in equilibrium state it is ordered solid solution (η-phase) existed under high temperature (825^0C) only. So, in the thin film the stabilization of Fe_5Si_3 phase proceeds, the formation of Fe_5Si_3 occurs without decomposition of the solid solution Fe(Si). Early, the formation of $FeSi_2$ [4], FeSi [5] and other was observed. The stabilization of Fe_5Si_3 is shown for the first time. Two types of resistance- temperature dependences separated by a "transition point" corresponded to film thickness about 100 nm are found. Specific points observed in R-T-dependencies of iron films correspond to passing of processes: reset, polygonization and recrystallization of structure. With that, at a film thickness less than 100 nm recrystallization of the structure absent which is associated with less defects of structure compared to the films with thickness bigger than 100 nm. During increasing of thickness the defects are reduced whereupon the recrystallization temperature is increased. It is found that in thin iron films greater influence of dislocations on the electrical conductivity in comparison with pinholes is observed. That is, the nature of the size effect found when the film thickness to 100 nm is the polygonization grains process which leads to lower electrical resistance.

CONCLUSION

The formation of phases in the iron films depends on the structure and consists of two stages: a) the formation of a solid solution Fe (Si) in the transition area "film/substrate"; b) stabilization of the high temperature phase Fe_5Si_3 at room temperature. At the same time the formation of solid solutions is initiated by reset structure process and the subsequent grains polygonization. The observed size effect is appeared in the fact that the recrystallization of the iron film structure is observed only when the thickness is less than 100 nm.

REFERENCES

[1] Fine M.E., Liu J.Z., Asta M.D. An unsolved mystery: The composition of bcc Cu alloy precipitates in bcc Fe and steels.//*Materials Science and Engineering A*. 2007. V.463. P. 271.

[2] Harry T., Bacon D. J. Computer simulation of the core structure of the <111> screw dislocation in α-iron containing copper precipitates: I. Structure in the matrix and a precipitate//*Acta Mater*. 2002. V.50. P.195.

[3] Alvarez J., Parga A.L., Hinarejios J.J., Figuera J. Initial stages of the growth of Fe on Si(l 11)7x7.//*Phys. Rev. B*. 1993. V.47. P.16048.

[4] Chrost J., Hinarejes J.J., Segovia P., Michel E.G., Miranda R. Iron silicides grown on Si(100): metastable and stable phases//*Surf. Sci.* 1997. V. 371. P.297.

[5] Gallego J.M., Miranda R. The Fe/Si(100) interface//*J. Appl. Phys*. 1991. V.69. №3. P.1377.

ATOMIC-FORCE VISUALISATION OF MOTT-TRANSITION IN VO2 NANOCOMPOSITE

A. V. Ilinskiy[1], V. A. Moshnikov[2], M. E. Pashkevich[3], N. V. Permyakov[2], and E. B. Shadrin[1,*]

[1]Ioffe Physical Technical Institute of the Russian Academy of Sciences, St. Petersburg, Russia
[2]St. Petersburg Electrotechnical University LETI, St. Petersburg, Russia
[3]St. Petersburg State Polytechnical University, St. Petersburg, Russia

ABSTRACT

The electron beam can be used to control the temperature of the semiconductor–metal phase transition. The structure that is formed on the VO_2-nanocomposite surface using electron_beam irradiation is studied with the aid atomic force methods. The physical principle of such a control is based on the donor properties of the backdonation σ bonds

Keywords: Vanadium dioxide, phase transition, strong correlations

INTRODUCTION

Variations in the PT parameters due to an increase in the electron-beam irradiation dose are similar to variations related to the hydrogenation of the VO_2 film [1]. Variations in the PT parameters indicate a decrease in the band gap between 3*d*|| and π* bands that is normally related to the formation of the donor type defects in VO_2 [2].

In the course of PT, the correlation effects in the heated sample lead to a decrease in a gap of 0.7 eV between the lower 3*d* subband and π* band owing to the correlation motion of bands determined by the thermal transition of electrons from the lower 3*d* subband to the π* band (Figure 5). We must take into account the correlation interaction of electrons. In this case, (i) the Fermi distribution of electrons with extremely low tails of about 0.03 eV at a temperature of 340 K is transformed into the Migdal distribution with tails of about 0.4 eV, (ii) the positions of energy bands depend on electron populations [3].

* Corresponding author E.B.Shadrin, Ioffe Institute, St. Petersburg, Russia, Tel.: + 79095798026. E-mail: shard.solid@mail.ioffe.ru.

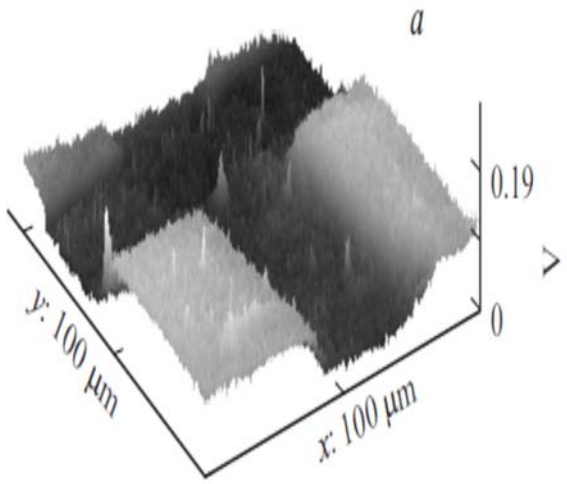

Figure 1. Figure 2. Bands of (a) high_temperature metal and (b) low 3D surface_potential distribution at temperatures of temperature semiconductor phases of vanadium dioxide. 20°C.

This circumstance leads to a positive feedback between the band gap and populations: a decrease in the band gap provides an increase in the rate of the thermal generation of electrons to the π* band, which causes a decrease in the band gap. Thus, the population of the π* band by electrons provided by the donor_type defects leads to a decrease (due to correlation effects) in the band gap from 0.7 eV to a level that is determined by the donor concentration [4]. Therefore, we obtain a decrease in the temperature of the thermal structural PT of the material from semiconductor phase to metal phase.

We assume that the oxygen vacancies that are generated by electron_beam irradiation serve as donordefects. Indeed, the electron beam with a medium energy of 7 keV passes through the film with a thickness of 80 nm to the glass_ceramic substrate and generates secondary electrons with a solid energy spectrum in the interval 0–50 eV. The escape energy of the oxygen atom for the VO2 lattice (several electronvolts) is close to the energy of the formation of oxygen vacancy in rutile (7.74 eV). Such an energy is available in the solid spectrum of secondary electrons. Thus, the beam of secondary electrons generates vacancies with donor properties. Donor electrons provide a decrease in the energy of the π* band and, hence, a decrease in the temperature of the semiconductor–metal PT. A large decrease in the energy of the π* band (by 0.7 eV) leads to the overlapping with the lower $d\|$ Hubbard subband, so that the dielectric phase is transformed into the metal phase at room temperature – Figure 1.

Figure 2 presents the axonometric images of the potential relief of the fragment of the VO2 film at a temperature of 20°C that is lower than the temperature of the structural PT in the film grains.

The analysis of the images yields the absence of difference between the heights in the irradiated and unirradiated regions, whereas a significant potential difference between the irradiated and unirradiated regions corresponds to the difference of conductivities in the presence of voltage across the sample. We conclude that the electron beam irradiated square fragments exhibit higher conductivity and the potential profile is formed in spite of the

topographical homogeneity of the film. Such a process leads to significant variations in the optical and electrophysical properties of the film, so that extremely high gradients of the refractive index (up to 0.5×10^6 m^{-1}) and conductivity (up to 10^9 S m^{-1}) can be formed on the film surface.

REFERENCES

[1] W. Bruckner, H. Opperman, W. Reichelt, E. I. Terukov, and F. A. Tschudnovskii, Vanadiumdioxide (Akamemie Verlag, Berlin, 1983).
[2] R. A. Aliev and V. A. Klimov, Phys. Solid State 46, 532 (2004).
[3] V. Il'insky, O. E. Kvashenkina, and E. B. Shadrin, Semiconductors 45, 1153 (2011).
[4] M. Gatti, F. Bruneval, V. Olevano, and L. Reining, Phys. Rev. 99, 26402 (2007).

CORRELATION MECHANISM OF THE ELECTRONIC COMPONENT OF THE METAL-INSULATOR PHASE TRANSITION IN VO2 NANOCOMPOSITE

A. V. Ilinskiy[1,*], O. E. Kvashenkina[2] and E. B. Shadrin[1]

[1]Ioffe Physical Technical Institute of the Russian Academy of Sciences, Russia
[2]St. Petersburg State Polytechnical University, Russia

ABSTRACT

Development of a method for separating of purely electronic phase transition component of VO_2-films and the determination of its characteristics is main result of this study.

Keywords: vanadium dioxide, phase transition, strong correlations

INTRODUCTION

In undoped VO_2 films, the electronic phase transition (PT) without hysteresis begins close to room temperature. It high increases the film reflectance by increasing of temperature, yielding the anhysteretic curve $\Delta r(T)$ (curve *2* in Figure 1). At temperatures $Ti = Tc + \Delta Ti$ differented from one another for each *i*-th group of grains with equalized size, the electronic transition initiates the structural PT in each of such group. In both tetragonal and monoclinic phases the electronic PT without hyseresis continues in all groups of grains above this temperature, (as in that have made fase transition, and that have not made). The anhysteretic electronic transition is ended, reaching saturation at temperature of ~140°C. By summarizing the above, we can conclude that the nature of the electronic component of the thermal PT in crystalline VO_2 films consists of the formation of a decreasing of the energy of many particle electronic states and the gradual disappearance of the gap in the electronic spectrum because of occurrence of free electrons in the empty allowed bands of a strongly correlated material. Free electrons appear in empty allowed bands during the thermal breakage of σ bonds of V–V dimers of the monoclinic phase. This breakage is strongly enhanced by the correlation electron–electron interaction[1-4].

The procedure of experimental separation of the electronic component of the thermal PT in its pure form is based on the following circumstance. By moving along the heating branch along the major loop to a certain temperature T_k we go back to cooling direction of sample in the range of 2-3 °C. In thise case the reflectance decrease in according to the behavior of the purely Mott electronic transition without interaction for the structural transition[5].

* Corresponding author A. V. Ilinskiy, Ioffe Institute, St. Petersburg, Russia, Tel.: + 79213759624. E-mail: ilinskiy@mail.ioffe.ru.

For the heating branch of the major loop, monotonic heating by 5–6°C was performed, then heating was terminated $T = Tk$, after which the temperature was reversed followed by cooling by 2–3°C, and heating by 5–6°C was per formed again, and the entire cycle was repeated. In the cooling branch of the major loop, the temperature was gradually decreased followed by a "stop" at $T = Tk$, then the temperature run was reversed as heating by 2–3°C followed by cooling by 5–6°C and repetition of the entire cycle. As a result of such a "multistage" procedure, the obtained major thermal hysteresis loop $\Delta r(T)$ contained a number of anhysteretic segments in the heating and cooling branches (Figure 2). To interpret the obtained experimental data, we constructed a mathematical model of the formation of only the temperature dependence of the reflectance of an individual film microcrystal, but also that of a set of VO_2 crystallites, which determines the experimentally observed total reflectance of the VO_2 film.

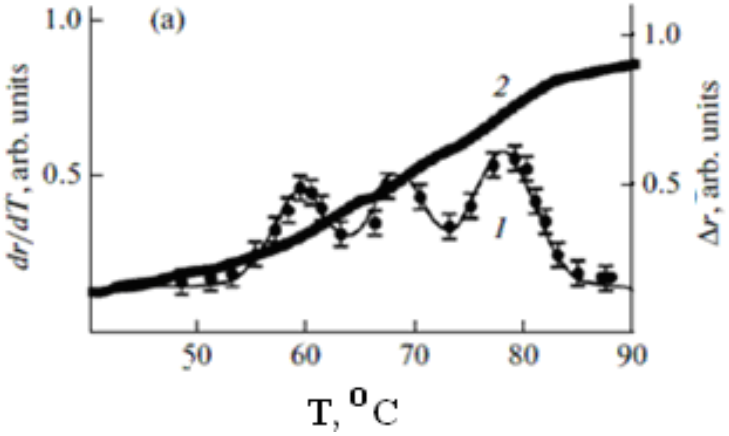

Figure 1. Temperature distributions dr/dT (curve *1*) and $\Delta r(T)$ (curve *2*), constructed by the experimental data of Figure 2.

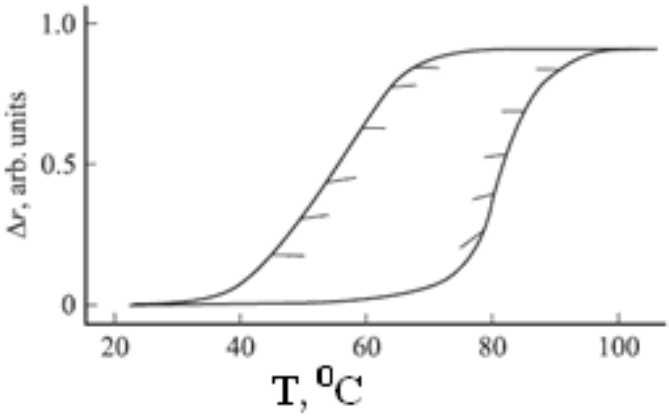

Figure 2. Anhysteretic changes in the VO_2 film reflectance (short segments), resulting from a slight deviation in temperature (from the heating and cooling branches of the major thermal hysteresis loop).

When constructing the major hysteresis loop of the film, we assume that the total change in the reflectance $\Delta r(T)$ of the film is defined by the arithmetic sum of contributions to this change by thermal changes in the reflectances Δri of individual film nanocrystallites. Summation considers the difference in the contributions of grains of different sizes to the reflectance, the size distribution of the numbers of grains and the related width and height distribution of the numbers of elementary loops.

Figure 3 shows the result of analysis, i.e., the temperature dependence of the variation in the reflectance $\Delta r(T)$ of an individual nanocrystallite (elementary loop),

This change reflects the purely Mott electronic transition in this range. In Figure 3, this process of an accelerated increase in the reflectance corresponds to the portion *b* in the dependence $\Delta r(T)$. The reflectance increase results from the thermal transfer of electrons from the lower $3d||$ subband to the descending π^* band. According to [19], the portion *b* corresponds to a 4% increase in the reflectance (Figure 3d). It follows from the above that the electronic PT component initiates the structural PT. Thus, the described set of abrupt changes in the band positions at $T = Tc + \Delta T$ causes an abrupt jump (upward in temperature) in the electron concentration in the π^* band, hence, in the sample reflectance, which is indicated by segment *c*. In the case of the reverse process of decreasing the sample temperature, all described PT stages exactlyreproduce each other. The decrease in the tetragonal *R*_phase reflectance is described by curves *d* and *e* in Figure 3, which correspond to a decrease in the electron concentration in the π^* band and, accordingly, an increase in the concentration of dimer σ bonds due to newly restored ones. As the critical concentration of dimer σ bonds is reached at $T = Tc - \Delta T$, the reverse abrupt structural PT from the tetragonal phase to the monoclinic phase, i.e., the reverse Peierls transition, occurs. Simultaneously, an abrupt decrease in the electron concentration in the π^* band, initiated by this PT, and an abrupt decrease in the reflectance (vertical segment *f*) occur. Finally, a further temperature decrease causes a further decrease in the crystal's reflectance in the monoclinic phase, which is also described by curve *a* in Figure 3. Within the proposed model, the electronic PT component in VO2 is anhysteretic, and the structure component in the VO2 microcrystal exhibits thermal hysteresis with an elementary loop width of $2\Delta T$.

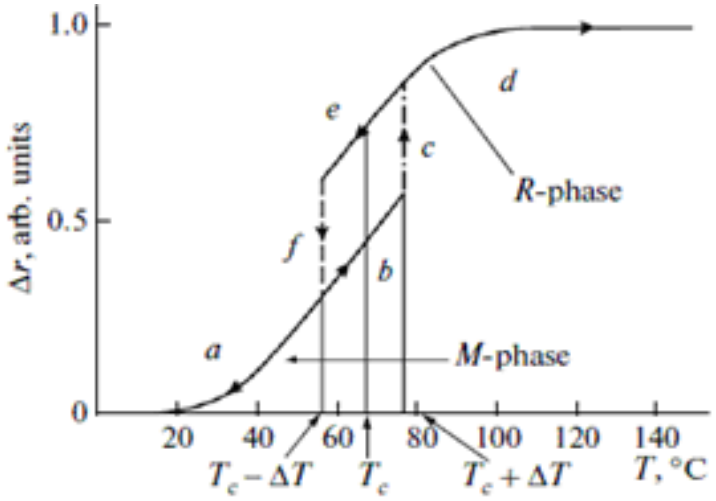

Figure 3. Elementary hysteresis loops of an individual nanocrystallite.

REFERENCES

[1] N. F. Mott, *Metal–Insulator Transitions* (Nauka, Moscow, 1979; Taylor Francis, London, 1974).
[2] W. Bruckner, H. Opperman, W. Reichelt, E. I. Terukov, and F. A. Tschudnovskii, *Vanadium Dioxide* (Akamemie_Verlag, Berlin, 1983).
[3] Bugaev, B. P. Zakharchenya, and F. A. Chudnovskii, *Metal–Semiconductor Phase Transition and Its Application* (Nauka, Leningrad, 1979) [in Russian].
[4] V. Il'inskii, O. E. Kvashenkina, and E. B. Shadrin, Semiconductors **45**, 1153 (2011).
[5] V. Il'inskii, O. E. Kvashenkina, and E. B. Shadrin, Semiconductors **46**, 422 (2012).

ON THE MODELING OF GAS-SENSITIVE PROPERTIES OF THE POROUS COMPOSITES SIO2-MEXOY WITH FRACTAL STRUCTURE

A. P. Sigaev[1], I. A. Averin[11], S. E. Igoshina[1], A. A. Karmanov[1], I. A. Pronin[1,2], V. A. Moshnikov[2], G. V. Vishnevskaya[1] and M. V. Kuznetsova[1]

[1]Penza State University,
Penza, Russia
[2]St. Petersburg Electrotechnical University "LETI,"
St. Petersburg, Russia

ABSTRACT

A model of gas sensitivity, taking into account the molecular and Knudsen diffusion of gases in porous nanocomposites SiO_2-Me_xO_y is developed. It has been shown that their gas sensing properties depend not only on the qualitative and quantitative composition, but also on the prevailing type of gas diffusion, which is determined by the concentration and size of the pores in the material.

Keywords: sol-gel technology, nanocomposites, diffusion, gas sensors, modeling

INTRODUCTION

Currently, gas sensors and multisensor systems of the "electronic nose" type are widely demanded in various fields of human activity. They are used in environmental monitoring, non-invasive medical diagnostics, criminalistics, mineral extraction, etc. The existing sensors do not fully satisfy the requirements in terms of gas sensitivity, selectivity, power consumption and performance. In order to improve their characteristics different methods and approaches are used, including those based on the use of nanotechnology principles [1].

The porous nanocomposites SiO_2-Me_xO_y (where Me are transition *d*-metals, such as Sn, In, Zn) with fractal structure are promising materials for sensitive elements of gas sensors [2]. The internal volume of such nanocomposites (Figure 1) is available for the molecules of the gas phase, the active surface being much higher than their external geometric dimensions. The most suitable method for the synthesis of these materials is the sol-gel process [3].

[1]*E-mail: nano-micro@mail.ru

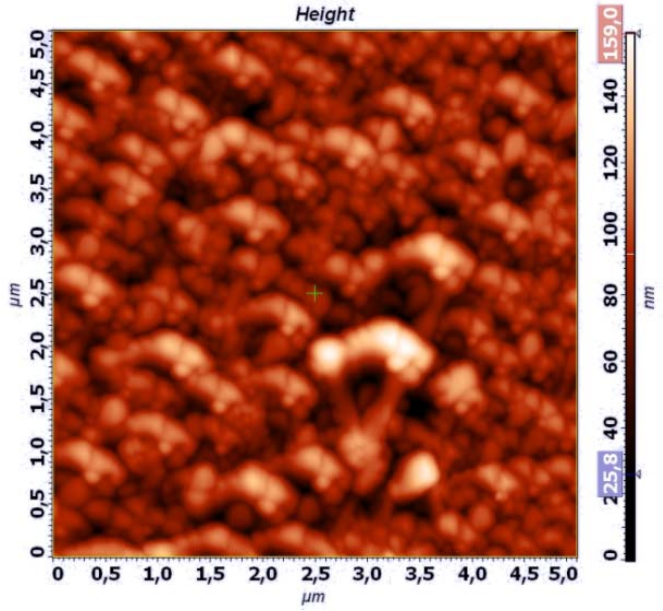

Figure 1. A typical AFM image of the porous nanocomposites SiO_2-SnO_2 surface.

To describe the interaction of gases with the sensitive elements of sensors, various models are used, among which are the following ones: the thin continuous layer model; the potential barriers at grain boundaries model; the open bridges model; the closed bridges model; the whole grain modulation resistance model. These models have their advantages and disadvantages, however, they are not suitable for describing the gas-sensitive properties of nanocomposites SiO_2-Me_xO_y, because they do not explicitly take into account their porosity and the fractal type of structural organization.

Based on [4] results, a model was developed that takes into account the molecular and Knudsen diffusion of gases and allows to determine the resistance change (R_g/R_0) of porous nanocomposites SiO_2-Me_xO_y when exposed to gases, both at a constant concentration, and while changing with a constant speed:

$$\frac{R_g}{R_0} = \frac{1}{1 + \frac{a}{L}\sqrt{\frac{ND_T}{K+\lambda}}\,\mathrm{th}\left(L\sqrt{\frac{K+\lambda}{ND_T}}\right)C_0\exp(\lambda t)},$$

where C_0 is the initial concentration of gas molecules; λ is the growth rate of the concentration of gas molecules [c^{-1}]; L is thickness of the nanocomposite material; $0 \le t \le t_{max}$ is the gas exposure time; N is the number of pores in the film; K is the constant of the surface reaction [c^{-1}]; D_T is the theoretical diffusion coefficient; a is a constant depending on the gas type (positive is for the reducers and negative is for the oxidants) and specific mechanisms of the interaction of gases with films based on the semiconductor oxides [ppm^{-1}].

Figure 2 shows the relative resistance change of films based on tin dioxide-silicon dioxide under the influence of the reducing gases (ethanol vapor). The comparative analysis of the results shows that the resulting model adequately describes the experimental data.

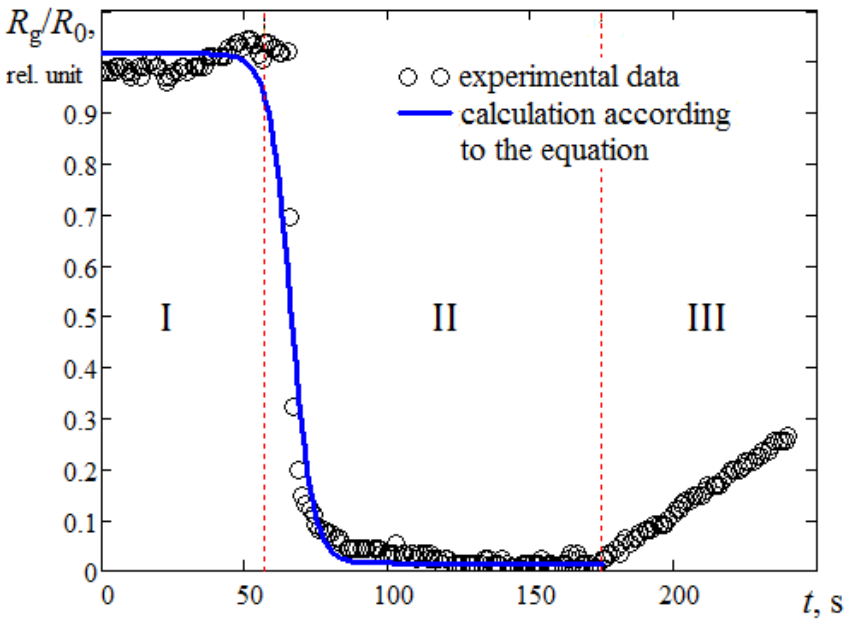

Figure 2. The relative resistance change of nanocomposite films SiO_2-SnO_2 under the influence of the reducing gases (ethanol vapor).

The graph in Figure 2 contains three typical areas characterizing the relative resistance change of porous nanocomposite layers. Area I corresponds to the resistance layer in the air in the absence of the analyzed gases. There is a sharp decrease in resistance in area II, when exposed to the reducing gases (ethanol vapor), the concentration of which increases at a constant rate until it reaches the value of C_{max} = 1000 ppm. Area III corresponds to the reduction of the resistance layer after the reducing gases exposure cessation.

CONCLUSION

It should be noted that the proposed model does not only describe the gas sensing properties of nanocomposites SiO_2-SnO_2, but also determines the predominant type of diffusion in the material, which is important for the further prediction of sensors parameters.

This work was financially supported by the Russian Ministry of Education in the framework of the basic task of the state of PSU No. 2014/151 (project code 117), and the Foundation for Assistance to Small Innovative Enterprises in Science and Technology (program “UMNIK,” No. 0015027).

REFERENCES

[1] Pronin I.A., Averin I.A., Yakushova N.D., Dimitrov D.T., Krasteva L.K., Papazova K.I., Chanachev A.S., Bojinova A.S., Georgieva A.T., Moshnikov V.A. Theoretical and experimental investigations of ethanol vapour sensitive properties of junctions

composed from produced by sol-gel technology pure and Fe modified nanostructured ZnO thin films//*Sensors and Actuators A: Physical*. 2014. V. 206. P. 88-96.

[2] Moshnikov V.A., Gracheva I.E., Pshchelko N.S., Anchkov M.G., Levine K.L. Investigating properties of gas-sensitive nanocomposites obtained via hierarchical self-assembly//*Smart Nanocomposites.* 2011. V. 2. № 2. P. 165-179.

[3] Pronin I.A., Goryacheva M.V. Principles of structure formation and synthesis models produced by the sol-gel method SiO_2-Me_XO_Y nanocomposites//*Surface and Coatings Technology*. 2013. V. 235. P. 835-840.

[4] Sakai G., Matsunaga N., Shimanoe K., Yamazoe N. Theory of gas-diffusion sensitivity for thin film semiconductor gas sensor//*Sensors and Actuators B*. 2001. V.80. P. 125-131.